THEORETICAL AND EXPERIMENTAL STUDY OF ABSORPTION AND ABSORPTION/DIFFUSION REFRIGERATING MACHINES USING AMMONIA AS A REFRIGERANT: SIMULATION UNDER STEADY-STATE AND DYNAMIC REGIMES AND EXPERIMENTAL CHARACTERIZATION OF A PILOT

Rami Mansouri

DOCTORAL THESIS

Theoretical and experimental study of absorption and absorption/diffusion refrigerating machines using ammonia as a refrigerant: Simulation under steady-state and dynamic regimes and experimental characterization of a pilot

Rami Mansouri

Supervisors: Dr. Mahmoud Bourouis

Dr. Ahmed Bellagi

Department of Mechanical Engineering

Department of Energy Engineering

UNIVERSITAT ROVIRA I VIRGILI

Tarragona, 2016

UNIVERSITAT ROVIRA I VIRGILI

ESCOLA TÈCNICA SUPERIOR D'ENGINYERIA QUÍMICA
DEPARTAMENT D'ENGINYERIA MECÀNICA

Av. Països Catalans, 26
43007 Tarragona (Spain)
Tel. +34 977 559 602
Fax +34 977 559 691
secmec@urv.cat
www.etseq.urv.es/DEM/

Dr. Mahmoud Bourouis and Dr. Ahmed Bellagi state that the present study, entitled "*Theoretical and experimental study of absorption and absorption/diffusion refrigerating machines using ammonia as a refrigerant: Simulation under steady-state and dynamic regimes and experimental characterization of a pilot*", presented by **Mr. Rami Mansouri** for the award of the degree of Doctor, has been carried out under our supervision at the Department of Mechanical Engineering of Universitat Rovira i Virgili (URV) and at the Department of Energy Engineering of Monastir University (ENIM), and that it fulfils all the requirements to be eligible for the International Doctorate.

Tarragona, July 2016

Doctoral Thesis Supervisors

Dr. Mahmoud Bourouis

Dr. Ahmed Bellagi

Dedicated to my family

Acknowledgements

I wish to express my sincere gratitude to my supervisor **Dr. Mahmoud Bourouis** at the University Rovira i Virgili, whose help, stimulating suggestions, expertise, understanding, patience and encouragement have helped me during the whole time I have dedicated to this research and to the writing of this thesis. I appreciate his extensive knowledge and multifold skills in many areas.

I also wish to express my sincere gratitude to my supervisor **Dr. Ahmed Bellagi** at the Monastir University without whom this work would not have been possible. Words fail me to enumerate all his educational and scientific qualities. I am particularly grateful to him for his advice, for all the hours he devoted to this research during the years of my thesis. I have learned a lot with him and this work has been a real pleasure thanks to him.

I am deeply grateful to my family and particularly to my mother, **Najeh Chaara**, who has dedicated her life to her children, and to my sister, **Waed Mansouri**, my brothers, **Jassem Mansouri** and **Dr. Wael Mansouri**, for their constant confidence in me. Their support was a great source of strength and encouragement. Their contributions to my studies and my life are beyond any gratitude I could express.

How can I forget my father, **Khaled Mansouri**, who will always remain near to me in the most difficult moments of my life. He gave me love and dedicated his life to his children's studies. I present this thesis as a gift to honor him.

Finally, I express my thanks to my colleagues from the National Engineering School of Monastir (**ENIM**), Tunisia, and my colleagues from the University Rovira i Virgili of Tarragona (**URV**), Spain.

Contribution by the Author

Articles in Peer-reviewed Scientific Journals

1. R. Mansouri, I. Boukholda, M. Bourouis, A. Bellagi. Modelling and testing the performance of a commercial ammonia/water absorption chiller using ASPEN-Plus platform. Energy, 2015, 93, 2374-2383.
2. R. Mansouri, M. Bourouis, A. Bellagi. Experimental investigations and modelling of a small capacity diffusion-absorption refrigerator in dynamic mode. Applied Thermal Engineering, 2017, 113, 653-662.
3. R. Mansouri, M. Bourouis, A. Bellagi. Steady state investigations of a commercial diffusion-absorption refrigerator: Experimental study and numerical simulations. Applied Thermal Engineering, 2018, 129, 725-734.

Papers presented in Conferences

1. R. Mansouri, R. Ben Jemaa, M. Bourouis, A. Bellagi. Experimental dynamic modelling of a commercial diffusion-absorption refrigerator. International Conference on Clean Cooling Technologies in the MENA Region, I3CT_MENA'2015, October 5-6, 2015, Tipaza (Algeria).
2. R. Mansouri, S. Mazouz, M. Bourouis, A. Bellagi. Experimental study and theoretical analysis of a commercial diffusion-absorption refrigerator. International Conference on Clean Cooling Technologies in the MENA Region, I3CT_MENA'2015, October 5-6, 2015, Tipaza (Algeria).
3. R. Mansouri, R. Ben Jemaa, I. Boukholda, M. Bourouis, A. Bellagi. Simulation of an absorption refrigeration machine operating with alkane mixtures. 3ème conférence Internationale des énergies renouvelables, CIER-2015, December 21-23, 2015, Sousse (Tunisia).
4. R. Mansouri, R. Ben Jemaa, I. Boukholda, M. Bourouis, A. Bellagi. Performance evaluation of a commercial absorption chiller. The 7th International Renewable Energy Congress, IREC-2016, March 22-24, 2016, Hammamet (Tunisia).
5. R. Mansouri, M. Bourouis, A. Bellagi. Black-box Dynamic Modelling of an Absorption Diffusion Refrigerator. VIII Congreso Ibérico/VI Congreso Iberoamericano de las Ciencias y Técnicas del Frío, CYTEF 2016, Mayo 3-6, 2016, Coimbra (Portugal).

Abstract

The main objective of the present thesis is to develop detailed models for absorption and diffusion-absorption refrigeration machines using ammonia as a refrigerant. The models could be useful to evaluate, analyzeandpredict the operation and performance of these machines under steady-state and dynamic regimes. This work also aims to present a detailed methodology of an experimental characterization of a small capacity diffusion-absorption refrigerator (DAR).

Case Study 1: Gas-fired absorption chiller

A steady-state simulation model of a commercial 3-ton ammonia/water gas-fired absorption chiller (10 kW cooling capacity) using the flow-sheeting software Aspen-Pluswas developed and validated. First, an appropriate thermodynamic property model for the ammonia/water fluid mixture over wider ranges of temperature ($273.16 \leq T \leq 613.15$ K) and pressure ($0 < P \leq$ 210 bar) was selected. To this purpose nine models implemented in the software library were pre-selected and tested, but none of these models predicted the vapor-liquid equilibrium (VLE) with sufficient accuracy. The interaction parameters of these models were then determined by fitting the equations of state (EOS) to VLE data. It was finally found that the Boston-Mathias modified Peng-Robinson eos with fitted parameters predicted most accurately the VLE in the temperature and pressure ranges encountered in commercial absorption chillers. A simulation model of the absorption chiller was then developed. The simulation results were found to be well in agreement with data from literature at a cooling air temperature of 35ºC. The heat transfer characteristics (UA) of the various heat exchangers of the chiller were then determined and the model modified so that it would accept them as input parameters. The comparison between simulation predictions and bibliographical data at air temperatures of 26.7 and 38ºC was also well in concordance.

Case Study 2: Low capacity DAR in steady-state mode

A small capacity commercial diffusion-absorption refrigerator (cooling capacity of 7 W) was tested under conditions of different heat input to the generator. The temperatures at the inlet and outlet of each thermal component were continuously recorded. All the essential features of the refrigerator were determined experimentally, especially the heat exchange capacities of the refrigerated room "cabinet" and the evaporator, found to be respectively $(UA)_{cab} = 0.554\ \mathrm{WK^{-1}}$ and $(UA)_{int} = 0.3\ \mathrm{WK^{-1}}$. The best performance of the refrigerator was reached experimentally with an electric power supply of 46 W and a generator temperature of 167°C. The COP of the refrigerator was found to be 0.159. An Aspen-Plus model was then developed for the diffusion-absorption refrigerator investigated. The operating conditions and the assumptions introduced as inputs in the simulations were based on experimental tests. The predicted temperatures were well in agreement with the measured ones for the heating rates of 46W, 56W and 67W. The deviations between the predicted and measured COP and cooling capacity were less than 1%. This indicated that the model developed represented fairly well the functioning of the commercial diffusion-absorption refrigerator working under a steady-state regime.

Case Study 3: Low capacity DAR in dynamic mode

A dynamic black-box model was then developed for the refrigerator based on the experimental data and using the Matlab identification package to correlate the power input to the generator and the cooling capacity of the refrigerator. A first order transfer function with a delay was found to describe quite accurately the time evolution of the cooling capacity for all the heat rates supplied to the generator that were taken into consideration. In a further step, regressed analytical expressions of the transfer function parameters, as a function of the generator heat supply, were incorporated into the cooling capacity function. A generalized dynamic black-box model was thus obtained for the refrigerator and was

validated using the Matlab Simulink® environment. The predictions made by the model were found to be well in agreement with the experimental data. In particular, the predictions for COP under steady state conditions agreed satisfactorily with the experimental data yielding a maximum relative deviation of about 8%.

Resumen

El objetivo principal de la presente tesis es el desarrollo de modelos detallados para las máquinas de refrigeración por absorción y difusión-absorción que utilizan el amoniaco como refrigerante. Los modelos pueden ser útiles para predecir, evaluar y analizar el funcionamiento y el rendimiento de estas máquinas en los regímenes de estado estacionario y dinámico. Esta tesis también tiene como objetivo presentar una metodología detallada para la caracterización experimental de un refrigerador de difusión-absorción (DAR) de pequeña capacidad.

Caso de estudio 1: Enfriadora de absorción accionada con gas natural

Un modelo de simulación en estado estacionario de una enfriadora comercial de absorción de amoniaco/agua de 3 toneladas de potencia (capacidad de enfriamiento de 10 kW) y accionamiento con gas natural fue desarrollado y validado utilizando el software Aspen-Plus. En primer lugar, fue seleccionado un modelo de propiedades termodinámicas apropiado para la mezcla amoníaco/agua en amplios intervalos de temperatura ($273.16 \leq T \leq 613.15$ K) y presión ($0 < P \leq 210$ bar). Nueve modelos implementados en la librería del software fueron pre-seleccionados y probados, pero ninguno de estos modelos predijo el equilibrio líquido-vapor (VLE) con suficiente precisión. Por ello, los parámetros de interacción de estos modelos fueron determinados mediante el ajuste de las ecuaciones de estado (EOS) con los datos del equilibrio líquido-vapor (VLE). Finalmente, se encontró que la ecuación de estado (EOS) de Boston-Mathias Peng-Robinson modificada con parámetros ajustados predice con mejor precisión el equilibrio liquido-vapor en los intervalos de temperatura y presión encontrados en las enfriadoras de absorción comerciales. A continuación, se desarrolló un modelo de simulación de la enfriadora de absorción. Se encontró que los resultados de la simulación estaban de acuerdo con los datos de la literatura a una temperatura del aire de

enfriamiento de 35ºC. Las características de transferencia de calor (UA) de los diferentes intercambiadores de calor dela enfriadora fueron también determinadas y el modelo fue modificado de modo que los aceptaría como parámetros de entrada. La comparación entre las predicciones de la simulación y los datos bibliográficos a temperaturas del aire de enfriamiento de 26.7 y 38°C estuvieron también en concordancia. Por lo tanto, se concluyó que el modelo Aspen-Plus propuesto podría ser una herramienta muy útil para predecir las condiciones internas de funcionamiento y el coeficiente de operación de la enfriadora de absorción comercial a diferentes temperaturas del aire de enfriamiento teniendo en cuenta el tamaño real de los intercambiadores de calor.

Caso de estudio 2: Refrigerador de difusión-absorción de pequeña potencia en régimen estacionario

Un refrigerador comercial de difusión-absorción de pequeña capacidad (capacidad de enfriamiento de 7 W) fue ensayado a diferentes condiciones del calor suministrado al generador. Las temperaturas en la entrada y salida de cada componente térmico fueron registradas continuamente. Todas las características esenciales del refrigerador fueron determinadas experimentalmente, especialmente las conductancias térmicas de la cámara refrigerada y el evaporador, las cuales son $(UA)_{cab} = 0.554\ \mathrm{WK^{-1}}$ y $(UA)_{int} = 0.3\ \mathrm{WK^{-1}}$, respectivamente. El mejor rendimiento del refrigerador se alcanzó experimentalmente con una fuente de alimentación eléctrica de 46 W y una temperatura del generador de 167°C. Se encontró que el COP del refrigerador fue de 0.159. A continuación, un modelo Aspen-Plus fue desarrollado para el refrigerador de difusión-absorción investigado. Las condiciones de operación y las suposiciones introducidas como entradas en las simulaciones, fueron basadas en las pruebas experimentales realizadas con el refrigerador. Las temperaturas predichas estaban de acuerdo con las temperaturas medidas para las potencias de accionamiento de 46,

56 y 67W. Las desviaciones entre el COP predicho y el calculado a partir de los datos experimentales, y la capacidad de refrigeración fueron menores del 1%. Esto indica que el modelo desarrollado representa satisfactoriamente el funcionamiento del refrigerador de difusión-absorción comercial en régimen estacionario de operación.

Caso de estudio 3: Refrigerador de difusión-absorción de pequeña potencia en régimen dinámico

Un modelo dinámico de caja negra fue desarrollado para el refrigerador en base a los datos experimentales y utilizando el paquete de identificación Matlab para correlacionar la potencia suministrada al generador y la capacidad de refrigeración del refrigerador. Se encontró que una función de transferencia de primer orden con un retardo describe con precisión suficiente la evolución en el tiempo de la capacidad de refrigeración para todas potencias seleccionadas del calor suministrado al generador. En una etapa posterior, expresiones analíticas, ajustadas en función del calor suministrado al generador, de los parámetros de la función de transferencia fueron incorporadas en la función de la capacidad de refrigeración. Un modelo dinámico generalizado de caja negra fue obtenido para el refrigerador y validado utilizando el entorno Matlab Simulink®. Se encontró que las predicciones hechas por el modelo concuerdan bien con los datos experimentales. En particular, las predicciones para el COP bajo condiciones de estado estacionario concuerdan satisfactoriamente con los datos experimentales siendo la desviación relativa máxima del orden del 8%.

Résumé

Le principal objectif de cette thèse est le développement de modèles détaillés pour des machines frigorifiques à absorption et à diffusion-absorption, utilisant l'ammoniac comme fluide de travail.

Les modèles pourraient être utiles pour évaluer, analyser et prédire le fonctionnement et les performances de ces machines en régime permanent et dynamique. Cette thèse vise également à présenter une méthodologie détaillée pour la caractérisation expérimentale d'un réfrigérateur diffusion-absorption de faible capacité.

Cas d'étude 1: Climatiseur à gaz

L'étude porte sur un climatiseur à gaz commercial du 10 kW de puissance utilisent le mélange ammoniac-eau comme fluide de travail. Un modèle de simulation en régime permanent de cette machine a été développé à l'aide du logiciel Aspen-Plus et validé. Tout d'abord, un modèle des propriétés thermodynamiques approprié pour le mélange ammoniac-eau couvrant de larges plages de température ($273.16 \leq T \leq 613.15$ K) et de pression ($0 < P \leq 210$ bar) a été sélectionné. À cet effet, neuf modèles de la bibliothèque du logiciel ont été présélectionnés et testés. Aucun ne prédisait l'équilibre vapeur-liquide avec une précision suffisante. Les paramètres d'interaction de ces modèles ont été alors déterminés en ajustant les équations d'état aux données d'équilibre. Il a été finalement constaté que l'équations d'état Peng-Robinson Boston-Mathias avec des paramètres ajustés prédit le plus fidèlement les données dans les plages de température et de pression rencontrées dans les machines frigorifiques à absorption commerciales. Les résultats des simulations du fonctionnement du climatiseur se sont avérés en bon accord avec les données de la littérature par une température de l'air de refroidissement de 35°C. Ensuite, les caractéristiques de transfert de chaleur (UA) des différents échangeurs de chaleur du climatiseur ont été déterminées et le modèle Aspen-Plus modifié de manière à accepter ces caractéristiques comme paramètres d'entrée. La

comparaison entre les prédictions des modèles et les données bibliographiques par des températures du medium de refroidissement de 26.7 et 38ºC montrait une bonne concordance.

Cas d'étude 2: Réfrigérateur à absorption-diffusion de faible capacité en régime stationnaire

Une machine frigorifique commerciale à absorption-diffusion de faible puissance (7 W) a été testée pour différentes puissances motrices fournies au générateur. Les températures à l'entrée et à la sortie de chaque organe de la machine ont été enregistrées en continu. Toutes les caractéristiques essentielles du réfrigérateur ont été déterminées expérimentalement, en particulier les capacités d'échange de chaleur de la cabine et de l'évaporateur, respectivement $(UA)_{cab} = 0.554\ \mathrm{WK^{-1}}$ et $(UA)_{int} = 0.3\ \mathrm{WK^{-1}}$. La meilleure performance du réfrigérateur est obtenue avec une alimentation électrique de 46 W et une température de générateur de 167°C. Le COP de la machine est alors de 0.16. Les températures prédites par les modèles Aspen-Plus pour les puissances de chauffe 46W, 56W et 67W se sont révélées en bon accord avec les températures relevées sur l'appareil testé. Les écarts entre les valeurs mesurées et prédites du COP et de la puissance frigorifique sont inférieurs à 1%.

Cas d'étude 3: Réfrigérateur à absorption-diffusion de faible capacité en mode dynamique

Enfin, un modèle dynamique de type boîte noire a été développé pour ce réfrigérateur en exploitant le logiciel Matlab Simulink®. Il a été constaté qu'une fonction de transfert de premier ordre avec retard décrit correctement la relation entre la puissance thermique stimulante et la puissance frigorifique produite dans la cabine. Le comportement en régime instationnaire du réfrigérateur lors de la phase de démarrage est ainsi bien décrit par ce modèle. En outre, la prédiction du COP en régime stationnaire se trouve en bonne concordance avec les données expérimentales, l'écart relatif maximum étant d'environ 8%.

Contents

Chapter 3

Chapter 4

Chapter 5

List of Figures

List of Tables

List of Symbols and Abbreviations

Symbols

COP	coefficient of performance (-)
x	concentration of ammonia (-)
P	pressure (bar)
Q	heat transfer rate (W)
T	temperature (ºC)
t	time (min)
UA	overall heat transfer coefficient (W K^{-1})
F	unit step function (-)
G_R	transfer function (-)
K_p	static gain (-)
s	Laplace variable (-)
I	Laplace transform of the input function(-)
Y	Laplace transform of the output function (-)

Abbreviations

COP	coefficient of performance
VLE	vapor-liquid equilibrium
ENRTL-RK	Electrolyte NRTL/Redlich-Kwong
RKS-BM	Redlich-Kwong-Soave-Boston-Mathias
PENG-ROB	Standard Peng-Robinson
PR-MHV2	Modified Peng-Robinson-Huron-Vidal
PR-WS	Peng-Robinson-Wong-Sandler

NRTL-HOC	Non-Random-Two-Liquid/Hayden O'Connell
SRK	Soave-Redlich-Kwong
WILS-RK	Wilson/Redlich-Kwong
PR-BM	Peng-Robinson-Boston-Mathias
LMTD	log-mean temperature difference
DET	valve
COND, CNDNSER	condenser
EVAP	evaporator
ABS	absorber
SHX, SOL-HX	solution heatexchanger
PREAB	pre-absorber
GEN	generator
PUMP	pump
RECT	rectifier
GGHX, G-HX	gas heat exchanger
BBL-PUMP	bubble pump

Greek Symbols

φ	the applied voltage (V)
θ_p	time constant (min)
τ_p	time delay (min)

Subscripts

i	inlet
o	outlet
gen	generator

evap	evaporator
cab	refrigerated room cabinet
loss	heat losses
int	indoor of the refrigerated room
amb	outdoor of the refrigerated room
LMevap	the logarithmic mean temperature difference at the cold and hotsides of the evaporator
f	instantaneous cooling capacity

Chapter 1

Introduction

The market of refrigeration and air conditioning is rapidly expanding all around the world because of the increase of the needs for comfort by a growing world population. This fast evolution has entrained a galloping consumption of energy in general and in electrical energy in particular. As this form of energy is mainly produced by combustion of fossil energy resources (oil, gas, coal), these cover approximately 80 % of the world energy demand today, this combustion contributes for a large part to the emissions of greenhouse gases, essentially CO_2. Moreover CFC and HCFC refrigerants used in common refrigerators and chillers working according to the technique of vapor compression are destructive for the ozone layer which protects the life on earth and, consequently, highly harmful. To reduce the emissions to the atmosphere of the greenhouse gases on one side and gases responsible for holes observed in the ozone layer, on the other side, several protocols and international agreements were signed: protocol of Montreal in 1987 to limit the use of the CFC and HCFC refrigerants, Kyoto protocol in 1998 for the CO_2 and the greenhouse gases, etc. These agreements have the objective to bring the signatory countries to reduce their greenhouse gas emissions by at least 5 % compared with the level of 1990, during the period of commitment from 2008 to 2012. In 2015, the United Nations Climate Change Conference (COP21) was held in Paris, France. The objective of this conference was to achieve, for the first time in over 20 years of the United Nations negotiations, a binding and universal agreement on climate, from all the nations of the world, with the aim of keeping global warming below 2°C. On April 2016, 174

countries signed the agreement and began adopting it within their own legal systems (through ratification, acceptance, approval, or accession).

The absorption and diffusion-absorption cooling technologies represent an interesting alternative to the technique of vapor compression as they are heat powered. Indeed, these techniques require a marginal use of electrical energy. Besides, the refrigerants which are used are compatible with the environment. Two working fluid mixtures mostly used in these machines are:

a. Aqueous solutions of lithium bromide (H_2O/LiBr), water being the refrigerant.
b. Aqueous solutions of ammonia (NH_3/H_2O), ammonia being the refrigerant.

The application of the absorption technique is particularly interesting if a free source of heat (waste heat, solar energy, etc.) is available.

1.1. Justification

Current research concerning absorption and diffusion-absorption refrigerating machines is carried out according to two main directions. Firstly, there are investigations aiming at deepening the understanding of functioning of these machines and at studying their performance at various operating conditions. Secondly, there are other investigations focused on improving the performance of the NH_3/H_2O and H_2O/LiBr refrigerating machines and the search for new fluid mixtures susceptible to be used as working pairs in such machines. In this thesis, detailed models will be developed to predict, evaluate and analyze the detailed behavior of functioning and the performance of ammonia-based absorption and diffusion-absorption refrigerating machines under steady-state and dynamic regimes. This thesis also aims to present a detailed experimental analysis on the operation of a small capacity diffusion-absorption refrigerator, which will be useful to understand the optimal operation

conditions of this machine and collect experimental data to be used for validation purposes of the models developed.

1.2. Aims and objectives

The main objective of this thesis is to perform a theoretical and experimental study on ammonia-based absorption and diffusion-absorption refrigerating machines. The specific objectives are as follows.

1. Choice of the appropriate thermodynamic model to predict the properties of the ammonia based working fluids in Aspen-Plus platform.

2. Steady-state modeling in Aspen-Plus platform of a commercial gas-fired air-cooled NH_3/H_2O absorption chiller.

3. Experimental investigations and characterization of a commercial diffusion-absorption refrigerator (DAR) working with the fluid mixture $NH_3/H_2O/H_2$ under diverse operating conditions.

4. Steady-state modeling in Aspen-Plus platform of the diffusion-absorption refrigerator investigated experimentally.

5. Dynamic modeling and simulation of the functioning of the diffusion-absorption refrigerator investigated experimentally.

1.3. Thesis structure

The investigations carried out in the thesis are organized into the chapters described below.

Chapter 1: Introduction

In this chapter, the framework and objectives of the thesis are presented.

Chapter 2: Bibliographic review

This chapter presents an overview on the evolution of cooling techniques and technologies and the operating principles. It also reports on the state of the art of absorption and diffusion-absorption refrigeration systems. Moreover, it presents an overview of the ammonia based working fluids used or considered for use in these machines.

Chapter 3: Choice of the thermodynamic model to predict the properties of the ammonia based working fluids in Aspen-Plus

Simulation of absorption and diffusion-absorption refrigerating machines requires the knowledge and/or the reliable prediction of the thermodynamics properties of the working fluids. This chapter is dedicated to the choice of the appropriate thermodynamic model for the binary working fluid mixtures considered in this thesis, namely (NH_3/H_2O) for absorption systems and the ternary mixture ($NH_3/H_2O/H_2$) for absorption/diffusion systems. As the simulations of the various refrigeration machines are carried in the environment of the Flow-Sheeting software Aspen-Plus, this part of the thesis is limited to the models available in the rich library of the software, with data regression when needed. The choice of the appropriate model was based on the quality of prediction of the liquid-vapor equilibrium of the considered fluid mixtures.

Chapter 4: Steady-state modeling and operational analysis of a commercial gas-fired absorption chiller in Aspen-Plus

This chapter consists of two parts. The first one presents the Aspen-Plus simulation of a commercial gas-fired air-cooled NH_3/H_2O absorption chiller. The purpose is to analyze and predict its behavior and to determine the heat transfer characteristics (UAs) of its various components. In the second part, simulations of the chiller at different ambient temperature conditions are performed based on the UA values obtained. The model predictions are compared with experimental and simulation data from the open literature.

Chapter 5: Experimental investigations and characterization of a small capacity diffusion-absorption refrigerating (DAR) machine

In this chapter, experiments are performed on a small capacity commercial diffusion-absorption machine at various operating conditions. The experimental data base will allow us to perform a complete characterization of the DAR machine and the validation of the simulation models developed in the next chapters. This chapter includes the experimental determination of the heat transfer characteristics of the different components, the cooling capacity and the coefficient of performance (COP) of the DAR machine.

Chapter 6: Steady-state modeling of a small capacity diffusion-absorption refrigerating (DAR) machine

The objective of this chapter is to develop a realistic and reliable model for the simulation of a small capacity diffusion-absorption refrigerating (DAR) machine. The model has to comply with following constraints: it must be autonomous but also able to be integrated into other models, for example into a system of residual energy recovery or into a free source of heat. It has to require only the following input data: driving heat temperature, temperature of the cooling medium, efficiency of the various heat exchangers and the available heating power or

the required cooling capacity. The model developed is validated with experimental data from the investigations carried out in the previous chapter.

Chapter 7: Dynamic modeling and operational analysis of a small capacity diffusion-absorption refrigerating (DAR) machine

In this chapter, the operation of the diffusion-absorption refrigerating machine, investigated experimentally, is modeled using transfer functions and Laplace transforms. The dynamic modeling of the DAR machine is based on a black-box approach and makes use of the experimental data base of chapter 5. A generalized dynamic model of the functioning of this commercial DAR machine is then developed and validated.

Chapter 8: General conclusions and Recommendations

This chapter gives a summary of the methodology employed, the most relevant results achieved in this thesis as well as the future investigations which can be carried out in this topic.

Chapter 2

Bibliographic review

This chapter is devoted to present an overview on the absorption and diffusion-absorption refrigeration systems and the working fluid mixtures used in these machines. Firstly, a description of the basic principle of absorption refrigeration systems and a review of various investigations conducted on the absorption refrigerating machines are presented. Secondly, an overview of the ammonia based working fluids used or considered for use in absorption refrigeration systems is presented. Finally, a literature review on the research conducted on the diffusion-absorption refrigerating machines is reported.

2.1. Introduction

Due to the rapid increase in global demand for energy and the need to reduce greenhouse gas emissions, the interest in finding new efficient ways of using energy is growing. Cooling technologies are of great economical, energetic and environmental importance. The conventional vapor compression refrigeration and air conditioning systems are driven by electrical energy which consumes worldwide huge amounts of this kind of energy and also contributes to the greenhouse effect in the atmosphere. Priority should be given to the investigation and use of alternative driving energy sources instead of electricity for cooling applications. The interest is focused on the absorption cooling technology as it is an attractive alternative and sustainable solution to replace vapor compression units. Indeed, waste heat rejected in many industries is at higher temperatures than the heat source temperatures required for driving most of the absorption cooling systems [1-2]. The use of thermally driven cooling systems can help in reducing problems related to global warming, such as the green-house effect due to CO_2 emissions from the combustion of fossil fuels in thermal power plants.

Absorption refrigeration systems use natural fluid mixtures, such as ammonia/water (NH_3/H_2O), water/lithium bromide (H_2O/LiBr) and methanol/lithium bromide (CH_3OH/LiBr) as working pairs, instead of the harmful chloro-fluoro-carbon and chloro-hydro-fluoro-carbon (CFC/CHFC) gases used in conventional vapor compression refrigeration and air conditioning systems which contribute to the greenhouse effect in the atmosphere.

The idea of eliminating the pump circulating the solution and making the pressure uniform in all components of the absorption refrigeration systems occurred first to Geppert in 1899 [3]. To allow the refrigerant to evaporate at low temperatures in the evaporator, a third compound i.e. an inert gas was introduced. A diffusion-absorption refrigeration cycle or a pumpless vapor absorption refrigeration cycle is of great significance in noiseless refrigeration

applications. The diffusion-absorption cycle is unique in that it runs without any mechanical energy input. This is achieved by pumping the working fluid using a thermally driven bubble pump. Another unique feature of this cycle is that it is essentially noise free. The first diffusion-absorption refrigeration (DAR) machine using this technique for cold production was developed by the Swedish engineers von Platen and Munters in 1928 [4]. In this refrigerator, ammonia was used as a refrigerant, water as an absorbent and hydrogen as an inert gas to equalize the pressure. Since the invention of the diffusion-absorption refrigeration systems, much research has been conducted in order to make them more attractive for use as domestic refrigerators and to improve their performance. Most of these investigations were focused on improving the performance by reducing the heat supplied to the generator. Many aspects were then discussed, such as the mechanical design of the various components of these systems, the thermodynamic cycles and the nature of the working fluids.

2.2. Absorption refrigeration machines

The operation principle of the absorption refrigeration cycle has been known since 1777. The first continuously working absorption refrigeration system using ammonia and water as the refrigerant and the secondary fluid, respectively, was invented by Carré in 1859. Figure 2.1 (a) schematically shows such an absorption refrigeration system. This most simple continuous absorption cycle consists of the following components: generator, condenser, evaporator, absorber, two throttling devices (two expansion valves) and a pump. In the generator the so-called rich solution, i.e. a mixture rich in refrigerant, is heated to drive refrigerant vapor of the solution. The remaining liquid, being weak in refrigerant, passes back through a throttling device to the absorber. The concentrations of the rich and weak solutions are denoted in Figure 2.1 (a) as X_R and X_A, respectively. The vapor which has been separated from the rich solution is liquefied in the condenser. The concentration of the vapor is given as X_D. After being throttled it enters the evaporator where the refrigerant is evaporated at a low

temperature by taking up heat, thus performing the cooling effect. The vapor leaving the evaporator is absorbed by the weak solution in the absorber. The pump feeds the obtained rich solution back to the generator.

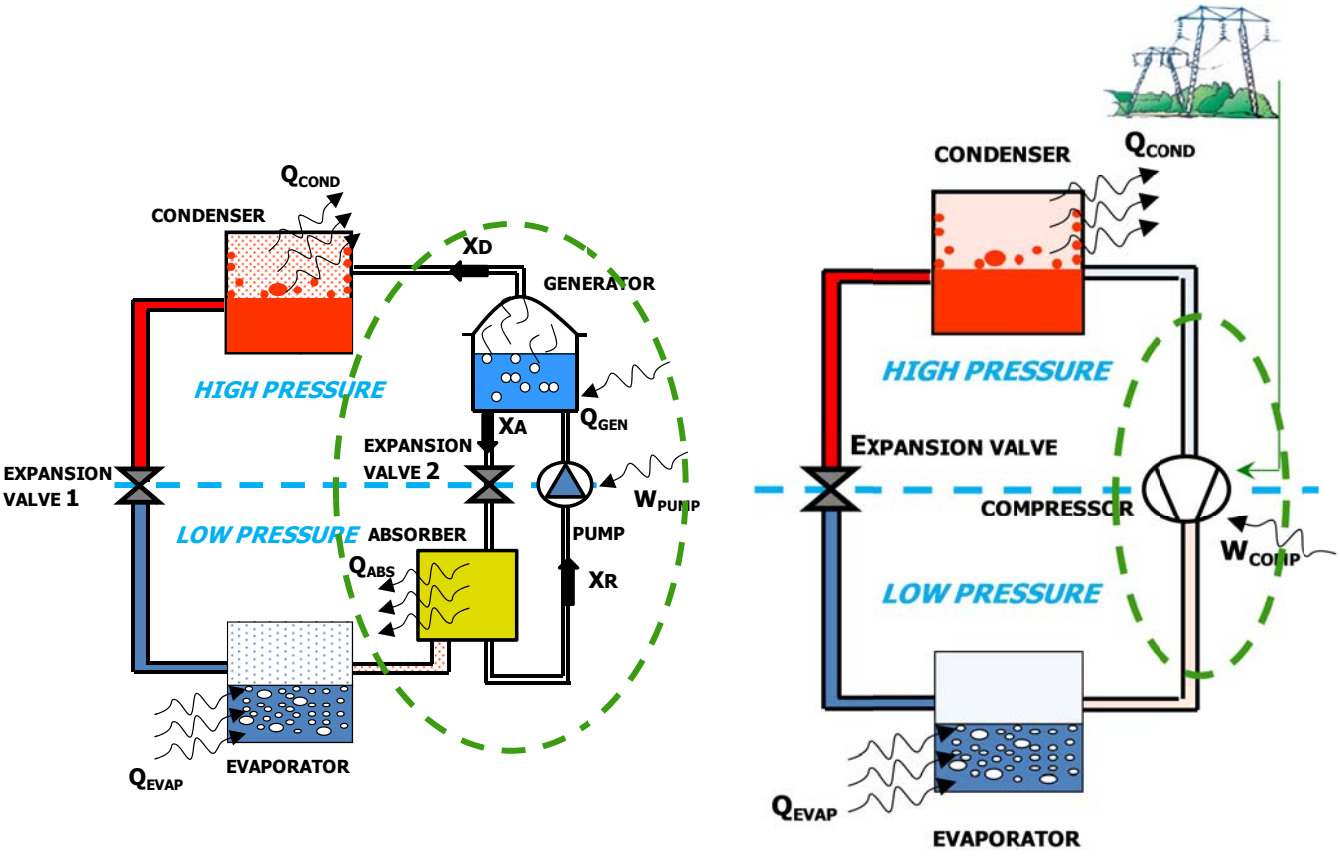

(a) Absorption cycle (b) Compression cycle

Figure 2.1. Schematics of the absorption and vapor compression refrigeration cycles.

Figure 2.1 (b) shows that the absorption refrigeration cycle is similar to the conventional vapor compression cycle. Both systems contain a condenser at the high-pressure side and an evaporator at the low pressure side. In the vapor compression cycle the compression is performed by a mechanical compressor; while in the absorption cycle compression is obtained by a sub-system consisting of a generator, an absorber, a solution pump and a throttling

device. This sub-system is often referred to as the thermal compressor, which characterizes the main feature of absorption refrigeration cycles. While in vapor compression refrigeration systems all the energy supplied to operate the cycle consists of mechanical energy, absorption refrigeration systems are mainly powered with thermal energy and only a small amount of mechanical energy (1-10% of the thermal energy depending on the operation conditions) is required to drive the solution pump. Although the pressure heads are in principle the same for the mechanical compressor and for the solution pump, the amount of mechanical energy needed for compression will differ to a large extent because pumping a liquid uses less energy than compressing a gas. The performance of absorption refrigeration systems is significantly dependent on the thermodynamic properties of the working fluid [5]. A basic requirement of the refrigerant/absorbent combination is that, in liquid phase, they must have a margin of miscibility within the operating temperature range of the cycle. The mixture refrigerant/absorbent should also be chemically stable, non-toxic, and non-explosive. Many working fluids are recommended in the literature. A survey on the working fluids for absorption cycles provided by Marcriss [6] suggested that, there are some 40 refrigerant compounds and 200 absorbent compounds available. However, the most commonly used working fluids are NH_3/H_2O and H_2O/LiBr. Since the invention of absorption systems, NH_3/H_2O fluid mixture has been usually used for both cooling and heating purposes. Both NH_3 (refrigerant) and H_2O (absorbent) are highly stable in a wide range of operating temperature and pressure. NH_3 has a high latent heat of vaporization, which is required for the efficient performance of the system. It can be used for low temperature applications, as the freezing point of NH_3 is -77°C. Since both NH_3 and H_2O are volatile, the absorption cycle requires a rectifier to strip away H_2O that normally evaporates with NH_3. Without a rectifier, H_2O would accumulate in the evaporator and offset the system performance. There are other disadvantages of NH_3 such as its high operating pressure, toxicity and corrosiveness.

However, NH_3/H_2O is environmentally friendly and low cost. The use of H_2O/LiBr (water being the refrigerant) in absorption refrigeration systems began around 1930 [7]. Two exceptional features of H_2O/LiBr are the non-volatility of the absorbent (LiBr) and an extremely high heat of vaporization of H_2O. However, using H_2O as a refrigerant limits the low temperature application to that above 0°C. H_2O/LiBris therefore usually used in chillers for air-conditioning purposes. The system must be operated under vacuum conditions. At high concentrations, the solution is prone to crystallization. It is also corrosive to some metals and expensive. The thermodynamic properties of H_2O/LiBr are well established in references [8-12]. Some chemical products may be added to H_2O/LiBr as a corrosion inhibitor [13-16] or to enhance heat and mass transfer processes [17-21]. The characteristics of the thermodynamic properties of the two conventional working fluids NH_3/H_2O and H_2O/LiBr are summarized in Table 2.1 [22].

Renz and Steimle [23] identified the suitable properties of the refrigerant, absorbent and refrigerant/absorbent combinations for absorption refrigeration systems. The search for a good refrigerant/absorbent combination has to consider all the items mentioned in Table 2.2.

Absorption refrigeration systems are generally classified as direct or indirect-fired, and as single, double or triple-effect. In direct-fired units, the heat source can be natural gas or some other fuel that is burned in the unit. In general, increasing the number of effects is intended to increase the COP using higher driving temperature levels [24]. Table 2.3 shows a list of the absorption refrigeration technologies available in the market with their available range of cooling capacity [25-26].

Table 2.1. Characteristics of the thermodynamic properties of NH_3/H_2O and $H_2O/LiBr$ [22].

Property	NH_3/H_2O	$H_2O/LiBr$
Refrigerant	NH_3	H_2O
High latent heat	good	excellent
Vapor pressure	too high	too low
Low freezing temperature	excellent	limited applications
Low viscosity	good	good
Absorbent	H_2O	LiBr
Low vapor pressure	poor	excellent
Low viscosity	good	good
Mixture		
No solid phase	excellent	limited applications
Low toxicity	poor	good
High affinity between refrigerant and absorbent	good	good

Table 2.2. Suitable properties for working fluids in absorption refrigeration systems [23].

Working fluid	Suitable properties	Reasons
Refrigerant	- High latent heat - Moderate pressure at condensing temperature - Relatively low freezing point - Low ozone depletion potential	- To reduce mass flow - To avoid thick walled equipment and piping - Limit on evaporator the temperature - Environmental hazards
Absorbent	- Negligible vapor pressure (low volatility) - Easily absorbs refrigerant (strong affinity for the refrigerant)	- No rectification requirement - Fundamental requirement for absorption
Solution	- Negative deviation from Raoult's law - Low specific heat - Working pressure should below or near to atmospheric pressure - Low specific volume - Work even at temperature below zero degree	- To reduce mass flow rate - To reduce exergy losses in solution heat exchanger duty - Reduce pump work(to minimize equipment weight and leakage) - Reduce pump work - For refrigeration purpose
All fluids	- High thermal conductivity - Low viscosity - Low surface tension - Low toxic, non flammable - Chemically stable, non-corrosive - Cost	- To improve heat transfer - To increase heat transfer coefficient, reduce pipe pressure losses and pump work - To improve absorber operation - Safety purposes - To increase system life - Low and available

Table 2.3. Absorption cooling machines available in the market [25-26].

Company	Country	Type	Working fluids	Cooling capacity [kW]
AGO	Germany	Single effect	NH_3/H_2O	30 - 1000
Broad	China	Single and double effect	H_2O/LiBr	150 - 23260
Carrier	U.S.A	Single and double effect	H_2O/LiBr	352 - 15977
Century Corporation	Corea	Single effect	H_2O/LiBr	350 - 5200
Climatewell	Sweden	Single effect With storage	H_2O/LiCl	10 - 20
Cooltec5	U.S.A	GAX	NH_3/H_2O	17.6 - 35
EAW Wergcall	Germany	Single effect	H_2O/LiBr	15 - 200
Ebara corporation	Japan	Single and double effect	H_2O/LiBr	158 - 2462
Entropie	France	Single Effect	H_2O/LiBr	300 - 6000
Hitachi	Japan	parallel double effect	H_2O/LiBr	106 - 19690
Kawasaki	Japan	Double and triple-effect	H_2O/LiBr	141 - 2462
LG	Corea	Single and double effect	H_2O/LiBr	352 - 5275
McQuay International	U.S.A	Single and double effect	H_2O/LiBr	350 - 5275
Pink	Austria	Single effect	NH_3/H_2O	12
Rinnai Osaka gas	Japan	Double effect	H_2O/LiBr	6.7
Robur	Italy	Single effect	NH_3/H_2O	12.8 - 17.7
Sanyo	China	Single and double effect	H_2O -LiBr	105 - 5274
Shuangliang	China	Single and double effect	H_2O/LiBr	211 - 11605
Solarice	Germany	Single effect	NH_3/H_2O	25 - 40
SolarNext	Germany	Single effect	H_2O/LiBr and NH_3/H_2O	18 - 50
Sonnenklima	Germany	Single effect	H_2O/LiBr	10
Thermax	India	Single and double effect	H_2O/LiBr	35 - 12000
Trane	USA	Single and double effect	H_2O/LiBr	390 - 5925
Yazaki	Japan	Single and double effect	H_2O/LiBr	17.6 - 703
York	U.S.A	Single and double effect	H_2O/LiBr	422 - 4840

2.3. Ammonia-water absorption refrigeration systems

The mixture refrigerant/absorbent NH_3/H_2O is widely used as a working fluid in absorption refrigeration systems investigated. Various investigations focused on the thermodynamic analysis and performance evaluation of NH_3/H_2O absorption refrigeration machines are available in the open literature. Raghuvanshi and Maheshwari [27] developed empirical relations for evaluating the characteristics and performance of a single stage NH_3/H_2O vapor absorption system. The heat and mass transfer equations and appropriate equations describing the thermodynamic properties of the working fluid at all thermodynamic states were evaluated. An energy analysis of each component has been carried out and numerical data of different streams of the cycle were tabulated. Finally the variations of various thermodynamic parameters were simulated and analyzed. They concluded that as the generator temperature, the condenser temperature, the absorber temperature increase the COP of the system decreases and as the effectiveness of the heat exchanger increases the COP of the system is also increased. Kong *et al.* [28] developed a mathematical model to analyze the performance of a single stage NH_3/H_2O absorption chiller equipped with a vertical sieve tray tower (VST) with complete condensation. The chiller was also experimentally tested with different heat input values between 4800 and 6400 W for a high pressure of 14 bar. The cooling capacity was found to be between 1900 and 2200 W with COP ranging from 0.32 to 0.36. The experimental results were found to lie between 75% and 85% of the calculated values. Ben Ezzine*et al.* [29] developed a thermodynamic simulation model of an NH_3/H_2O double effect, double-generator absorption chiller. The second law of thermodynamics was applied to quantify the irreversibility in each component of the chiller. Results indicated that the absorber, solution heat exchangers, and condenser have the greatest potential to improve the chiller's energy efficiency. Also they indicated that focusing on irreversibility is a more direct way of analyzing the potential for improving the efficiency of an NH_3/H_2O absorption chiller.

Ge *et al.* [30] presented the simulation of a low-temperature gas-fired NH_3/H_2O absorption chiller for refrigeration applications. The model was developed to investigate microturbine-based tri-generation systems for application in the food retail industry. The absorption chiller model was developed in the TRNSYS environment by integrating the main component models in the system and formed part of an overall TRNSYS-based supermarket model. The chiller model was validated against experimental results obtained on a 12 kW absorption chiller. The model was subsequently used to investigate the influence of important design and operating parameters on the performance of the chiller. Jawahar *et al.* [31] analyzed an NH_3/H_2O absorption cooling system using the pinch point analysis, to recover maximum internal heat from the streams, thereby increasing the system performance. The system was simulated for generator temperatures between 120°C and 150°C, sink temperatures between 25°C and 45°C and evaporator temperatures ranging from -10°C to 10°C. Based on the maximum internal heat that could be obtained using this approach the conventional cycle was modified without the need for rectification and its performance was compared. The COP of the proposed cycle was found to be 17 to 56% higher than that of a conventional cycle with respect to the operating conditions analyzed. Sozen and Ozalp [32] investigated an NH_3/H_2O absorption refrigeration system in which an ejector was integrated at the absorber entrance to improve the overall efficiency. The authors reported that the COP was improved by 49% and the circulation ratio was reduced by 57%. Abu-Ein *et al.* [33] presented a theoretical analysis of a solar powered NH_3/H_2O absorption refrigeration system. The effects of the operating temperatures and effectiveness of the solution and refrigerant heat exchangers on the component thermal loads and the coefficient of performance (COP) were investigated. A commercial NH_3/H_2O absorption refrigeration chiller manufactured by Robur was experimentally tested by Horuz and Callander [34]. The authors investigated the response of the chiller to variations of the chilled water flow rate, inlet temperature and level in the

evaporator drum at variable heat inputs by modifying the air-cooled components. A water-cooled absorber and a water-cooled condenser were incorporated into the system in order to test the experimental system under a wider range of condenser and absorber pressures. Darwish *et al.* [35] analyzed the Robur absorption refrigeration chiller using Aspen Plus flowsheet simulator, which has databases for the physical-chemical properties of chemical substances. The calculated values of various performance parameters were compared with the experimental and some manufacturers' data reported in the literature on the same unit. They concluded that there was a good agreement between the two sets of data and the use of Aspen Plus simulator in this kind of thermodynamic cycle analysis was valid. Priedeman *et al.*[36] tested a gas operated, 17.5 kW ammonia/water GAX system under steady state operation at 35°C ambient conditions. The COP of the system was found to be 0.68 at a full load condition. Simulation was also carried out, and the results of the experimentation were found to be in close proximity with the simulation results. Ng *et al.*[37] investigated a 7 kW gas fired NH_3/H_2O absorption chiller with a generator heat exchanger, an absorber heat exchanger and a regenerative GAX configuration. The COP of the system was about 0.8 at an operating condition of a generator temperature of 200°C, condenser temperature of 44°C, absorber temperature of 41°C and evaporator temperature of 5°C. The study revealed the significance of the process average temperature in the analysis of the chiller. Based on thermodynamic considerations, the authors derived a proper process average temperature for the non-isothermal processes occurring in the absorption chiller, and quantified the inaccuracies that derived from an incorrect process average temperature, in predicting chiller performance and in estimating optimal operating conditions. Zheng *et al.*[38] simulated a single stage ammonia absorption system and a GAX cycle, and reported that the COP and the exergy efficiency of the latter were 31% and 78% respectively higher than those of the former, at the heat source, cooling medium and cold temperatures of 120°C, 25°C and 5°C, respectively. Based on the

concept of exergy coupling, the absorption cycle was divided into the heat pump and heat engine sub-cycles. By means of the energy grade factor enthalpy diagram, a thermodynamic analysis was carried for both frameworks, which showed that the exergy demand of the heat pump sub-cycle in the GAX cycle was the same as that of a single stage cycle. A reduction in the external heat loss, external exergy loss and the internal exergy loss of the heat engine sub-cycle, reduced the energy consumption, and an increased benefit was obtained for the overall cycle. Mansouri *et al.* [39] developed and validated a steady-state simulation model of a commercial 3-ton NH_3/H_2O absorption chiller using the flow-sheeting software Aspen-Plus. The simulation results were found to be in good agreement with data from literature at a cooling air temperature of 35 ºC. The heat transfer characteristics (UA) of the various heat exchangers of the machine were then determined and the model was modified to make it accept these (UA) as input parameters. A comparison of the simulation predictions at cooling air temperatures of 26.7ºC and 38ºC with the bibliographical data showed a good concordance. The proposed model could be very useful for the analysis and performance prediction of the commercial absorption chiller investigated.

2.4. Non-conventional ammonia-based absorption refrigeration systems

Growing interest in absorption refrigeration systems has led to research on new ammonia-based working fluids. Several investigations have been carried out, to eliminate the rectifier and make simpler the structure of the absorption system; certain substitute working fluids have been studied to a greater extent. The most popular substitutions are the binary ammonia/salt solutions of $NH_3/LiNO_3$ and NH_3/NaSCN, which offer the advantages of high solubility in ammonia and no corrosion of steel [40]. In general, the refrigeration and heat pump cycles reached higher COP values using the $NH_3/LiNO_3$ fluid mixture. Wang *et al.* [41]

investigated an improved absorption refrigeration cycle using $NH_3/LiNO_3$ with staged absorption. The improved cycle used a series of absorbers among which one was cooled by the external medium and the others were cooled by refrigerant at staged pressures between the evaporation and condensation pressures. The results of this study demonstrated that the improved cycle was able to steadily run when driven by low-grade thermal sources as low as 65°C, and to produce deep refrigeration temperature as low as -40°C. In addition, the boiling point difference between the refrigerant and absorbent is sufficiently large that the generated NH_3 vapor is 100% pure, and the rectifier can be eliminated [42]. Davis *et al.* [43] tested a number of solutions with different concentrations in the temperature range of -14°C to 35°C to select good absorbents for ammonia. The substances were tested with positive results. Among the substances tested, $LiNO_3$ appears to offer the highest absorptive value. Chinnappa [44] theoretically and experimentally investigated an intermittent absorption refrigeration cycle employing NH_3/H_2O and $NH_3/LiNO_3$. A simplified approximate expression was presented for the theoreticalCOP of both working fluids. Best *et al.* [45-56]presented tables of flow ratios, the Carnot COP and the enthalpy-based COP under possible operating temperatures and concentrations for NH_3/H_2O, $NH_3/LiNO_3$ and NH_3/NaSCN absorption systems used for cooling and heating applications. Antonopoulos and Rogdakis [57] predicted the hourly performance of solar-driven $NH_3/LiNO_3$ and NH_3/NaSCN absorption systems in the Athens area. Sun [58] simulated the performance of single-stage absorption chillers using NH_3/H_2O, $NH_3/LiNO_3$ and NH_3/NaSCN as working fluids, indicating that $NH_3/LiNO_3$ and NH_3/NaSCN may be suitable alternatives to NH_3/H_2O and that the performance of NH_3/NaSCN is slightly better than that of $NH_3/LiNO_3$. Rivera and Rivera [59] presented the theoretical performance of an intermittent solar absorption refrigeration system operating with an $NH_3/LiNO_3$ mixture and concluded that the overall efficiency of the system was between 0.15 and 0.4 depending on the generation and condensation temperatures. Zhu and Gu [60]

conducted a second-law-based thermodynamic analysis of an NH_3/NaSCN absorption system. The COP andexergetic efficiency of the absorption system were calculated under different operating conditions. The results showed that the COP increased with the increase of the heat source temperature and decreased with the increase of the cooling water temperature, but the exergetic efficiency did not show the same trends. Rivera and Best [61] described the experimental results obtained regarding the heat transfer in forced convective boiling for NH_3/H_2O and $NH_3/LiNO_3$ mixtures flowing upward in a uniformly heated vertical tube. Venegas *et al.* [62] simulated an $NH_3/LiNO_3$ absorption system in two different applications, namely refrigeration and heat pump cycles, powered by low temperature heat sources, and compared its performance with the systems using H_2O/NH_3 and NH_3/NaSCN. Results showed that the $NH_3/LiNO_3$ absorption system achieved the highest COP in both refrigeration and heat pump applications. Moreno-Quintanar *et al.* [63] reported experimental data on the operation of a solar powered intermittent absorption refrigeration system with both $NH_3/LiNO_3$ and $NH_3/(LiNO_3+H_2O)$ for ice production. They concluded that the ternary fluid mixture produced a higher amount of ammonia during the desorption process at water concentrations of 20 % and 25 % in the absorbent. The authors also observed that at a water concentration of 10 % in the absorbent, there is no difference in the performance of both $NH_3/(LiNO_3+H_2O)$ and $NH_3/LiNO_3$ absorption systems. It was also concluded that with the $NH_3/(LiNO_3+H_2O)$ mixture the solar coefficients of performance were up to 24 % higher than those obtained with the $NH_3/LiNO_3$ mixture (varying from 0.066 to 0.093) and that the initial generation temperatures were up to 5.5ºC lower than those required for the $NH_3/LiNO_3$ mixture. The authors finally highlighted that no traces of water in the ammonia vapor were observed at any point during the experimental tests. Ventas *et al.* [64] numerically evaluated the performance of an $NH_3/LiNO_3$ absorption chiller with an integrated low-pressure compression booster between the evaporator and the absorber. Their results showed that this

configuration allowed to reduce the activation temperature keeping the COP at the same value of that could be achieved with the conventional configuration at a higher activation temperature.

Bourouis *et al.* [65] obtained the first patent for a water-cooled or air-cooled single stage absorption chiller using $NH_3/LiNO_3$ for solar cooling applications. These absorption chillers have as a main characteristic the use of brazed plate heat exchangers in all thermal components. Zamora *et al.* [66] presented an experimental characterization of two pre-industrial prototypes of the $NH_3/LiNO_3$ absorption chiller patented by Bourouis *et al.* [65], a water-cooled one and an air-cooled one. The nominal cooling capacity of the air-cooled prototype was 9.3 kW at 15°C, 35°C and 90°C of chilled water, ambient air and hot water temperatures, respectively. The nominal cooling capacity of the water-cooled prototype was 12.9 kW at 15°C, 35°C and 90°C of chilled water, cooling water and hot water temperatures, respectively. The results also showed that at an ambient air temperature of 41°C the air-cooled prototype was still able to provide 64% of its nominal capacity at 35°C. Zamora *et al.* [67] also reported on the experimental characterization at part-load operation mode of the water-cooled pre-industrial prototype. The results showed that the degradation coefficient was 0.7985, which matches the value obtained by dividing the remaining electrical consumption generated during the OFF half cycles by the total energy consumption. The authors reported that at part-load operation mode it is much more convenient to use an ON-OFF control to achieve a higher electrical coefficient of performance than to modify the hot water temperature. Táboas *et al.* [68] reported the performance of ammonia/water and ammonia/salt mixture absorption cycles for refrigeration purposes in fishing ships. The result showed that the evaporation temperature of $NH_3/LiNO_3$ system could reach -18.3°C with COP about 0.3 when the system is driven by waste heat energy from jacket water in diesel engines. They concluded also that the coefficients of performance of ammonia/salts systems are higher than

those of ammonia/water systems under the same operation conditions. Amaris *et al.* [69] presented an experimental investigation on the ammonia absorption process in tubular bubble absorbers using $NH_3/LiNO_3$ as a working pair at operating conditions of interest for absorption chillers. They showed that the absorption rate achieved with the micro-finned tube is up to 1.7 times higher than with the smooth tube at a solution mass flow rate of 40 kg h^{-1}. They concluded also that absorption mass flux increases when tube diameter is reduced and decreases when tube length is increased. Also, Amaris *et al.* [70] presented an experimental investigation to quantify the individual and simultaneous effects of two passive techniques, namely CNTs (carbon nanotubes) and advanced surfaces, on the performance of an $NH_3/LiNO_3$ tubular bubble absorber. Results showed that the maximum absorption mass flux achieved with the CNT binary nanofluid and the smooth tube is up to 1.64 and 1.48 times higher than reference values at cooling-water temperatures of 40 and 35°C, respectively. They found also that simultaneous use of CNT nanoparticles and advanced surfaces resulted in a more pronounced increase in the absorption mass flux and solution heat transfer coefficient with respect to the smooth tube absorber with $NH_3/LiNO_3$ as a working pair. Oronel *et al.* [71] presented an experimental study of bubble absorption in a plate heat exchanger using binary and ternary mixtures, ammonia/lithium nitrate and ammonia/(lithium nitrate + water), at operating conditions of air-cooled absorption systems driven by low temperature heat sources. They concluded that the mass absorption flux, heat transfer coefficient, subcooling and mass transfer coefficient increased as the solution flow rate was increased for both working pairs. The mass absorption flux achieved with the binary mixture was enhanced as the cooling-water inlet temperature was decreased and the mass absorption flux and the solution heat transfer coefficient achieved with the ternary mixture were around 1.3-1.6 and 1.4 times higher, respectively, than those of the binary mixture under similar operating conditions.

2.5. Diffusion-absorption refrigeration machines

Diffusion-absorption refrigeration (DAR) systems are widely used in supermarkets, domestic freezers, and hotel rooms, etc. This technique for producing cold was patented in 1928 by the two Swedish engineers Van Platen and Munters [72] (Figure 2. 2). The unique feature of the DAR cycle, as compared to a conventional ammonia/water absorption cycle, is that it operates at a uniform pressure. The working fluid is a mixture of three components: ammonia as a refrigerant, water as an absorbent, and an auxiliary inert gas, frequently hydrogen or helium. The inert gas is necessary to reduce the partial pressure of the refrigerant in the evaporator, and allow for it to evaporate at low temperatures and for the production of useful cold. DAR systems are silent because they have no moving parts.

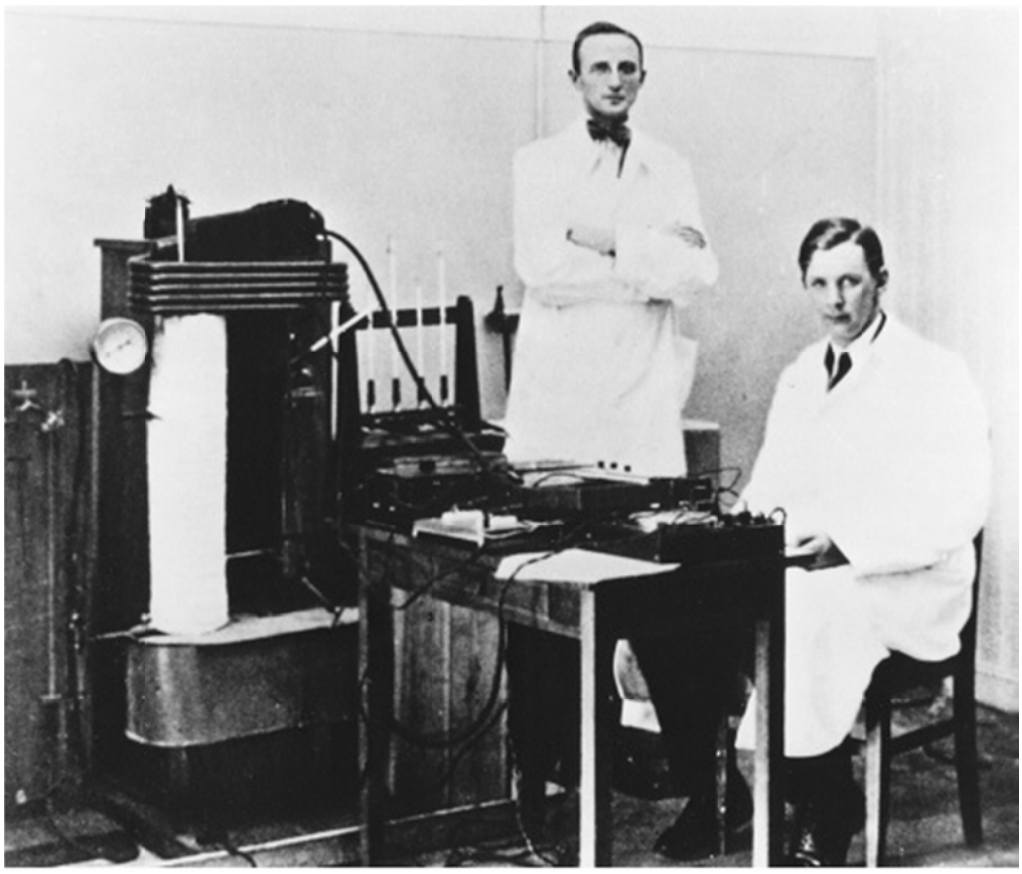

Figure 2.2.Van Platen and Munters and their refrigerating machine [72].

Over the years, investigations have been published on the performance of various configurations of DAR cycles using graphical, numerical and experimental approaches.

Kouremenos *et al*. [73] investigated the use of helium as an alternative to hydrogen. The authors observed a similar behavior of both inert gases. Zohar *et al.* [74] developed a thermodynamic model for an Electrolux DAR system and analyzed its performance with both inert gases and found that the COP of the system operating with helium was 40% higher than that of the system operating with hydrogen. They further reported that higher COP values were obtained for an ammonia mass fraction of 30% in the rich solution and 10% in the weak solution. Zohar *et al.* [75] compared the configurations of a DAR cycle both with and without condensate sub-cooling prior to the evaporator entrance. They showed that in the DAR cycle without sub-cooling there was a 14-20% higher COP than in the DAR cycle with condensate sub-cooling. Zohar *et al.* [76] examined numerically the performance of a DAR system operating with the organic absorbent DMAC which was associated to five different refrigerants and with helium as an inert gas. They compared the performance of their systems with that of the system operating with ammonia-water and helium and found out that that the latter had the highest COP values. Ben Ezzine *et al*. [77] investigated the feasibility of a DAR system operating with the working fluid system DMAC-*R*124-He and coupled to a solar collector. They reported that both the COP and the temperature of the cooling effect depended largely on the effectiveness of the absorber and the generator temperature. For solar cooling applications, this working fluid mixture could be an alternative to the conventional ammonia-water-hydrogen mixture. Starace and De Pascalis [78] developed an enhanced thermodynamic model to consider the more realistic operating conditions of the DAR cycle, such as the presence of some water (absorbent) in the refrigerant stream (ammonia). They used a magnetron activated thermal pump in order to reduce the start-up time of the refrigerator. The model's predictions were validated on a prototype built by coupling a domestic magnetron to a small purposely modified commercial DAR. A maximum deviation was noticed to be roughly 2% in the weak solution mass flow rate and lower than 5% in the COP between the

predicted and measured data. Sayadi *et al*. [79] presented a HYSYS simulation model for a water-cooled DAR system using different binary mixtures of light hydrocarbons (C_3/*n*-C_6, C_3/cyclo-C_6, C_3/cyclo-C_5, propylene/cyclo-C_5, propylene/*i*-C_4 and propylene/*i*-C_5) as working fluids and helium as an inert gas. The driving heat in the generator was supposed to be supplied by evacuated tube solar collectors. The most appropriate binary mixture was found to be C_3/*n*-C_6 with a generation temperature of 126°C. Long *et al.* [80] investigated numerically the possibility of using TFE-TEGDME in the DAR system together with two cooling mediums, namely water at 32ºC and ambient air at 35ºC. The authors performed a parametric analysis on the effects of the cooling medium, the generation and evaporation temperatures and the effectiveness of the absorber on the system performance. They compared the performance of the TFE-TEGDME and NH_3-H_2O DAR systems in terms of COP and circulation ratio. They concluded that the TFE-TEGDME mixture is a good working fluid for DAR systems and found that with an absorber effectiveness of 0.8, the optimum generation temperature for the air-cooled TFE–TEGDME DAR system is around 170°C. A coefficient of performance (COP) up to 0.45 was obtained. However, the performance of the water-cooled system was better with a lower generation temperature of 130°C and a higher COP of 0.56. Rodriguez-Munoz and Belman-Flores [81] presented a review on diffusion-absorption refrigeration technology in which over 70 publications were analyzed. The authors concluded that diffusion-absorption technology represents an interesting and feasible alternative for small capacity refrigeration applications. Rattner and Garimella [82] proposed a fully passive DAR system operating with the working fluid mixture NH_3-NaSCN-He. Detailed design models for the various components of the system were elaborated. They reported *COP*s in the range of 0.11-0.26 at an ambient air temperature of 24ºC, low heat source temperatures of 110-130°C and passive air cooling. These authors reported [83] on the development of a prototype of the theoretically investigated machine,

activated by low temperature heat sources (110 - 130°C) and passively air-cooled. The cooling temperatures achieved were suitable for refrigeration (T_{evap}= 6 → 3°C, COP ~ 0.06) and air-conditioning (12 → 8°C, COP ~ 0.14; 18 → 14°C, COP ~ 0.17). Chen *et al.* [84] improved the coefficient of performance of the DAR system by 50%. They modified the design and construction of the generator by integrating a tube in tube solution heat exchanger into the generator. Vicatos [85] studied experimentally a modified domestic DAR in order to reduce the response time of the system. Koyfman *et al.* [86] presented an experimental investigation on the bubble pump performance in a DAR system. They used a solution of an organic solvent and HCFC as refrigerant. Their results showed that the performance of the bubble pump depends mostly on the motive head and the heat input to the bubble pump. Jacob *et al.*[87] conducted a theoretical and experimental study on a solar driven ammonia/water diffusion absorption cooling machine (DACM). They designed four prototypes for air-conditioning applications: water chillers with an evaporator temperature in the range of 6-12°C and ceiling cooling with an evaporator temperature of 15-18°C. The COP values achieved ranged from 0.10 to 0.45. Yıldız and Ersöz [88] designed a DAR system driven by electricity. They investigated numerically and experimentally the energy and exergy losses for each component of the system and compared the theoretical and experimental values. They concluded that the highest exergy losses took place in the solution heat exchanger. The experimental and predicted $COP$was around 0.19 and the exergy efficiency between 0.03 and 0.04. Mazouz *et al.* [89] carried out an experimental study of a commercial DAR machine using hydrogen as inert gas, in order to determine its performance parameters under various operating conditions. Steady state and dynamic methods were applied to evaluate the characteristics of the machine. The best performance of the machine was obtained with a heat supply of 42W, corresponding to a COP value of 0.12.

Chapter 3

Choice of the thermodynamic model to predict the properties of the ammonia based working fluids in Aspen-Plus

3.1. Introduction

The selection of a proper method for estimating the thermodynamic properties of the working fluid is one of the most important steps that can affect the simulation of absorption refrigeration cycles. Therefore, it is important to choose carefully an appropriate method to estimate the different properties of the working fluid. Aspen-Plus [90] includes a large databank of thermodynamic property and transport models with the corresponding mixing rules for estimating mixture properties. Before performing simulations in Aspen-Plus, it is important to ensure that the selected property method is the best reliable thermodynamic model. In fact there is scarce information in the open literature on how to choose an appropriate thermodynamic property model for the NH_3/H_2O mixture to simulate absorption refrigeration cycles in Aspen-Plus. In this chapter, the choice of the NH_3/H_2O mixture property model for use in the simulation of absorption refrigeration cycles is investigated in detail. To this purpose the predictions of the nine property models available in Aspen-Plus for this mixture are evaluated and compared with regressed experimental vapor-liquid equilibrium (VLE) data reported by Mejbri and Bellagi [91] in the pressure range from 2 to 25 bar and the temperature range -19 to 220ºC. In a second step, the Aspen-Plus Data Regression

System facility is used to fit the interaction parameters of the property models to the VLE data of reference [91]. The results are presented in the form of *T-x-y* diagrams.

3.2. Vapor-Liquid equilibrium

Consider a mixture of N fluid constituents at the temperature T and pressure P, divided between a liquid and a vapor phase. The conditionof thermodynamic equilibrium of this biphasic system is given by the equality of the chemical potentialsμ_i of each constituent $i$in both phases

$$\mu_i^v = \mu_i^l \quad (i = 1, N) \qquad (3.1)$$

or, equivalently, the equality of the fugacity

$$f_i^v = f_i^l \quad (i = 1, N) \qquad (3.2)$$

The fugacity f_i is defined as the effective partial pressure exerted by a constituent i of a mixture, and is related to the chemical potential by:

$$\mu_i - \mu_i^0 = RT \ln\left(\frac{f_i}{Z_i P}\right) \qquad (3.3)$$

The coefficients of fugacity, φ_i , is defined by:

$$\varphi_i = \frac{f_i}{Z_i P} \qquad (3.4)$$

With Z_i is the compressibility factor of constituent i

$$Z_i = \frac{PV}{RT} \qquad (3.5)$$

The calculation of the vapor liquid equilibrium, that is to say the determination of 2 N compositions of the vapor phase (y_i, $i = 1, N$) and the liquid phase (x_i, $i = 1, N$), leads to the resolution of the system (3.2) of N-equations associated with N balances of the species.

A fundamental problem then arises, that of linking fugacity and composition.

To resolve this issue, fugacity is defined for each φ_i species from the gas phase such as

$$f_i^v = \varphi_i y_i P \qquad \text{with} \qquad \lim_{P\to 0}\varphi_i = 1 \quad \forall_i \qquad (3.6)$$

This equation shows that the φ_i^v can be considered as a correction of the partial pressure ($y_i P$) of i. It is calculated either using the relation [92]:

$$\ln \varphi_i = -\frac{1}{RT}\int_\infty^V \left[\left(\frac{\partial P}{\partial n_i}\right)_{T,V,n_{i\neq j}} - \frac{RT}{V}\right] dV - \ln Z \qquad (3.7)$$

if one has an explicit equation of state in pressure $P = P\ (V, T, n_k)$.

or if the equation of state is explicit in volume $V = V\ (P, T, n_k)$, by the relation:

$$\ln \varphi_i = -\frac{1}{RT}\int_P^0 \left[\left(\frac{\partial V}{\partial n_i}\right)_{T,P,n_{i\neq j}} - \frac{RT}{P}\right] dP \qquad (3.8)$$

In the liquid phase an activity coefficient γ_i is defined to link the molar fraction of component i to its fugacity

$$f_i^l = \gamma_i x_i f_i^0 \qquad (i = 1, N) \qquad (3.9)$$

f_i^0 being the reference or standard fugacity. This is the fugacity of constituent i at the temperature, the pressure and reference composition of the considered system.

For a mixture of components that might exist in liquid and vapor in conditions contemplated of T and P, f_i^0 is the fugacity of pure liquid i ($x_i = 1$) at temperature T and total pressure P of the system, in which case:

$$f_i^0 = f_i^l\ (P, T, x_i = 1) = P_i^{sat}(T)\ \varphi_i^{sat}(T) \exp\left[\int_{P_i^{sat}}^P \frac{V_i^l(P,T)}{RT}\, dP\right] = (P_i\varphi_i)_{\text{sat}} F_i \qquad (3.10)$$

$P_i^{sat}(T)$ designating the pressure of the saturated vapor of constituent i at the system temperature, $\varphi_i^{sat}(T)$, fugacity coefficient of the saturated vapor-calculated using the relation (3.7) or (3.8), V_i^l, the molar volume of pure liquidof constituent i and F_i , the Poynting factor:

$$F_i = \exp\left[\int_{P_i^{sat}}^{P} \frac{V_i^l(P,T)}{RT}\, dP\right] \qquad (3.11)$$

The activity coefficient of constituent i, γ_i, for its part is deducted from the free molar excess liquid mixing enthalpy:

$$\bar{G}^{ex} = RT \sum_{i=1}^{N} x_i \ln \gamma_i \qquad (3.12)$$

using the relation

$$RT \ln \gamma_i = \left(\frac{\partial[n\bar{G}^{ex}]}{\partial n_i}\right)_{T,P,n_{i\neq j}} \qquad (3.13)$$

With n is the total number of moles in the particular liquid phase.

To do this, a model of $\bar{G}^{ex}$ is necessary. In practice, two methods are used to calculate the vapor-liquid equilibrium:

- The method $(\varphi - \varphi)$ also known as symmetric method the same equation of state is used to describe the behavior of both phases. In this case the equilibrium condition (3.2) becomes:

  $$\varphi_i^l x_i P = \varphi_i^v y_i P \qquad (3.14)$$

  or

  $$\varphi_i^l x_i = \varphi_i^v y_i \qquad (3.15)$$

  In this approach, the fugacity coefficients φ_i^l and φ_i^v are calculated using one or the other of equations (3.7) or (3.8).

- The method $(\gamma - \varphi)$ also known as asymmetric method. Two different routes are followed to describe the liquid state (activity coefficients) and the gas state (fugacity coefficient). The equilibrium is then given by the relation

  $$\gamma_i x_i f_i^0 = \varphi_i^v y_i P \qquad (3.16)$$

Equilibrium coefficient

In complex mixtures an equilibrium coefficient is defined for each component as:

$$K_i = \frac{y_i}{x_i} \qquad (3.17)$$

When the symmetric method ($\varphi - \varphi$) is used, equation (3.17) becomes:

$$K_i = \frac{\varphi_i^l}{\varphi_i^v} \qquad (3.18)$$

while for asymmetric method ($\gamma - \varphi$)

$$K_i = \frac{\gamma_i^l f_i^0}{\varphi_i^v} \qquad (3.19)$$

3.3. Thermodynamic property models

Ammonia/water mixtures have been used as a working pair in absorption refrigeration systems for several decades. Different equations are available in the literature [93-105] to calculate its thermodynamic properties: Virial equations of state, cubic equations of state, polynomial functions, Helmholtz free energy, Perturbation theory and Gibbs excess energy.

Schulz [94] presented a fundamental equation of state for this binary mixture. Ziegler and Trepp [95] modified the Schulz's equation of state and developed new correlations for predicting the equilibrium properties required in the analysis of absorption refrigeration cycles. The authors used the Gibbs excess energy equation to determine specific volume, specific entropy and specific enthalpy. The thermodynamic properties can be predicted with the new correlation up to a pressure of 50 bars and a temperature of 500 K. Renon *et al.* [96] derived an equation of state which can accurately estimate the properties of NH_3/H_2O mixtures. An extended Redlich-Kwong equation of state with two adjustable parameters was used to predict the VLE (vapor-liquid equilibrium) of the working fluid. Ruiter [97] presented a simplified thermodynamic model for the NH_3/H_2O mixture. The equilibrium pressure and the excess enthalpy of the gas and liquid phases were described using 11 coefficients.

Pátekand Klomfar [98] presented five equations to predict VLE properties. The use of these equations avoids iterative procedures when calculating thermodynamic properties of the NH_3/H_2O mixture. The equations were developed by fitting critically assessed experimental data using simple functional forms. The results were presented in form of an enthalpy-concentration diagram. Barhoumi *et al*. [99] reported a detailed work on the reformulation of the thermodynamic properties of the NH_3/H_2O mixture using the Gibbs energy function. For the liquid phase, a three constant Margules model of the excess free enthalpy was formulated. The vapor phase was considered a perfect mixture of real gases, each pure gas being described by a virial equation of state in pressure truncated after the third term. The model developed predicts the thermodynamic properties of the mixture with great accuracy in the three states, i.e. subcooled liquid, superheated vapor and liquid-vapor saturation in the temperature range of 200 to 500 K and a pressure up to 100 bars. Mejbri and Bellagi [91] modeled the thermodynamic properties of the NH_3/H_2O mixture using three different approaches: An empirical Gibbs free enthalpy model, the Patel-Teja cubic equation of state and the PC-SAFT (Perturbed Chain Statistical Associating Fluid Theory) equation of state. A comparison of these three methods proved the superiority of the PC-SAFT equation of state to predict and extrapolate the thermodynamic properties of the ammonia/water fluid mixture over a larger range of temperature ($273.16 \leq T \leq 613.15$ K) and pressure ($0 < P \leq 210$ bar). Also, the authors recommended the use of the Gibbs free enthalpy model for industrial applications that use NH_3/H_2O as a working fluid at moderate temperatures and pressures, such as absorption refrigeration.

3.4. Selection of the appropriate thermodynamic property model

The nine property models implemented in Aspen-Plus and considered for the calculation of the properties of the NH_3/H_2O mixture are listed in Table 3.1. This list includes cubic EOS methods (SRK, PR-WS and PR-MHV2, PENG-ROB, PR-BM, RKS-BM) as well as activity coefficient methods (ENRTL-RK, NRTL-HOC, WILS-RK). The tests of these models are performed in two steps. In the first one, *T-x-y* VLE predictions of each one of the Aspen-Plus property models are compared with the regressed data reported in [91] for 6 isobars, namely 2, 4, 10, 16, 20 and 25 bars.

Figures 3.1, 3.2 and 3.3 illustrate this comparison at 2, 10 and 25 bar, respectively. It is observed that the maximum equilibrium temperature deviation predicted by the considered nine property models implemented in Aspen-Plus and the data reported by Mejbri and Bellagi [91] is about 10ºC. As regards the ammonia mass fraction in the liquid phase, the values predicted by the property models SRK, PR-WS and PR-MHV2 are inconsistent in the whole pressure range. This is the case also of the three activity coefficient models (ENRTL-RK, NRTL-HOC, WILS-RK) at 10 and 25 bars, for which the deviations increase with increasing pressure. It is concluded that none of these property models reproduces the ammonia/water vapor-liquid equilibrium data with sufficient accuracy.

Table 3.1. Aspen-Plus thermodynamic property models tested.

Aspen-Plus property model	**Model name**
ENRTL-RK	Electrolyte NRTL/Redlich-Kwong
RKS-BM	Redlich-Kwong-Soave-Boston-Mathias
PENG-ROB	Standard Peng-Robinson
PR-MHV2	Huron-Vidal-Modified Peng-Robinson
PR-WS	Peng-Robinson-Wong-Sandler
NRTL-HOC	Non-Random-Two-Liquid/Hayden-O'Connell
SRK	Soave-Redlich-Kwong
WILS-RK	Wilson/Redlich-Kwong
PR-BM	Peng-Robinson-Boston-Mathias

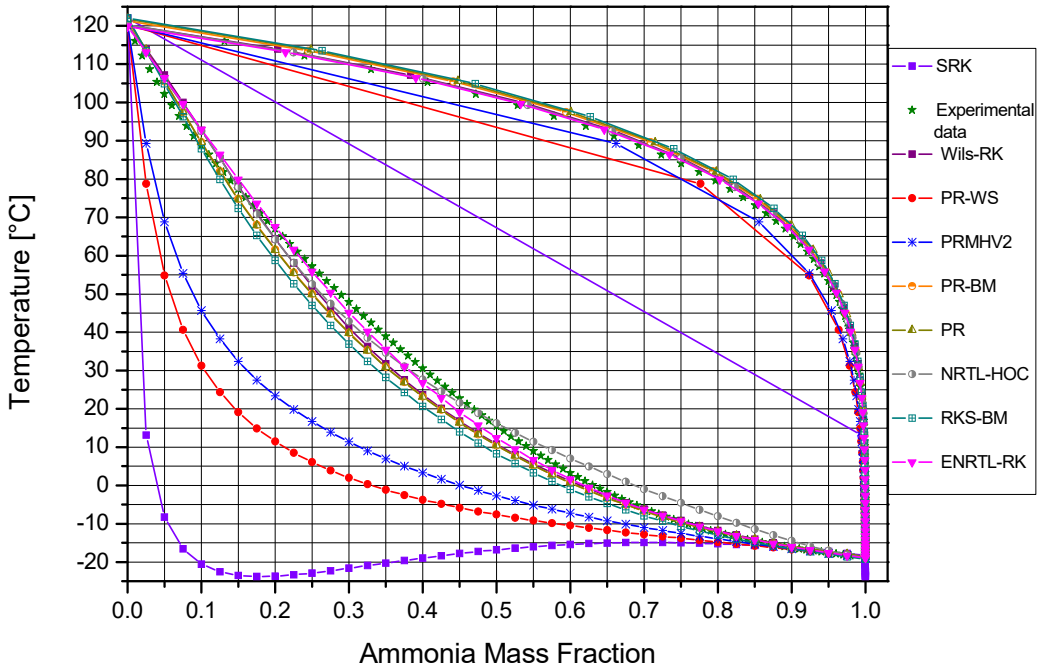

Figure 3.1. *T-x-y* VLE diagram at $P = 2$ bar for ammonia/water mixture (predicted by models with default interaction parameters).

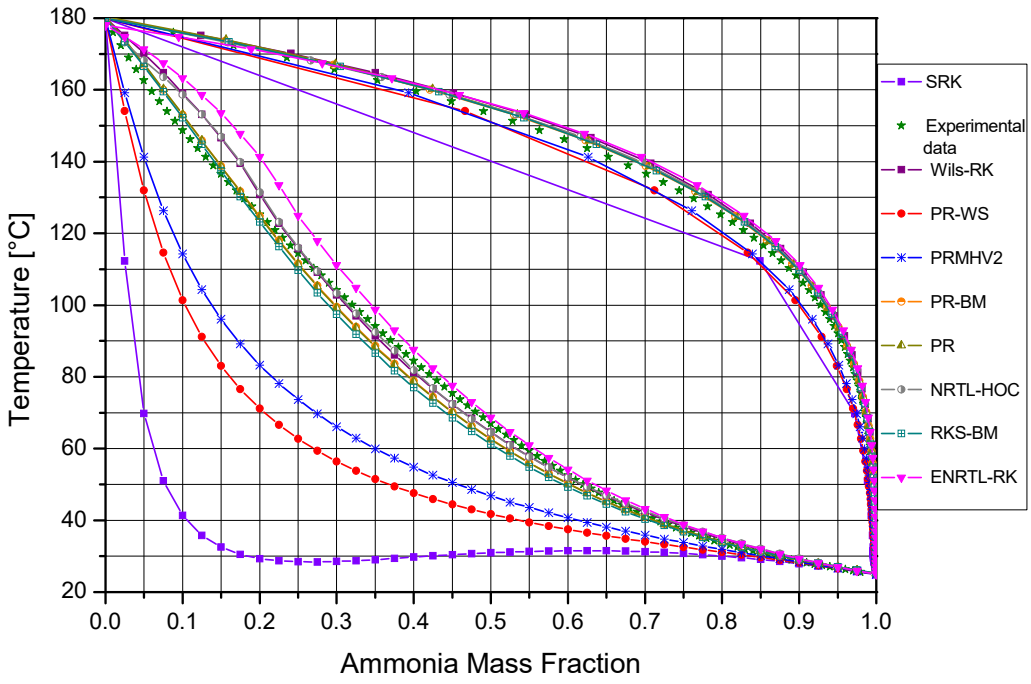

Figure 3.2. *T-x-y* VLE diagram at P = 10 bar for ammonia/water mixture (predicted by models with default interaction parameters).

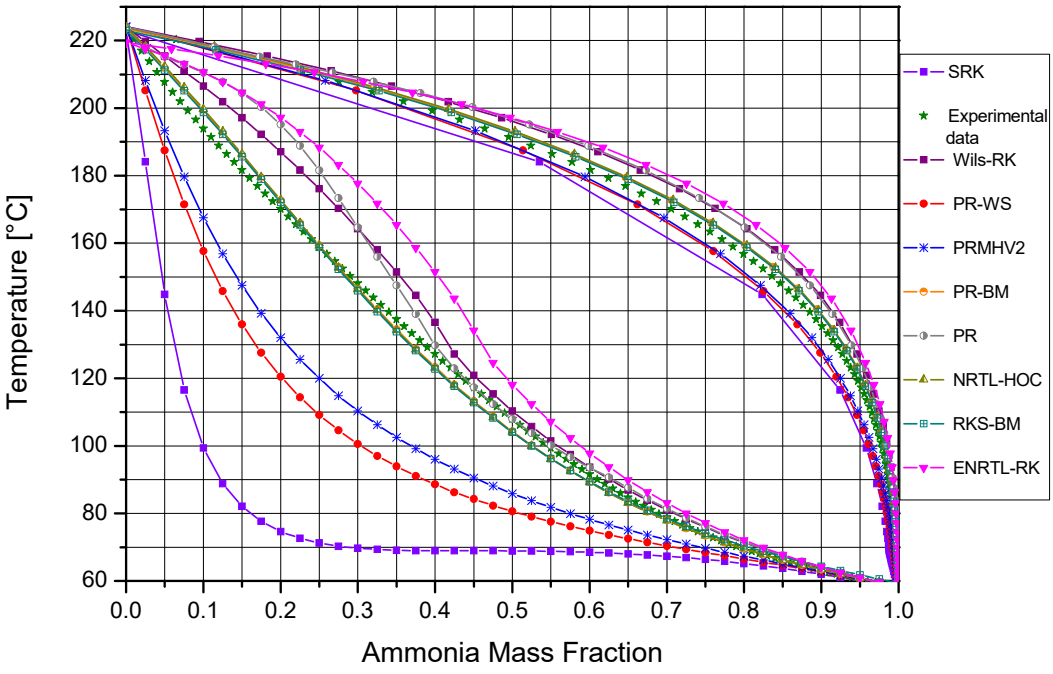

Figure 3.3. *T-x-y* VLE diagram at P = 25 bar for ammonia/water mixture (predicted by models with default interaction parameters).

In a second step, the data regression system of Aspen-Plus is used to fit the parameters of the property models by using the VLE data reported by Mejbri and Bellagi [91]. For cubic equations of state it is the interaction parameter k_{ij} —or its coefficients $k_{ij}^{(1)}, k_{ij}^{(2)}, k_{ij}^{(3)}$ if it is supposed temperature dependent that are fitted to the VLE data. Figures 3.4, 3.5 and 3.6 show the corresponding comparison at 2, 10 and 25 bar, respectively. As can be noted, all values of the ammonia mass fraction in the vapor phase predicted by the Aspen-Plus property models are now close to the data reported by Mejbri and Bellagi [91]. Regarding the ammonia mass fraction in the liquid phase, the PR-MHV2 model made the poorest predictions. These figures make also clear that the PR-BM model (Peng-Robinson eos with Boston-Mathias alpha function) is in better agreement with the considered vapor-liquid equilibrium data. The sum of squared errors for the nine Aspen-Plus property models tested and summarized in Table 3.2 confirms this conclusion. The calculation is based on the mean square error (EQM). It's a measure of the average deviation.

$$\text{EQM} = \sqrt{\frac{1}{N}\sum_{i=1}^{N}(F_i - Q_i)^2} \qquad (3.20)$$

With

$F_i$means the calculated value of the parameter in question,

Q_i, the observed value,

N, the number of check points.

This table shows also that with the help of data regression eight of the nine property models have been successfully fitted to make them predict VLE close to the experimental data. Just one property model fails to accommodate well the data: PR-MHV2. Based on these results, it is confirmed that the Peng-Robinson-Boston-Mathias equation of state (PR-BM), with fitted parameters, is the most appropriate property method among those implemented in Aspen-Plus

for the prediction of the ammonia/water vapor-liquid equilibrium in the investigated temperature and pressure ranges. Table 3.3 gives the default and regressed values of the parameters $k_{ij}^{(1)}, k_{ij}^{(2)}$ and $, k_{ij}^{(3)}$ for the considered cubic equation of state.

Peng-Robinson equation of state write:

$$P = \frac{R\,T}{(\bar{V}-b)} - \frac{a}{\bar{V}(\bar{V}+b)+b(\bar{V}-b)} \qquad (3.21)$$

Where P is the pressure, $\bar{V}$, the mixture molar volume, b, the mixture co-volume, a, the attraction term factor, and R the universal gas constant. The mixture a and b are deduced from the individual component constants a_i and b_i using the mixing rules

$$b = \sum x_i\, b_i \qquad (3.22)$$

$$a = \sum_{\boldsymbol{i}} \sum_{\boldsymbol{j}} x_i x_j \sqrt{a_i a_j}\left(1 - k_{ij}\right) \qquad (3.23)$$

In these equations x_i is the mole fraction of component i in the mixture and $k_{ij}$the binary interaction parameter of components $i$and j. Usually it is supposed that:

$$k_{ij} = k_{ji} \qquad (3.24)$$

It is this parameter that is deduced from VLE data by a regression procedure. To make the equation more flexible k_{ij} is often written as function of the temperature:

$$k_{ij} = k_{ij}^{(1)} + k_{ij}^{(2)}\,T + \frac{k_{ij}^{(3)}}{T} \qquad (3.25)$$

So that three parameters are fitted to the VLE data: $k_{ij}^{(1)}, k_{ij}^{(2)}andk_{ij}^{(3)}$.

The individual constants a_i and b_i are determined from the critical temperature and pressure of the compound, $T_{ci}$and P_{ci}, respectively:

$$a_i = \alpha_i(T)\left[0.45724\frac{R^2T_{ci}^2}{P_{ci}}\right] \quad (3.26)$$

$$b_i = 0.07780\frac{RT_{ci}}{P_{ci}} \quad (3.27)$$

In the $\alpha_i(T)$ function,

$$\alpha_i(T) = \left[1 + m_i\left(1 - \sqrt{T_r}\right)\right]^2 \quad (3.28)$$

T_r is the reduced temperature, $\frac{T}{T_{ci}}$, and m_i, a component specific parameter depending on the acentric factor ω_i,

$$m_i = 0.37464 + 1.54226\,\omega_i - 0.26992\,\omega_i^2 \quad (3.29)$$

$\alpha_i(T) = 1$ at the critical temperature.

The Boston-Mathias modification of the Peng-Robinson equation of state is as follow:

$$\alpha_i(T) = \left[\exp\left[c_i\left(1 - T_{ri}^{d_i}\right)\right]\right]^2 \quad (3.30)$$

with

$$d_i = 1 + \frac{m_i}{2} \;;\; c_i = 1 - \frac{1}{d_i} \quad (3.31)$$

It's intended to extend the validity of the equation of state for temperatures larger than the critical. In fact, this is necessary for the water/ammonia mixture considered as working fluid in the absorption chiller because temperatures between 180 and 200°C are needed in the generator to desorb the refrigerant. This temperature range is beyond the critical temperature of ammonia (405.5 K corresponding to 132.4°C).

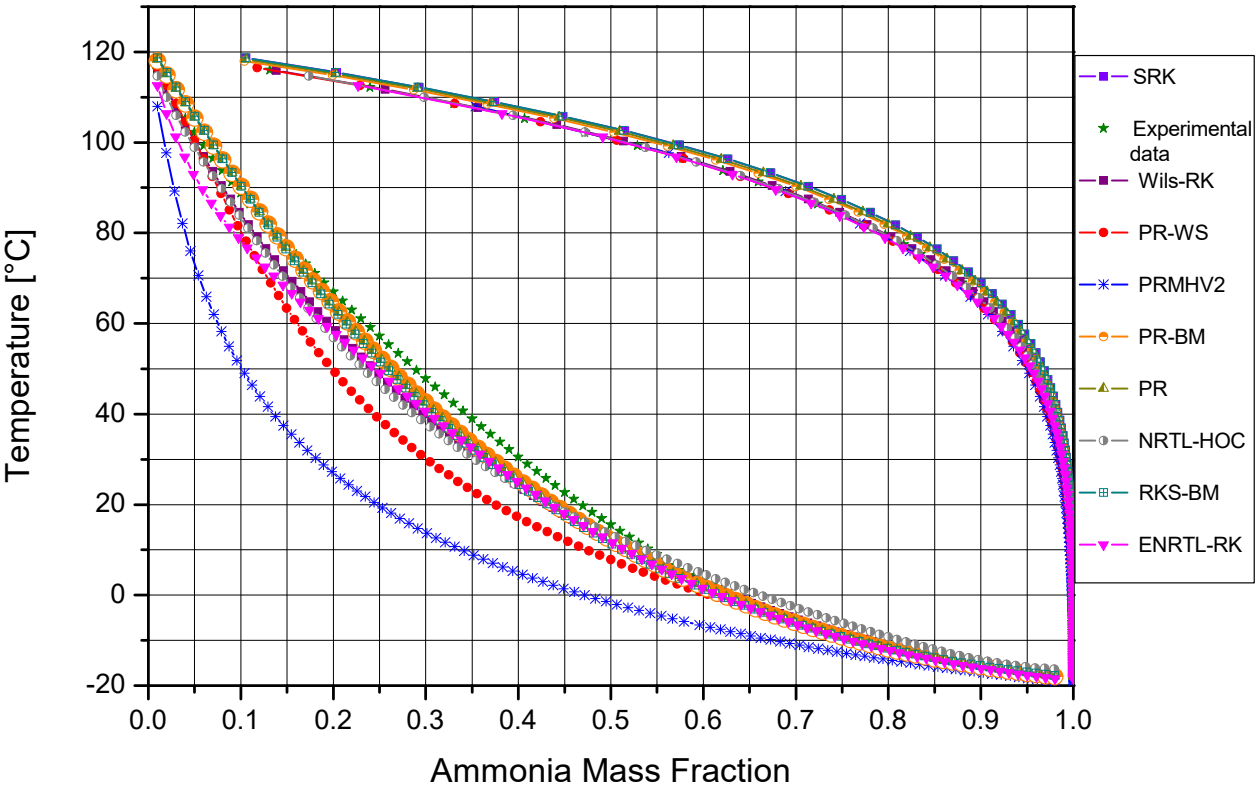

Figure 3.4. *T-x-y* VLE diagram at $P = 2$ bar for ammonia/water mixture (predicted by models with regressed interaction parameters).

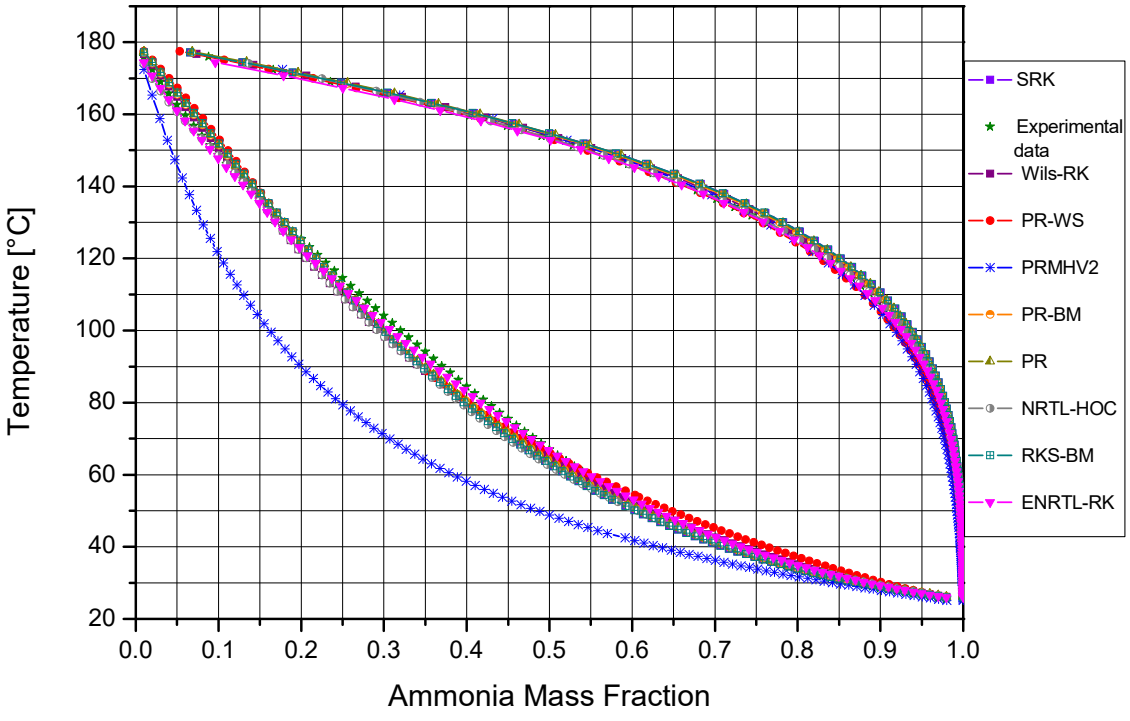

Figure 3.5. *T-x-y* VLE diagram at $P = 10$ bar for ammonia/water mixture (predicted by models with regressed interaction parameters).

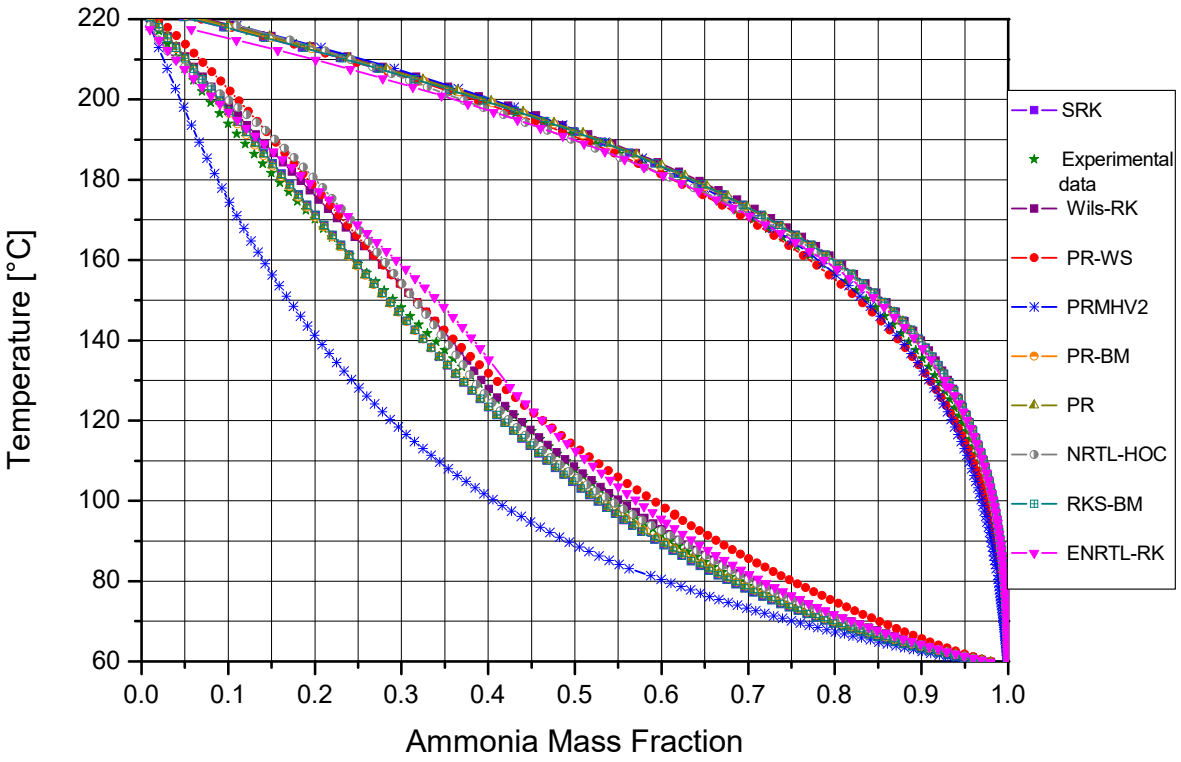

Figure 3.6. *T-x-y* VLE diagram at P = 25 bar for ammonia/water mixture (predicted by models with regressed interaction parameters).

Table 3.2. Sum of squared errors for the regressed thermodynamic property models tested.

Aspen-Plus property model	**Sum of squared errors**
PR-BM	36.55
PENG-ROB	38.36
WILS-RK	41.92
RKS-BM	44.86
SRK	45.07
ENRTL-RK	48.31
NRTL-HOC	53.00
PR-WS	80.42
PR-MHV2	226.62

Table 3.3. Interaction parameter k_{ij} for the considered cubic equations of state.

ASPEN-PLUS property model	$k_{NH_3H_2O}^{(1)}$ **Default**	$k_{NH_3H_2O}^{(2)}$ **Default**	$k_{NH_3H_2O}^{(3)}$ **Default**	$k_{NH_3H_2O}^{(1)}$ **Regressed**	$k_{NH_3H_2O}^{(2)}$ **Regressed**	$k_{NH_3H_2O}^{(3)}$ **Regressed**
PR-BM	-0.3147	$1.4\ 10^{-4}$	0	-1.0017	$1.1\ 10^{-3}$	119.82
PENG-ROB	-0.2589	0	0	-1.0610	$1.2\ 10^{-3}$	130.30
RKS-BM	-0.280	-0.280	0	-1.2146	$1.3\ 10^{-3}$	162.214
SRK	0	$1.77\ 10^{-5}$	0	-0.4246	$1.95\ 10^{-4}$	26.492

3.5. Conclusions

To predict and extrapolate the thermodynamic properties of ammonia/water fluid mixture over a wide range of temperature ($273.16 \leq T \leq 613.15$ K) and pressure ($0 < P \leq 210$ bar), nine different models implemented in Aspen-Plus were evaluated in two steps. Firstly, vapor-liquid equilibrium (VLE) calculated by each of the Aspen-Plus property models was compared with the regressed VLE data reported by Mejbri and Bellagi [91] at different pressures. It was concluded that none of these property models predicts the ammonia/water vapor-liquid equilibrium with sufficient accuracy. Secondly, the ASPEN-PLUS data regression tool was used to calculate the parameters of the ASPEN-PLUS property models by fitting the vapor-liquid equilibrium data reported by Mejbri and Bellagi [91]. It was found that the Peng-Robinson-Boston-Mathias equation of state (PR-BM) with regressed interaction parameters is the most suitable property model for the water/ammonia fluid mixture in the temperature and pressure ranges encountered in absorption refrigerating machines. It is concluded that simulations on Aspen-Plus flow-sheeting software of absorption refrigerating

machines working with NH_3/H_2O fluid mixture should be done using the Peng-Robinson-Boston-Mathias equation of state (PR-BM), with fitted parameters, as a property model.

Chapter 4

Steady-state modeling and operational analysis of a commercial gas-fired absorption chiller in Aspen-Plus

In the present chapter, an Aspen-Plus steady-state simulation model is developed using to analyze the performance of a commercial 3-ton gas-fired absorption chiller (10 kW cooling capacity) at different operating conditions. This air-conditioner uses ammonia/water as a working fluid and produces cold in form of ice water. This particular chiller has been chosen in this study for the following reasons:

i. Although absorption technique is used for cold production, its thermodynamic cycle presents some particularities and complex flow connections in comparison with conventional absorption machines. In particular a solution cooled absorber, called pre-absorber, is incorporated in the ROBUR chiller to improve its performances;
ii. The absorption chiller is a commercial unit and operational experimental data is available in the open literature.

The steady-state simulation model developed in the present work using the flow-sheeting software Aspen-Plus is intended to analyze the performance of the air-cooled ROBUR absorption chiller investigated experimentally by Klein [106]. This author carried out his experiments in an environmental chamber at three air-cooling temperatures, namely 26.7°C, 35°C and 38°C, with 14 temperature measurement points in the chiller.

4.1. Introduction

Several studies are focused on finding new ways to directly use thermal or solar energy to drive cooling machines. Investigations are being carried out on the development of new and hybrid cycle configurations and finding new potential working fluids.

Lazzarin *et al*. [107] reported a detailed work on a gas-fired 5-ton ammonia/water absorption chiller for refrigeration applications. The authors studied the performance of the chiller by modifying its initial charge and proposed some modifications on the machine to produce cold at temperatures as low as -25°C. Chua *et al*. [108] presented a general framework for thermodynamic modeling of an irreversible absorption chiller focusing on the design and tested their theoretical approach on a single-stage ammonia/water unit. Component models of the chiller have been assembled so as to quantify the internal entropy production and thermal conductance (UA) in a thermodynamically rigorous formalism, which is in agreement with the simultaneous heat-and-mass transfer processes occurring within the exchangers. Local thermodynamic balance (viz. energy, entropy, and mass balance) and consistency within the components is respected, in addition to the overall thermodynamic balance as determined by the inlet and outlet states of the components. For the absorbers, Colburn-and-Drew mass transfer equations are incorporated to describe the absorption process. Furthermore, the impact of various irreversibilities on the chiller performance is also evaluated through the use of a general macroscopic equation. Horuz and Callander [34] carried out experimental investigations on the 3-ton model (ROBUR Servel ACD-3600 gas-fired system) and studied the response of the system to variations of the chilled water flow rate, inlet temperature and level in the evaporator drum for variable heat inputs by modifying the air-cooled components. A water-cooled absorber and water-cooled condenser units were incorporated into the system in order to test the experimental system under wider range of condenser and absorber pressures. Darwish *et al*. [35] analyzed the ROBUR absorption refrigeration water/ammonia

(ARWA) system using the Aspen-Plus simulator. The results were compared with some manufacturer compiled data reported in the open literature. The performance parameters employed for the analysis were: coefficient of performance (COP), heat duties of the evaporator, absorber and condenser, concentration in the ammonia poor and ammonia rich solutions, and flow rates of the ammonia poor solution and refrigerant vapor leaving the evaporator. Agreement between the simulation results and the experimental measurements was observed. Some innovative modifications in the ROBUR cycle aimed at enhancing the generator operation showed a significant improvement in the COP. In particular, introducing a throttling process directly prior to the generator could alleviate the generator heat load and enhance the COP up to 20%. Rossa and Bazzo [109] investigated theoretically the feasibility of a small-scale cogeneration system for cold and electricity production. The system consisted of a 5-ton ROBUR absorption chiller and a 28 kWe natural gas micro-turbine whose exhaust gas was used to drive the absorption chiller. The authors reported a thermal efficiency of 41 % for the combined cooling and power system, which in turn represents an enhancement of 67% in the efficiency of a single natural-gas micro-turbine. El May *et al*. [110] developed a modular simulation program under Mathematica for absorption heat pumps, refrigerators and air conditioners. The modular approach is an easier way to simulate various complex configurations. As an application, the commercial ROBUR absorption machine was studied. The predicted results showed well agreement with experimental data from the open literature. El May *et al*. [111] presented and discussed the results of an energetic and exergetic analysis of a commercial air-cooled ammonia / water absorption machine with a cooling capacity of 10 kW. The comparison with a conventional single-effect absorption chiller operating under the same conditions showed that to achieve similar performances to those of the pre-absorber in the ROBUR chiller, an additional heat transfer area in the air-cooled absorber was required to ensure the complete absorption of the refrigerant. The second law analysis revealed that the

highest exergy dissipation (75%) is located in the driving compartment and that the irreversible absorption process was responsible for an important part (45%) of the COP degradation.

4.2. Working principle of the Robur absorption chiller

A schematic representation of the absorption chiller cycle is shown in Figure 4.1. In the generator, the ammonia/water mixture is heated by thermal energy input provided from a gas burner to desorb the refrigerant. The refrigerant vapors (12) flow to the rectifier where they are cooled by the ammonia rich solution on its way to the generator and which is thus preheated. This causes partial condensation of the water vapors purifying further the ammonia vapors. These flow to the air-cooled condenser where they are liquefied. The liquid refrigerant (8) circulates then to the refrigerant heat-exchanger and further to the refrigerant expansion valve. After reduction of its pressure, the refrigerant is introduced in the evaporator (10) where it evaporates by absorbing heat from the chilled water. The refrigerant vapor flows to the absorber where it is absorbed by the ammonia poor solution returning from the generator in two steps: first, in the pre-absorber where the absorption heat released is used to preheat the ammonia rich solution on its way to the generator (4) and then in the air-cooled absorber to complete the absorption process. 3D-Sketches of the internal view of the machine and its major components are presented in Figures 4.2 and 4.3.

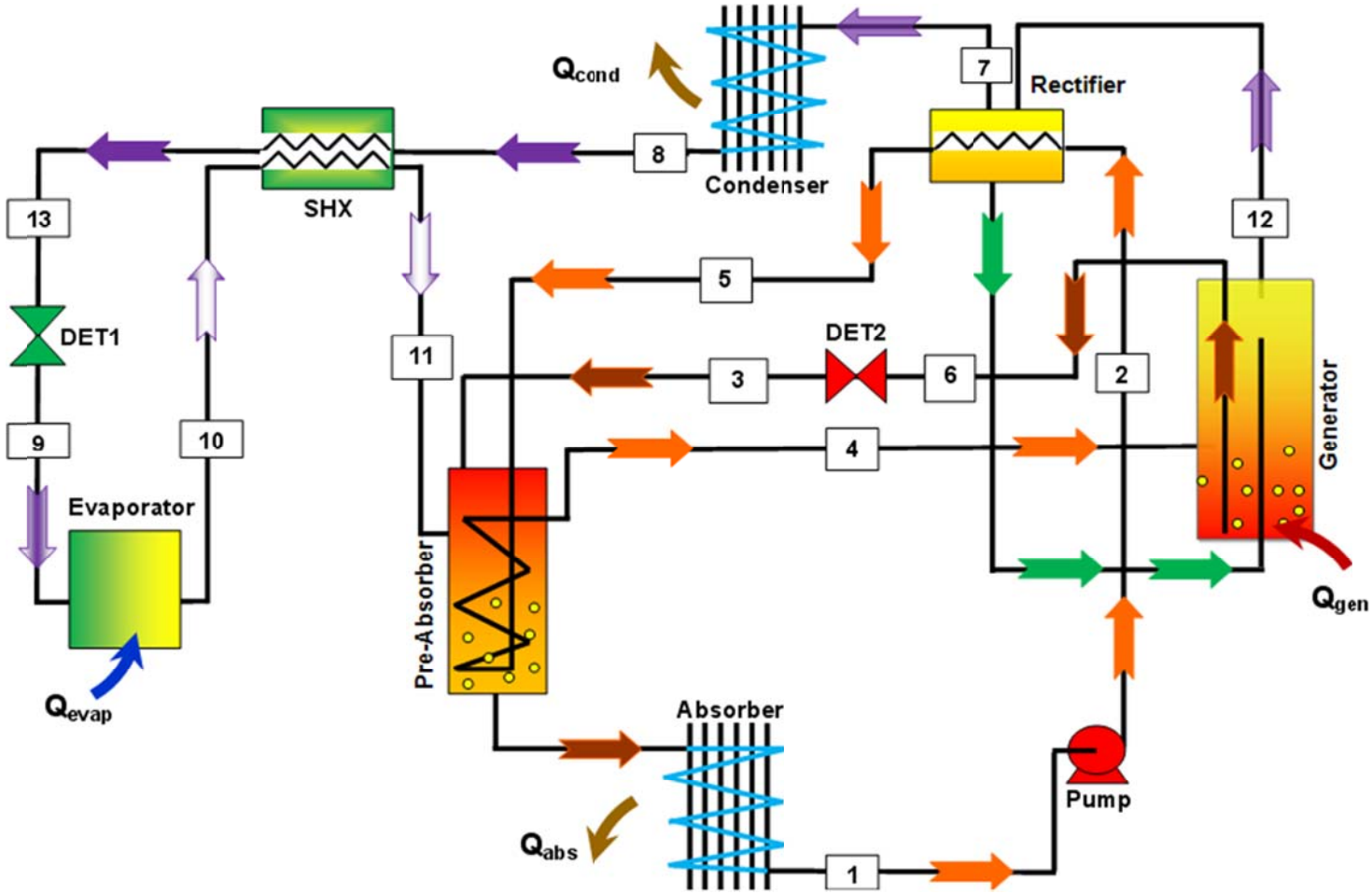

Figure 4.1. Schematic representation of the ROBUR absorption chiller.

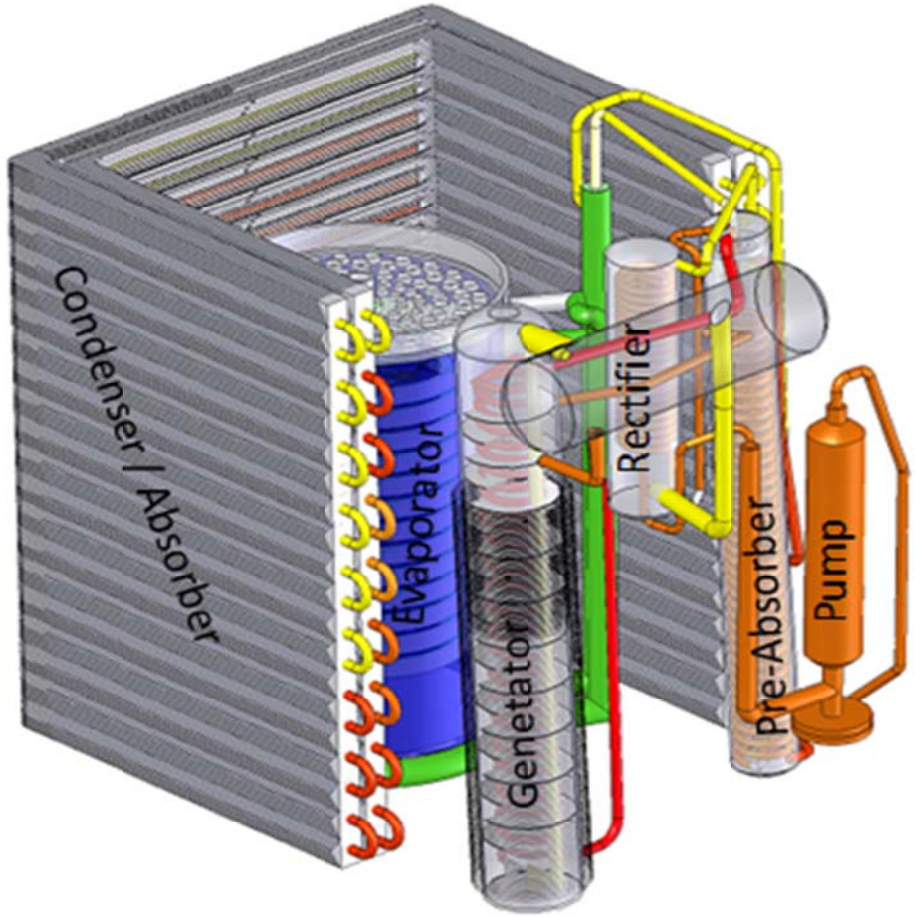

Figure 4.2. Internal view of the commercial absorption chiller.

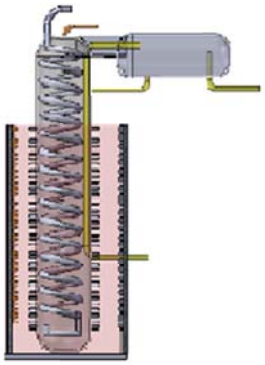

(a) Generator

(b) Evaporator

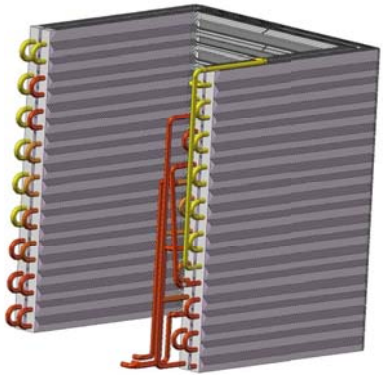

(c) Absorber and Condenser

(d) Pre-absorber

(e) Rectifier

(f) Solution pump

Figure 4.3. Schematic representation of the main components of the absorption chiller.

4.3. Models of the absorption chiller and its components

The analysis of the machine is performed in two steps. Firstly, the heat transfer characteristics of the major heat exchanging devices of the machine: condenser, evaporator, absorber and refrigerant heat exchanger are deduced from operating data of the chiller for 35ºC cooling air temperature.

The simulations results are then compared with experimental data of Klein [106] and those obtained by simulation of El May *et al*. [111]. In a second step, the model is then modified to include the (UA) values of the heat exchangers determined in the previous step as input parameters. To validate the model, the results are compared with the two sets of data from the literature [106, 111] at cooling air temperatures of 26.7ºC and 38ºC.

4.3.1. Simulation Model

The model developed for the absorption machine is represented in Figure 4.4. Table 4.1 summarizes the Aspen-Plus blocks for the different machine components as well as the input data used in these components for the simulation performed at 35°C cooling air temperature.

The state points in the chiller, shown in Figure 4.4, are defined as follows. The absorber exit is state point 1; the pump exit is state point 2; State point 5 represents the rectifier exit; the pre-absorber exit leading to the generator is state point 4; the solution exit of the generator leading to expansion valve 2 is state point 6; the expansion valve 2 (DET2) exit leading to the pre-absorber is state point 3. The vapor exit of the generator is state point 7; the condenser exit is state point 8. The refrigerant heat exchanger exit leading to expansion valve 1 (DET1) is state point 13; the refrigerant expansion valve 1 (DET1) exit is state point 9. The evaporator exit is state point 10; the refrigerant heat exchanger exit leading to the pre-absorber is state point 11, and the pre-absorber exit leading to the absorber is state point 14.

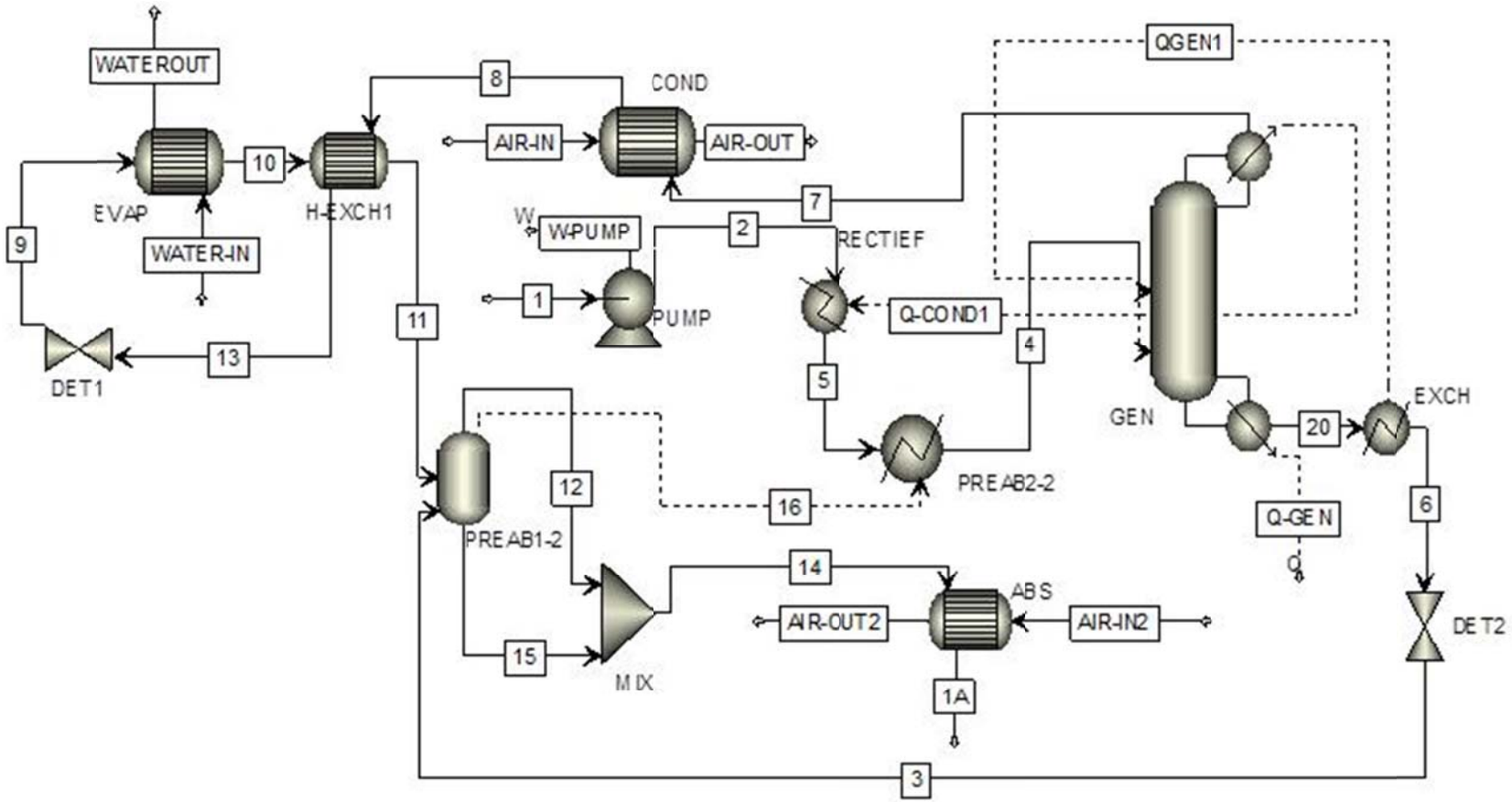

Figure 4.4. The absorption machine model in Aspen-Plus.

Table 4.1. Chiller's components and their models in Aspen-Plus with the corresponding input data.

Component	Aspen-Plus Block	Input data
Condenser (COND)	Two-flow heat exchanger HEATX	Pinch temperature: Hot outlet-Cold inlet = 13.5°C
Evaporator (EVAP)	Two-flow heat exchanger HEATX	Pinch temperature: Hot outlet-Cold inlet = 3°C
Absorber (ABS)	Two-flow heat exchanger HEATX	Pinch temperature: Hot outlet-Cold inlet = 10.2°C
Solution heat exchanger (SHX)	Two-flow heat exchanger HEATX	Pinch temperature: Hot outlet-Cold inlet = 16°C
Expansion valve1 (DET1)	VALVE	Outlet pressure = 4.936 bar
Pre-absorber (PREAB)	FLASH block and HEATER block	Pressure = 4.936 bar Exit temperature = 76°C
	MIXER	Pressure drop = 0 bar
Expansion valve2 (DET2)	VALVE	Outlet pressure = 4.936 bar
Generator (GEN)	RADFRAC	Reflux mass ratio = 0.09 Mass flow rate at the bottom = 55.06 kg/h
	HEATER	Pressure drop = 0 bar Exit temperature = 115°C
PUMP	PUMP	High pressure = 22.38 bar Isentropic efficiency = 1 **State point 1** - Pressure = 4.936 bar - Temperature = 45.2°C - Total mass flow = 90.718 kg/h - Vapor fraction = 0 - NH_3 Mass fraction = 0.437 - H_2O Mass fraction = 0.563

The calculation procedures used for the different state points of the chiller in the simulation carried out at 35ºC of cooling air temperature are summarized in Table 4.2.

Table 4.2. Calculation procedures used for the chiller simulation at 35ºC of cooling air.

State point	Calculation procedure
1	Saturated liquid; composition, total mass flow and pressure as inputs
2	Determined by the high pressure solution pump model
3	Determined by the solution valve 2 (DET2) model
4	Determined by the pre-absorber model
5	Determined by the rectifier model
6	Determined by the generator model
7	Determined by the generator model
8	Determined by the condenser model
9	Determined by the refrigerant valve 1 (DET1) model
10	Determined by the evaporator model
11	Determined by the vapor-liquid heat exchanger model
13	Determined by the vapor-liquid heat exchanger model
14	Determined by the pre-absorber model

Modeling a process in ASPEN-PLUS is based on the appropriate selection of the equivalent blocks of the software model-bank for the main components of the refrigerated machine.

- **Solution pump**

As shown in Figure 4.5, the solution pump is located between the state points 1 and 2. The default value of pump efficiency (100%) is used, as the effect of this parameter on the overall cycle performance is negligible. The inputs data for the pump model are:

- ❑ High pressure (pressure at the pump exit) = 22.38 bar
- ❑ Isentropic efficiency = 1

- Specifications of the state point 1:
  - Pressure = 4.936 bar
  - Temperature = 45.2°C
  - Total mass flow = 90.718 kg/h
  - Vapor fraction = 0
  - NH_3 mass fraction = 0.437
  - H_2O mass fraction = 0.563

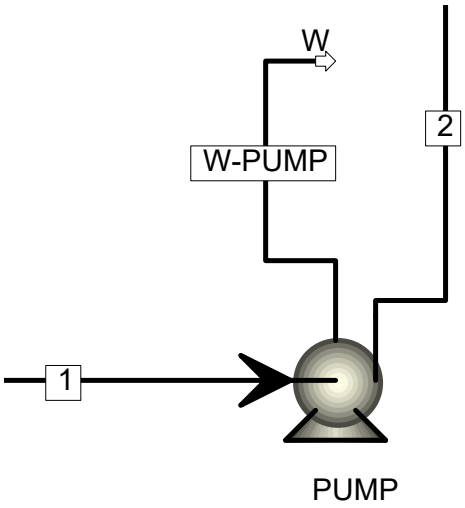

Figure 4.5. Solution pump model in Aspen-Plus.

- **Expansion valve1**

An expansion valve1 (DET1) is used between the state points 13 and 9 (Figure 4.6). The input data in the expansion valve1 (DET1) model is:

- Outlet pressure = 4.936 bar

Figure 4.6. Expansion valve1 (DET1) model in Aspen-Plus.

- **Expansion valve2**

An expansion valve2 (DET2) is used between the state points 6 and 3 (Figure 4.7). The input data in the expansion valve2 (DET2) model is:

- Outlet pressure = 4.936 bar

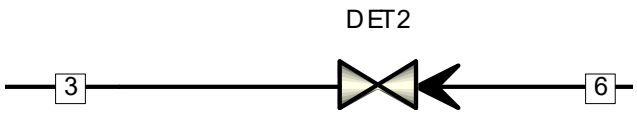

Figure 4.7. Expansion valve2 (DET2) model in Aspen-Plus.

- **Condenser**

A two-flow heat exchanger HEATX model is used for the air-cooled condenser (COND) between the state points 7 and 8 (Figure 4.8). The cooling medium air is modeled as a gas mixture comprised of 78 % nitrogen 21 % oxygen and 1 % argon by mole. The input data for the air-cooled condenser (COND) model is:

- Pinch temperature: Hot outlet-Cold inlet = 13.5°C

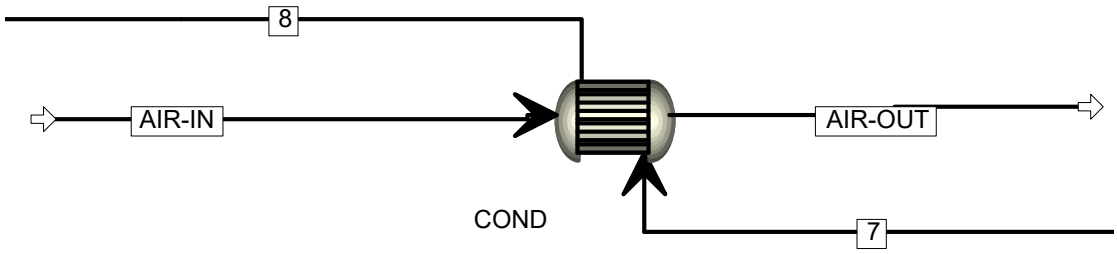

Figure 4.8. Air-cooled condenser (COND) model in Aspen-Plus.

- **Absorber**

A shown in Figure 4.9, a two-flow heat exchanger HEATX model is used for the air-cooled absorber (ABS) between the state point 14 and the absorber exit (state point 1A called "break point"). The cooling medium air is modeled as gas mixture comprised of 78 % nitrogen, 21 % oxygen and 1 % argon by mole. The input data for the air-cooled absorber (ABS) model is:

- Pinch temperature: Hot outlet-Cold inlet = 10.2°C

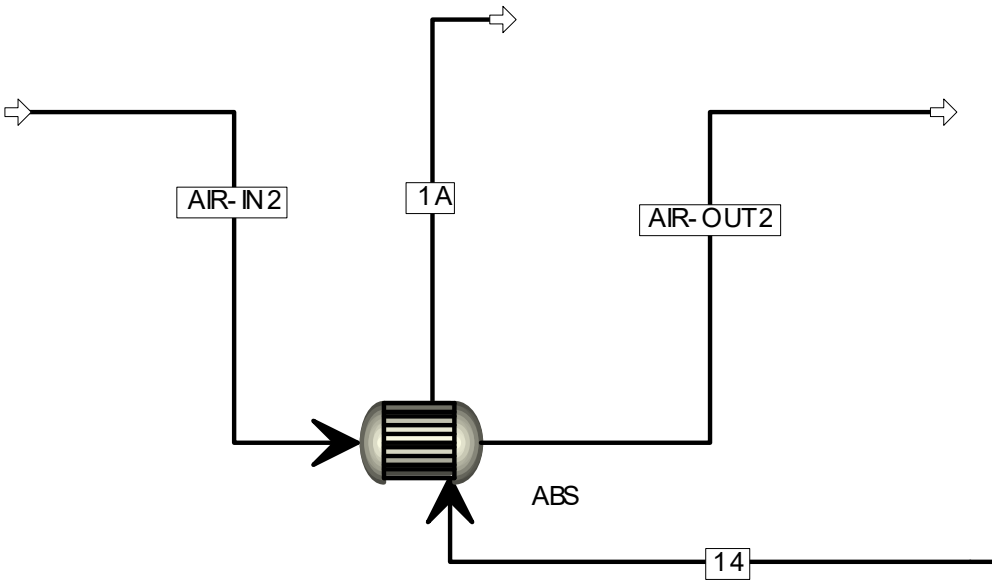

Figure 4.9. Air-cooled absorber (ABS) model in Aspen-Plus.

- **Evaporator**

As regards the water-cooled evaporator (EVAP), a two-flow heat exchanger HEATX model is used between the state points 9 and 10 (Figure 4.10). The cooling medium is pure water which is cooled from 12°C to 8°C. The input data for the water-cooled evaporator (EVAP) model is:

- Pinch temperature: Hot outlet-Cold inlet = 3°C

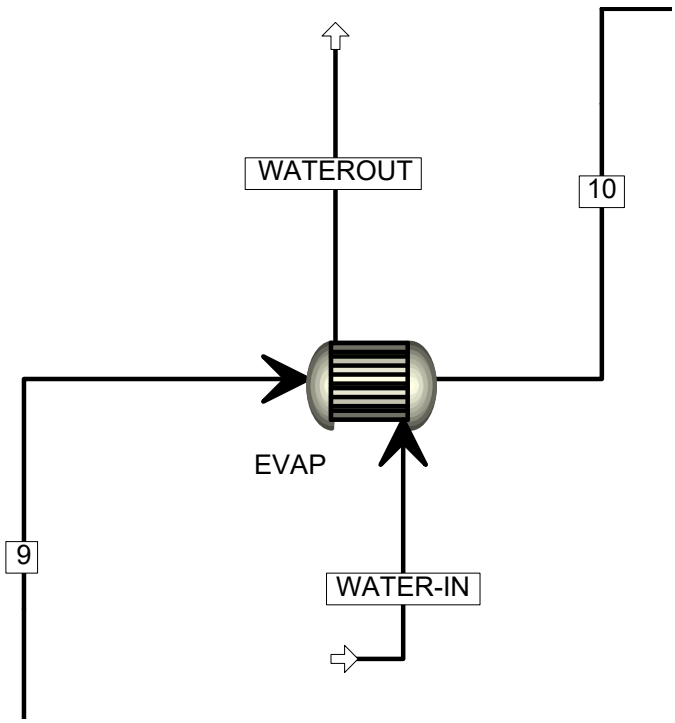

Figure 4.10. Water-cooled evaporator (EVAP) model in Aspen-Plus.

- **Solution heat exchanger**

As shown in Figure 4.11, a two-flow heat exchanger HEATX model is used for the solution heat exchanger (H-EXCH1) between the state points 10 and 11 and between the state points 8 and 13. The input data for the solution heat exchanger (H-EXCH1) model is:

- Pinch temperature: Hot outlet-Cold inlet = 16°C

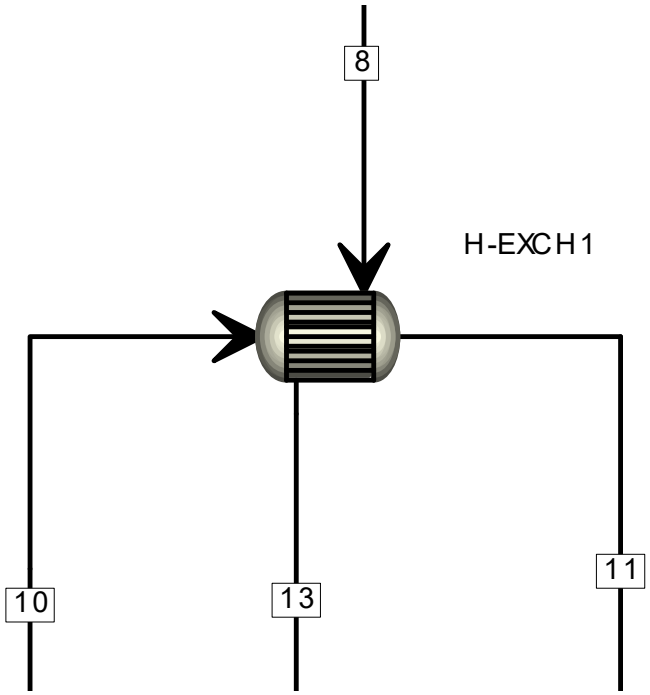

Figure 4.11. Solution heat exchanger (H-EXCH1) model in Aspen-Plus.

- **Generator**

To separate the refrigerant in the generator, a multi-stage rectification column with a condenser and a boiler is required (Figure 4.12). The generator (GEN) is modeled using a RADFRAC column connected with a HEATER connecting the state points 4, 7, 20 and 6. The inputs data for the generator (GEN) model are:

- Reflux mass ratio = 0.09
- Mass flow rate at the bottom = 55.06 kg/h
- Pressure drop = 0 bar
- State point 6 exit temperature = 115°C

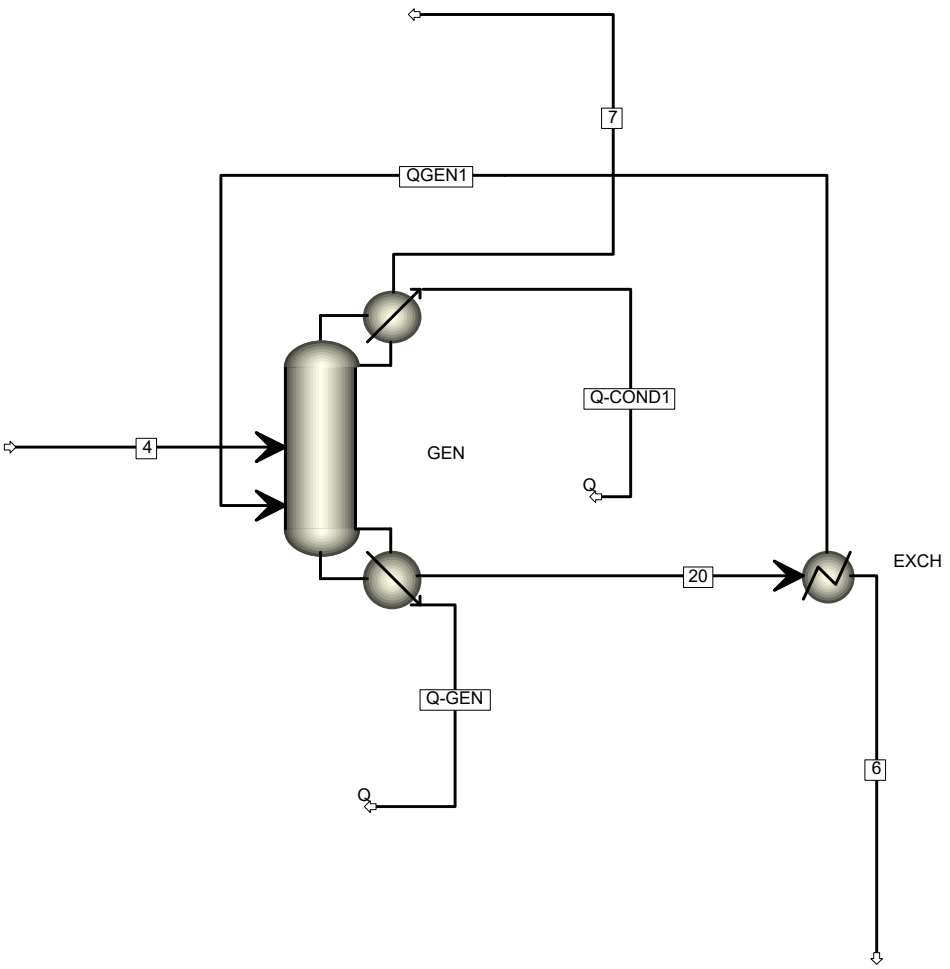

Figure 4.12. Generator (GEN) model in Aspen-Plus.

- **Pre-absorber and rectifier**

Regarding the pre-absorber and the rectifier, a simplified model combining a FLASH TANK and a HEATER is adopted to account for the complex heat and mass transfer processes taking place in this component (Figure 4.13). On one side, the hot ammonia poor solution from the generator (state point 3) is mixed with the cold refrigerant vapor coming from the evaporator (state point 11), resulting in a partial absorption and a liquid/vapor mixture leaving for the air-cooled absorber. On the other side, the ammonia rich solution (state point 5) on its way to the

generator preheated by the hot ammonia poor solution and by the heat released by the partial absorption process. The inputs data for the pre-absorber model are:

- Pressure = 4.936 bar
- State point 5 exit temperature = 76°C
- MIXER (MIX) Pressure drop = 0 bar

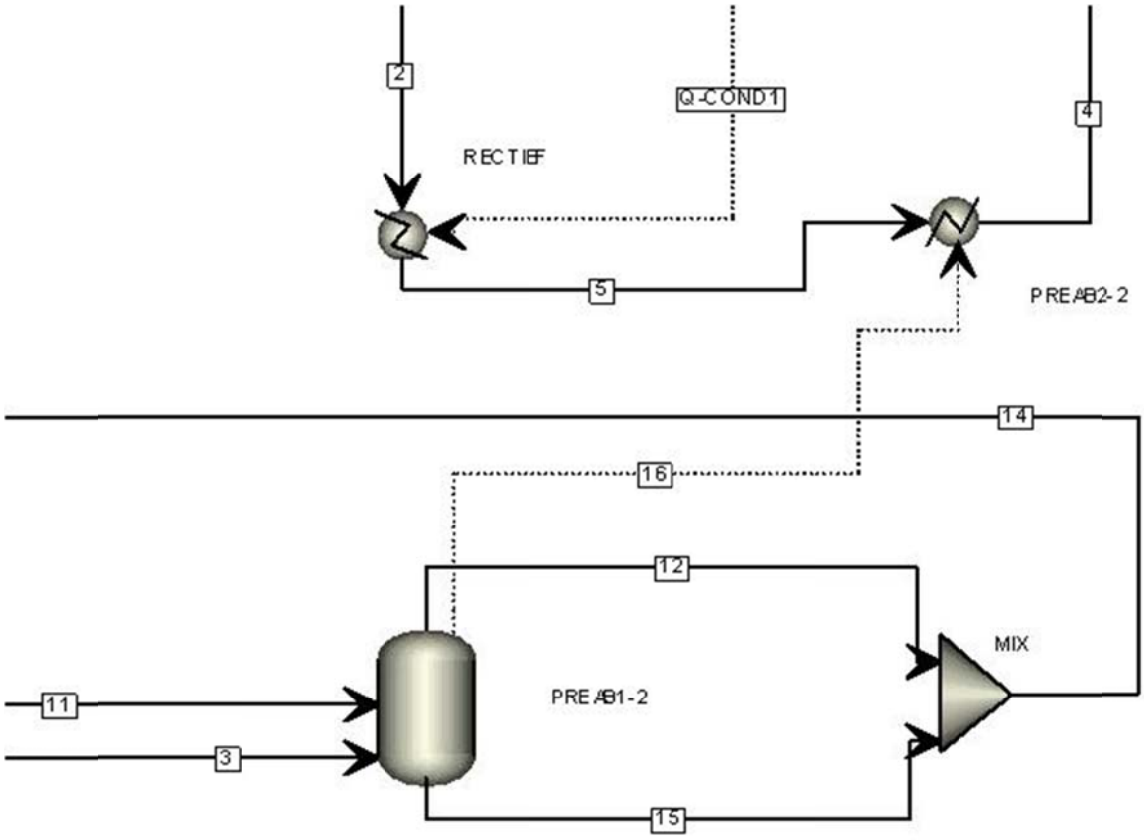

Figure 4.13. Models of the pre-absorber and rectifier in Aspen-Plus.

4.3.2. Simulation procedure

The simulation model developed in the present work uses in a first step a sequential modular approach in which each block is calculated separately. A “break point” is considered in the model for the cycle input conditions. This “break” point is inserted at state point 1, the solution pump inlet (Figure 4.4). The exit of the absorber (state point 1A) and the inlet of the

solution pump (state point 1) represent the same state, and consequently state point 1A should have the same characteristics as those given as inputs at the solution pump inlet after the simulations are run. This constitutes the convergence criterion for the simulations.

As Equation Oriented Modeling is a more effective way of solving complex problems, the simulations are run, in a second step, using the Equation-Oriented (EO) approach: the governing equations of the chiller model are solved simultaneously. To reach convergence in this approach, good initial estimates for all variables are necessary. Good practice is to begin the simulations in sequential modular mode and to initialize (synchronize) the EO solution procedure using the results of the sequential simulation after complete convergence.

4.4. Results and discussion

4.4.1. Heat transfer characteristics of the main thermal components of the chiller

The heat conductance, sometimes referred to as the heat capacity of the heat exchanger, is generally defined by the equation

$$\dot{Q} = (UA)\Delta T_{ln} \qquad (4.1)$$

Where $\dot{Q}$ is the heat duty and ΔT_{ln} the logarithmic mean temperature difference, LMTD, at the hot (subscript, *h*) and cold (subscript, *c*) ends of the exchanger,

$$\Delta T_{ln} = \frac{(T_{h,i} - T_{c,o}) - (T_{h,o} - T_{c,i})}{\ln\left[\frac{(T_{h,i} - T_{c,o})}{(T_{h,o} - T_{c,i})}\right]} \qquad (4.2)$$

with The subscripts *i* and *o* refer to the inlet and outlet, respectively.

As mentioned previously the start input values are introduced into the chiller simulation considering a "break" point at state point 1. A well-formulated model will conserve mass and

energy throughout the cycle, thus resulting in identical characteristics of the flows on either side of the break 1A. The cycle state points resulting from the Aspen-Plus model at 35ºC of cooling air temperature are given in Table 4.3.

The experimental data reported by Klein [106] and the simulation results obtained by El May *et al*. [111] are used to validate our Aspen-Plus model. The validation parameters employed are: driving heat input, coefficient of performance (COP) and temperature measured by Klein [106] at 14 locations in the chiller. In Figure 4.14, this comparison shows excellent agreement between the Aspen-Plus model results and Klein's data, except for state point 11 (refrigerant vapor leaving the refrigerant heat exchanger) for which the deviation is more than 10 ºC. The results are also well in agreement with the simulation results obtained by El May *el al*. [111], except at 4 state points namely 4 (ammonia rich solution entering the generator), 13 (Refrigerant liquid leaving the refrigerant heat exchanger), 14 (ammonia poor solution entering the absorber) and 11 (refrigerant vapor leaving the refrigerant heat exchanger) for which the temperature deviation is higher than 5ºC. The temperature values calculated in the present work and in El May *et al*. [111] for state point 11 are similar, which could mean that the experimental data from Klein [106] at this point is not of a good quality.

Table 4.4 shows the thermal loads in the main components and the COP of the absorption chiller reported by Klein [106] and the values obtained in the present work. As regards the thermal loads, the maximum deviation is observed in the driving heat in the generator which is less than 7%. The deviation obtained in the COP is about 5%.

Table 4.3. Aspen-Plus model simulation results for 35ºC cooling air temperature.

State point	From	To	Pressure (bar)	Temperature (°C)	Vapor fraction	Mass flow rate (kg/h)	NH_3 Mass fraction (%)
1A	Absorber	Pump	4.936	45.2	0	90.718	43.7
2	Pump	Rectifier	22.380	46.6	0	90.718	43.7
3	DET2	PREAB1-2	4.936	115.3	0	55.060	9.0
4	PREAB2-2	Generator	22.380	108.1	0.006	90.718	43.7
5	Rectifier	PREAB2-2	22.380	64.3	0	90.718	43.7
6	EXCH	DET2	22.380	115.0	0	55.060	9.0
7	Generator	Condenser	22.380	105.6	1	35.658	97.0
8	Condenser	H-EXCH1	22.380	48.5	0	35.658	97.0
9	DET1	Evaporator	4.936	4.9	0.073	35.658	97.0
10	Evaporator	H-EXCH1	4.936	9.5	0.819	35.658	97.0
11	H-EXCH1	PREAB1-2	4.936	16.7	0.901	35.658	97.0
12	PREAB1-2	Mixer	4.936	76.0	1	22.425	94.8
13	H-EXCH1	DET1	22.380	24.0	0	35.658	97.0
14	Mixer	Absorber	4.936	76.0	0.254	90.718	43.7
15	PREAB1-2	Mixer	4.936	76.0	0	68.293	26.9
20	Generator	EXCH	22.380	192.6	0	55.060	9.0

Table 4.4. Comparison between experimental data [106] and simulation results in terms of component heat duties and chiller COP for 35ºC cooling air temperature.

Parameter	Experimental value	Calculated value
$\dot{Q}_{generator}$ (kW)	17	15.91
$\dot{Q}_{evaporator}$ (kW)	9.59	9.51
$\dot{Q}_{condenser}$ (kW)	-	12.84
$\dot{Q}_{absorber}$ (kW)	-	12.85
COP	0.56	0.59

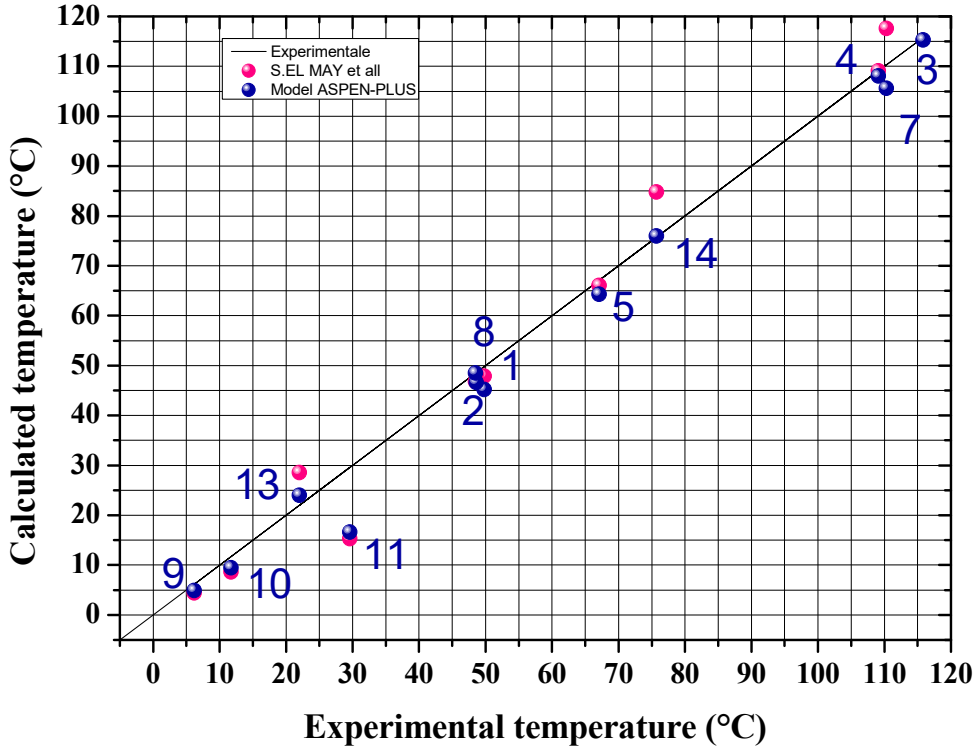

Figure 4.14. Temperature comparison at different locations in the chiller at 35ºC of cooling air temperature (UA values as output parameters of the model).

Next, the (UA)values for the condenser, evaporator, absorber and refrigerant heat exchanger (Table 4.5) were calculated.

Table 4.5.(UA) values of the heat exchangers calculated at 35ºC of cooling air temperature.

Heat exchanger	(UA) **(W/K)**
Condenser	390.0
Evaporator	3304.9
Absorber	630.0
H-EXCH1	55.9

4.4.2. Model predictions with (UA) values as input parameters

In this second step, the Aspen-Plus model for the absorption chiller is then modified to include the heat transfer capacities (UA) of the condenser, evaporator, absorber and refrigerant heat exchanger as input parameters for the simulations for cooling air temperatures of 26.7°C and 38°C. The obtained results for 26.7ºC cooling air temperature are represented in Figure 4.15 in comparison with the experimental data from Klein [106] and simulated temperatures reported by El May *et al*. [111]. As can be noted the results obtained in the present work are well in agreement with both sets of data. In the case of comparison with experimental data from Klein [106], the maximum deviations are observed in state points 4 (refrigerant vapor entering the generator) and 11 (refrigerant vapor leaving the refrigerant heat exchanger). Regarding the comparison with data obtained by El May *el al*. [111], the maximum deviation is observed in state point 14 (ammonia poor solution entering the absorber).

Figure 4.16 shows the same comparison for 38ºC cooling air temperature. In general terms, the results of the present work are in good agreement with data from Klein [106] and El May *et al*. [111]. The maximum deviations are obtained in state points 7 (Refrigerant vapor entering the condenser), 11 (refrigerant vapor leaving the refrigerant heat exchanger) and 13 (Refrigerant liquid leaving the refrigerant heat exchanger) for the comparison with experimental data from Klein [106] and in state points 11, 13, 14 and 3 (ammonia poor solution entering the pre-absorber) for the comparison with simulated data from El May *et al*. [111]. It is worth mentioning that the temperature values calculated in the present work and in El May *et al*. [111] for state points 11 and 13 are similar, which could mean that the Klein [106] experimental data at these points is not of such a good quality. Table 4.6 shows a comparison between experimental temperature data [106], the simulation results of [111] and the model calculated temperature for 38ºC cooling air temperature. Based on these results, it

is demonstrated that the version of the Aspen-Plus model that includes the (UA) values of the condenser, evaporator, absorber and refrigerant heat exchangers as input parameters could be very useful for predicting the internal operating conditions and the coefficient of performance of the ROBUR absorption chiller at different temperatures of the cooling air and taking in account the real size of the heat exchangers.

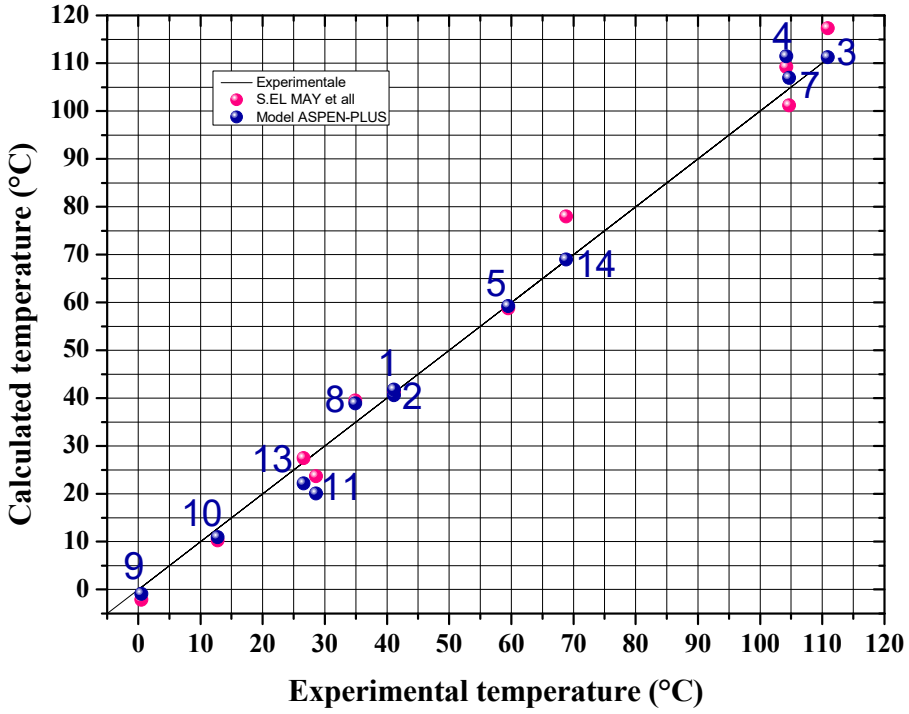

Figure 4.15. Temperature comparison at different locations in the chiller at 26.7ºC of cooling air temperature (UA values as input parameters in the model).

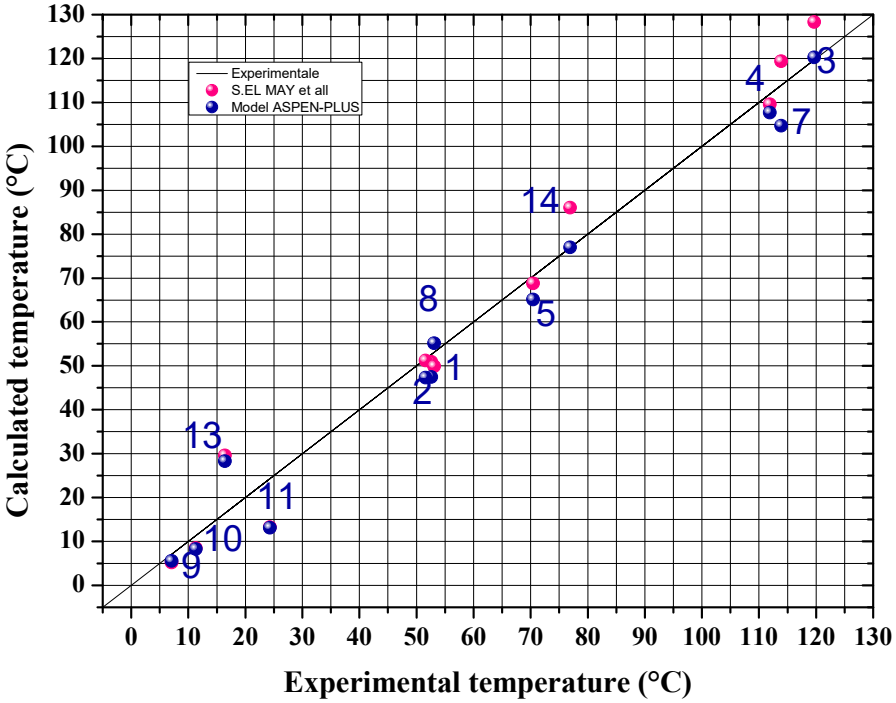

Figure 4.16. Temperature comparison at different locations in the chiller at 38ºC of cooling air temperature (UA values as input parameters in the model).

Table 4.6. Comparison between experimental temperatures [106], calculated temperatures from reference [111] and temperatures calculated by the Aspen-Plus model at 38ºC of cooling air temperature.

State point	Experimental data [106] Temperature (°C)	Calculated Data [111] Temperature (°C)	Aspen-Plus simulation results Temperature (°C)
1	52.6	50.9	47.4
2	51.6	51.2	47.3
3	119.7	128.3	120.2
4	111.9	109.6	107.6
5	70.4	68.8	65.1
7	113.9	119.4	104.7
8	53.1	49.9	55.2
9	7.1	5.2	5.5
10	11.3	8.5	8.2
11	24.3	13.3	13.1
13	16.4	29.6	28.2
14	76.9	86.0	77.0

4.5. Conclusion

In this chapter, a steady-state simulation model of a commercial 3-ton ammonia / water absorption chiller is developed and validated using the flow-sheeting software Aspen-Plus. First, the heat transfer characteristics of the condenser, evaporator, absorber and refrigerant heat exchanger were deduced from experimental data at 35ºC cooling air temperature. Then, the results were compared with experimental data published by Klein [106] and those calculated by El May *et al*. [111]. The comparison showed good agreement between the Aspen-Plus model results and the sets of data from the open literature. The model was then modified to include the (UA) values of the heat exchangers calculated in the previous step as input parameters. The results were compared with the experimental data from Klein [106] and those reported by El May *et al*. [111] at cooling air temperatures of 26.7ºC and 38ºC. The results showed agreement with the two sets of bibliographical data. Therefore, it is concluded that the proposed Aspen-Plus model can be very useful tool for predicting the internal operating conditions and the coefficient of performance of the commercial gas-fired absorption chiller at different temperatures of the cooling air and taking in account the real size of the heat exchangers.

Chapter 5

Experimental investigations and characterization of a small capacity diffusion-absorption refrigerating (DAR) machine

The present chapter reports on experimental investigations and performance characterization of a small capacity (7.5W) commercial diffusion-absorption refrigerator, designed for hotel rooms, activated by an electric heater. In order to:

i. Study the temperatures time evolution of the input and output parameters of the various components of the refrigerator;
ii. Deepen understanding of operation of the refrigerator;
iii. Analyze the refrigerator performance at different operating conditions;
iv. Build an experimental database to fully characterize the refrigerator operation and that will be used to validate a theoretical simulation models presented in the next chapters.

5.1. Introduction

As alternative to the compression-type refrigerators, there are diffusion-absorption refrigerators invented by the two Swedish engineers Balzar Von Platen and Carl Munters [4]. This system uses ammonia as refrigerant, water as absorbent and hydrogen as inert gas. Unlike conventional systems, the total pressure is constant throughout the Platen-Munters system, thus eliminating the need for mechanical pump or compressor. To allow the refrigerant (ammonia) to evaporate at low temperatures in the evaporator, a third inert gas (hydrogen) is needed. This system offers several advantages over conventional systems such as high reliability due to absence of moving parts, very little maintenance, silent operation. It can be powered by different electricity tensions and thermal energy sources (natural gas, LPG, etc). Due to the above advantages these systems find applications such as refrigerators for remote and rural areas, portable refrigerators, refrigerators for hotel rooms, etc.

The coefficient of performance (COP) of this kind of machines is however low. To give opportunity for energy savings for products in the growing markets of absorption-type refrigerating appliances, the electric type of these machines were included in the scope of the novel European Union regulation relative to energy labeling of household refrigerating appliances [112]. Since the invention of the diffusion-absorption refrigeration systems, much research has been conducted in order to make them more attractive for use as domestic refrigerators and to improve their performance. Most of these investigations were focused on improving the performance by reducing the heat supplied to the generator. Many aspects were then discussed, such as the mechanical design of the various components of these systems, the nature of the working fluids and the thermodynamic cycles.

5.2. Working principle

A 3-D scheme of the investigated refrigerator and its various components are represented in Figures 5.1 and 5.2, respectively. It is a small capacity refrigerator (44 litres), with internal

dimensions (height x width x depth = 490mm x 360 mm x 250 mm), designed for hotel rooms, activated by an electric heater, and operating with the ternary fluid mixture ammonia-water-hydrogen. The refrigerator is formed by a generator consisting of a bubble pump immerged in an externally heated boiler, a rectifier, a condenser, an evaporator, a gas heat exchanger (GHX), an absorber, a solution heat exchanger (SHX), and a liquid solution tank. Before the unit begins operation, the ammonia rich solution occupies part of the solution tank, the bubble pump and the boiler. The gas phase is constituted of hydrogen and ammonia water vapors. When heat is supplied to the generator, the temperature of the ammonia rich solution increases, and when the boiling point is reached bubbles of ammonia are generated. During their ascent in the tube, these bubbles lift the ammonia rich solution upward. At the exit of the pump, the liquid solution falls down into the boiler under the effect of gravity and the vapors continue their way to the air-cooled rectifier where a partial condensation takes place. Water-rich condensate falls back into the boiler and the almost pure ammonia vapor moves on towards the air-cooled condenser where it condensates by releasing heat to ambient air. Uncondensed vapor reaches the reservoir through a pressure equalizer tube. The liquid refrigerant leaving the condenser flows in a separate tube welded to the two-coaxial-pipe gas heat exchanger connecting the absorber and the evaporator. In the inner tube of this heat exchanger, the cold ammonia-hydrogen gas mixture coming from the evaporator flows, while the hydrogen exiting the absorber and returning to the evaporator circulates in the outer annulus. The refrigerant rich gas is introduced at the bottom of the absorber where it rises counter-currently to the ammonia lean solution fed at the top. The refrigerant dissolves in the ammonia lean solution by rejecting heat to the ambient. The resulting ammonia rich solution flowing out of the absorber tube ends up in the solution tank. From there it starts its way to the bubble pump via the solution heat exchanger where it is warmed up by the lean solution exiting the boiler and returning to the absorber.

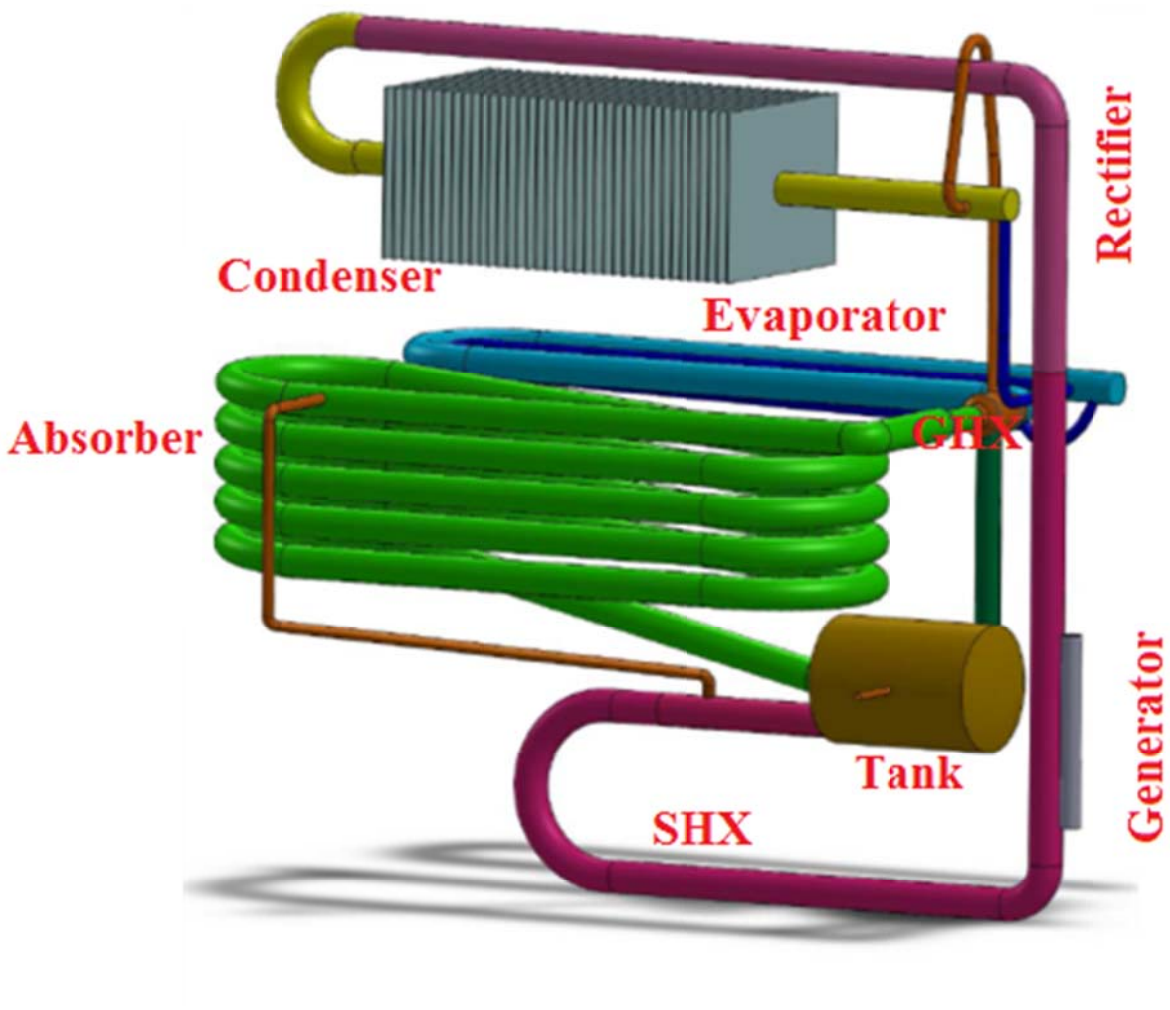

Figure 5.1. 3D-Schematic view of the diffusion-absorption refrigerator (DAR).

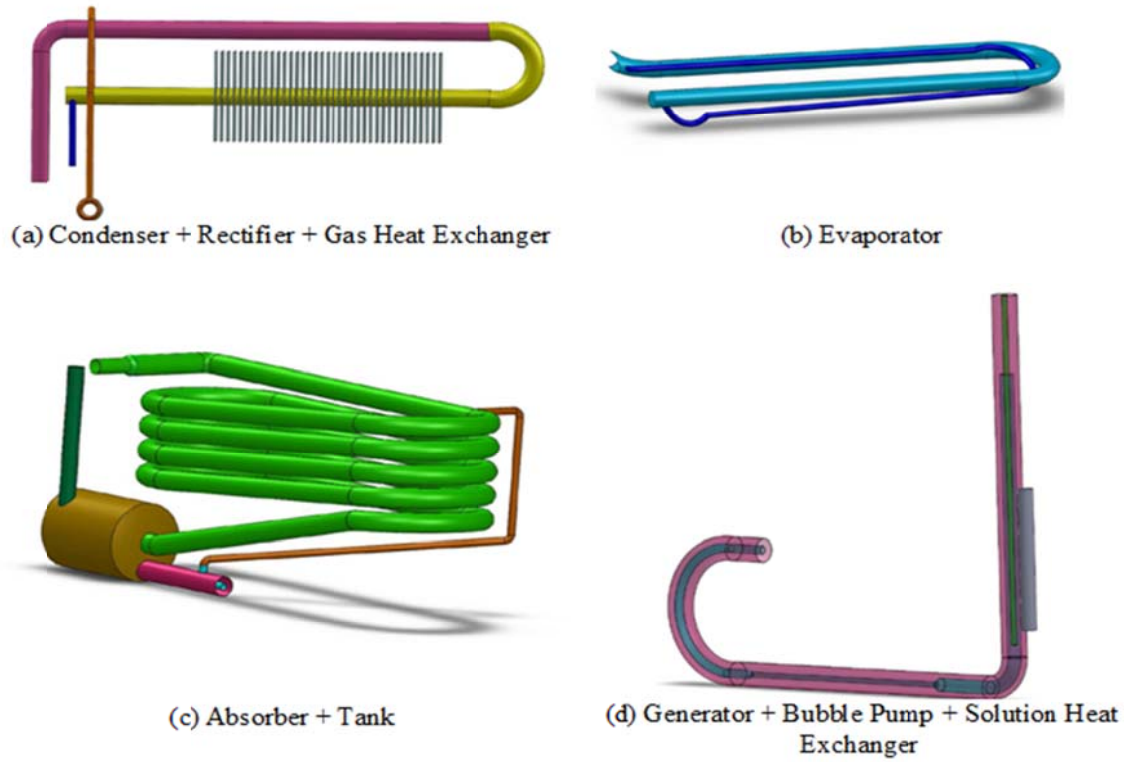

Figure 5.2. 3D-Schematic representation of the main components of the diffusion-absorption refrigerator.

5.3. Experimental set-up and procedure

5.3.1. Experimental set-up

In order to perform the tests, the refrigerator is equipped with 11 K-thermocouples placed at the entrance and exit of each of its components and connected up via a data acquisition unit (34970A AGILENT) to a computer where the data are monitored and stored (Figure 5.3). The locations of the thermocouples on the refrigerator, identified by their ID numbers, are given in Table 5.1. For all the tests, the thermostat was disconnected so that the refrigerator ran continuously in an air-conditioned environment with a set point temperature of 24°C. The ambient temperature T_a was also continuously measured and registered. The thermocouples were verified beforehand by placing them in a calibration ice-water bath. A fluctuation of

±0.5°C of the temperature measured was noticed. The electric heating device was connected to a power controller (Figure 5.3).

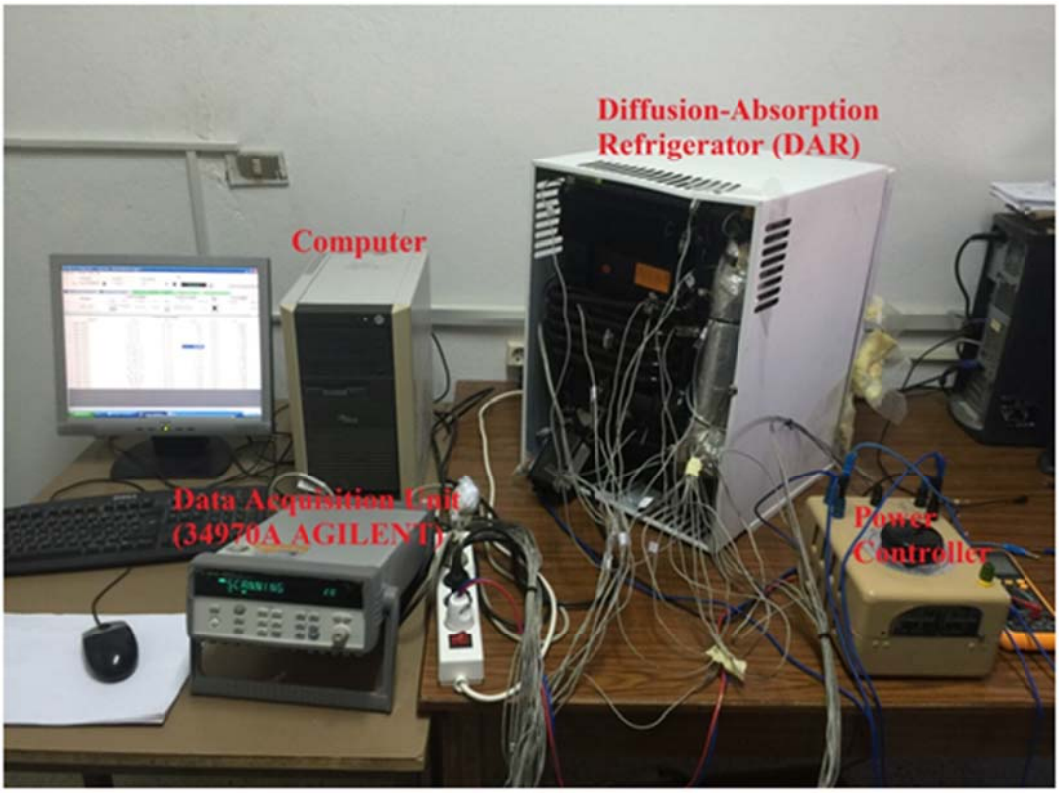

Figure 5.3. Experimental set-up of the diffusion-absorption refrigerator.

Table 5.1. Locations of the thermocouples.

Thermocouple locations	Thermocouple and stream ID
Generator gas outlet	101
Condenser outlet	103
Gas heat exchanger outlet	104
Evaporator outlet	105
Interior refrigerator	106
Absorber gas outlet	107
Absorber liquid outlet	108
Evaporator inlet	109
Liquid tank	110
Liquid generator outlet	112
Ambient air	115

5.3.2. Experimental procedure

The machine is normally equipped with a thermostat placed on the evaporator side to allow refrigeration at five levels. During our tests, the thermostat was disconnected to allow a continuous operation of the refrigerator. The experimental procedure consists of the following steps:

1. starting of Benchlink Data Logger;
2. Configuration of the different channels;
3. Setting the time intervals of data storage (60s);
4. Adjusting the power controller on the desired position and starting the every supplies
5. Monitoring the temperatures time evolution at the entrance and exit of each component of the refrigerator until a steady state regime is reached;
6. Shutdown of the refrigerator;

5.3.3. Performed tests

Several tests have been run in order to understand the operation of this refrigerator and to study its performance at different operating conditions. The first series of measurements have been performed by varying the power supplied to the generator. The second series of measurements have been carried out in order to evaluate the heat infiltration rate in the unit by introducing inside the machine an electric heater in form of an electric resistance cable (R = 135 Ω). The electric heater is connected to the power controller. Seven tests for different values of the applied voltage φ (V) to the resistor, have been performed, to vary the applied voltage, we act on the power controller.

5.4. Experimental characterization of the refrigerator

5.4.1. Refrigeration test results

A test set consisting of eleven experiments for different energy supply to the generator was performed: 35, 39, 44, 46, 48, 51, 53, 56, 58, 61 and 67W. Monitoring the temperature profiles allowed the determination of the minimum power supply needed to ensure the functioning of the refrigerator and its stability. As shown in Figures 5.4 and 5.5, it is observed that a supply of $\dot{Q}_{gen}$= 35W ensured the functioning of the refrigerator but not its stability, while with $\dot{Q}_{gen}$= 39W a steady operation of the refrigerator was reached after 150 minute.

Figure 5.6 shows how the temperature of the liquid stream at the generator exit fluctuates between 205°C and 155°C with a time period of 100 minute for a generator heat supply $\dot{Q}_{gen}$= 35W. For a generator heat supply of $\dot{Q}_{gen}$= 39W, a steady-state operation of the refrigerator is reached and the temperature of the solution leaving the generator stabilizes at 158°C after 150 minute. This Figure makes clear that when the electric power supplied to the generator is insufficient, the bubble pump does not start its operation because separate bubbles are produced in the pump tube: the flow regime is bubbly. With increasing heat supply, more bubbles are generated that also coalesce to form larger bubbles occupying entirely the section of the tube: the flow is now in slug regime. From this moment on, liquid can be efficiently entrained upwards. The frequency of slug formation increases with increasing heat supplied to the pump. For larger heat input, this frequency becomes larger and the pump operates more smoothly. It is concluded that, when the heating power supplied to the generator is below 39W, the bubble pump does not start its operation because no vapor bubbles are produced in the boiler section of the generator. Although, there is some ammonia vapor generated, it condenses and returns to the generator by rejecting heat to the ambient in

the rectifier, so no evaporation or absorption takes place which explains the presence of the fluctuations observed.

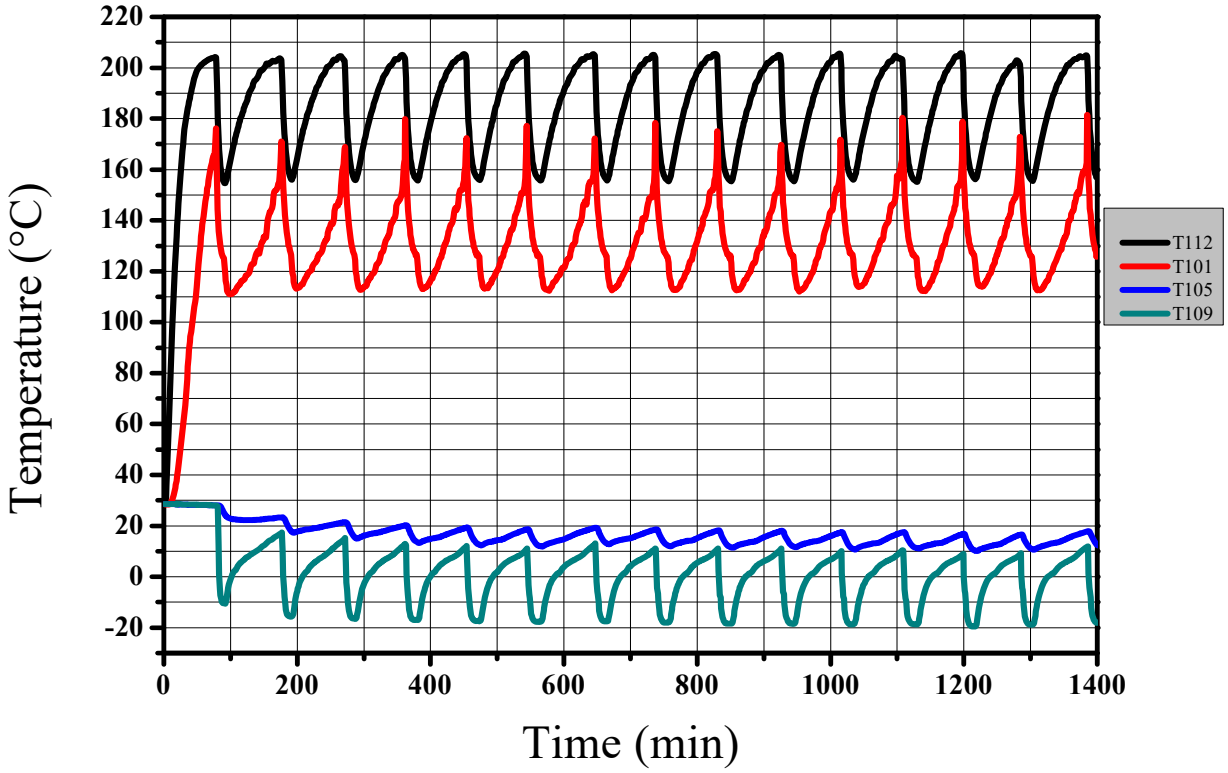

Figure 5.4. Temperature time evolution for generator heat supply of $\dot{Q}_{gen}$= 35W.

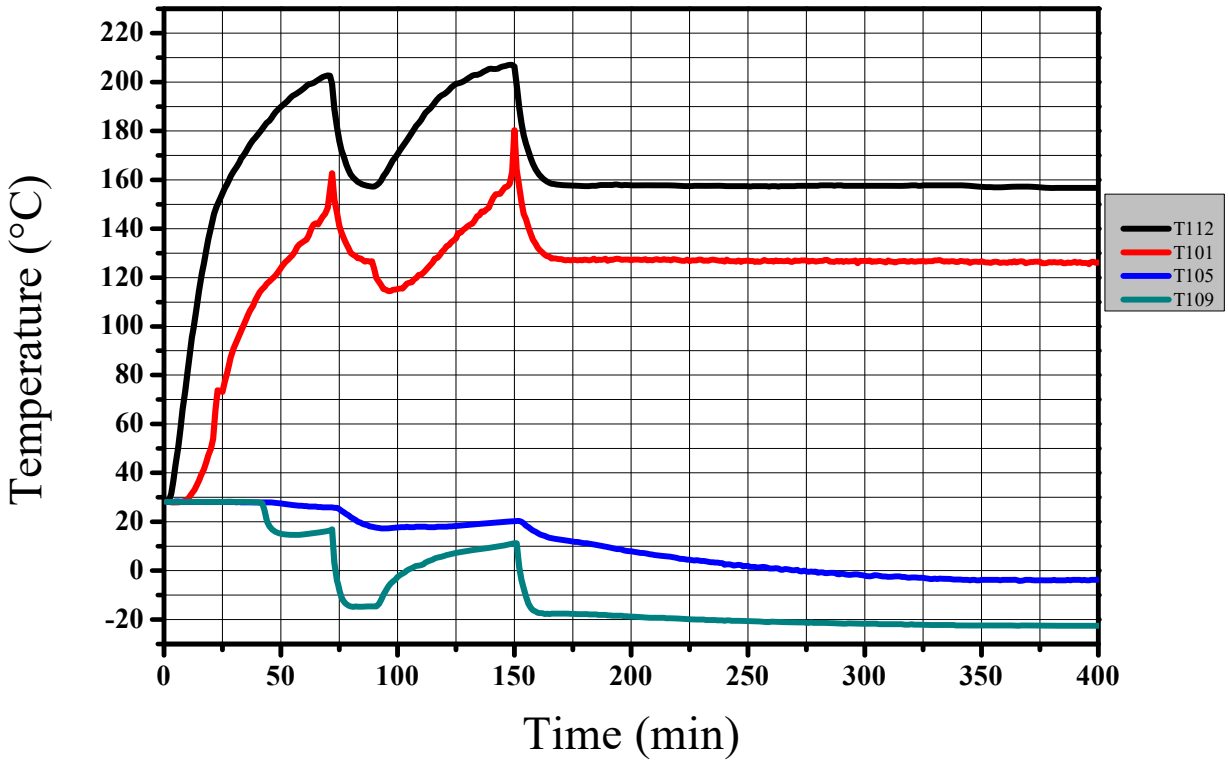

Figure 5.5. Temperature time evolution for generator heat supply of $\dot{Q}_{gen}$= 39W.

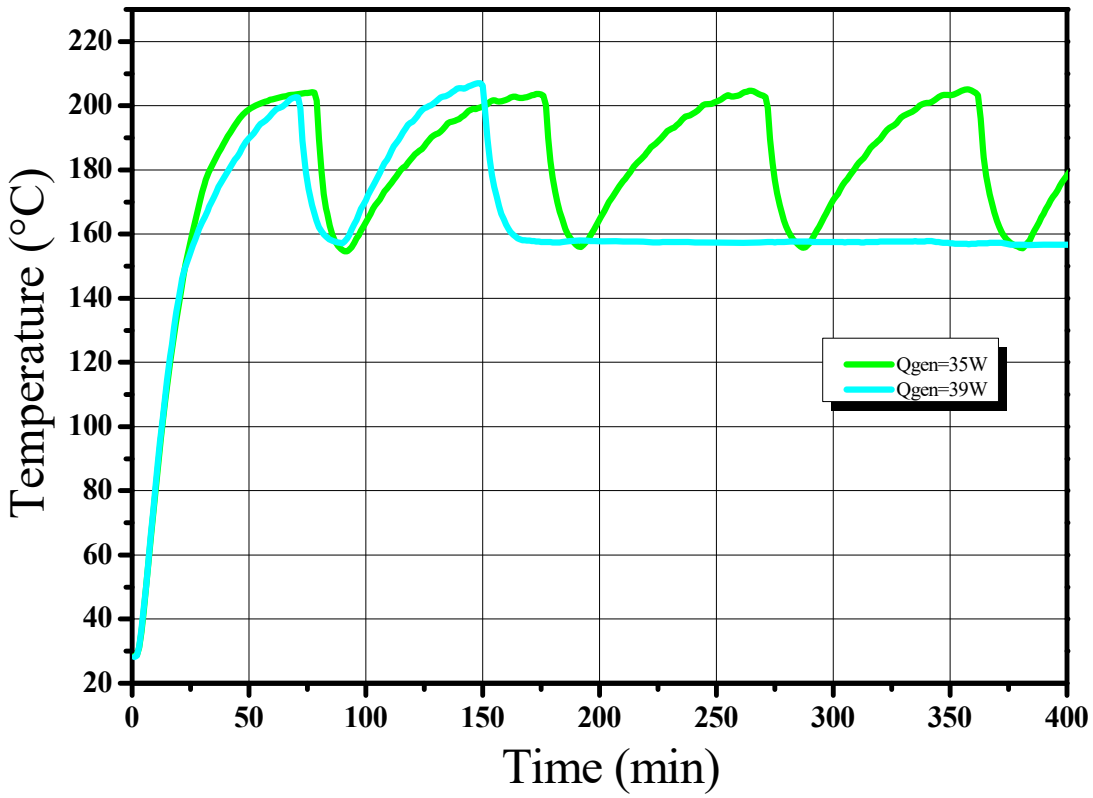

Figure 5.6. Temperature generator liquid out time evolution for (Generator heat supply $\dot{Q}_{gen}$= 35W and $\dot{Q}_{gen}$= 39W).

Figure 5.7 illustrates that, by increasing the heating power supplied to the generator, from $\dot{Q}_{gen}$= 44W to $\dot{Q}_{gen}$= 67W, the time fluctuations of the solution temperature at the generator exit decrease, therefore the time required for the machine to reach a stable regime decreases also.

Figures 5.8, 5.9 and 5.10 show that the time required for the machine to reach a stable regime is 38 minute, 31 minute and 25 minute for a generator heat supply $\dot{Q}_{gen}$= 51W, $\dot{Q}_{gen}$= 56W, $\dot{Q}_{gen}$= 61W, respectively.

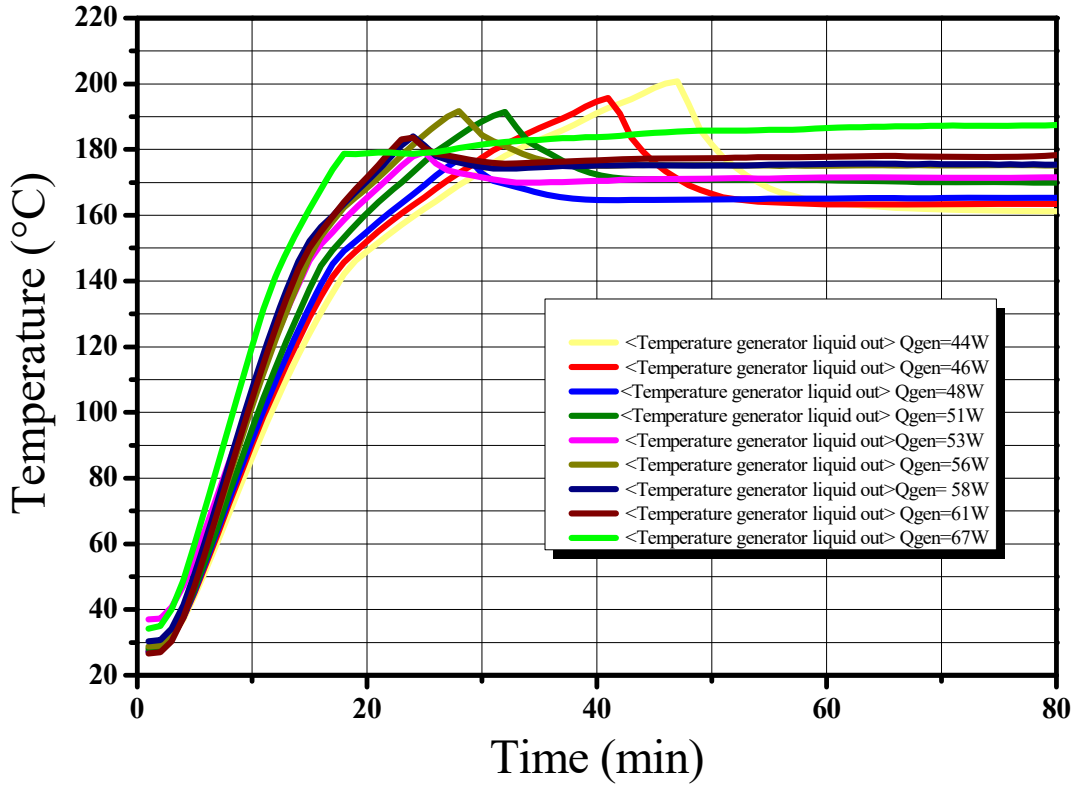

Figure 5.7. Temperature generator liquid out time evolution for different heat supply to the generator.

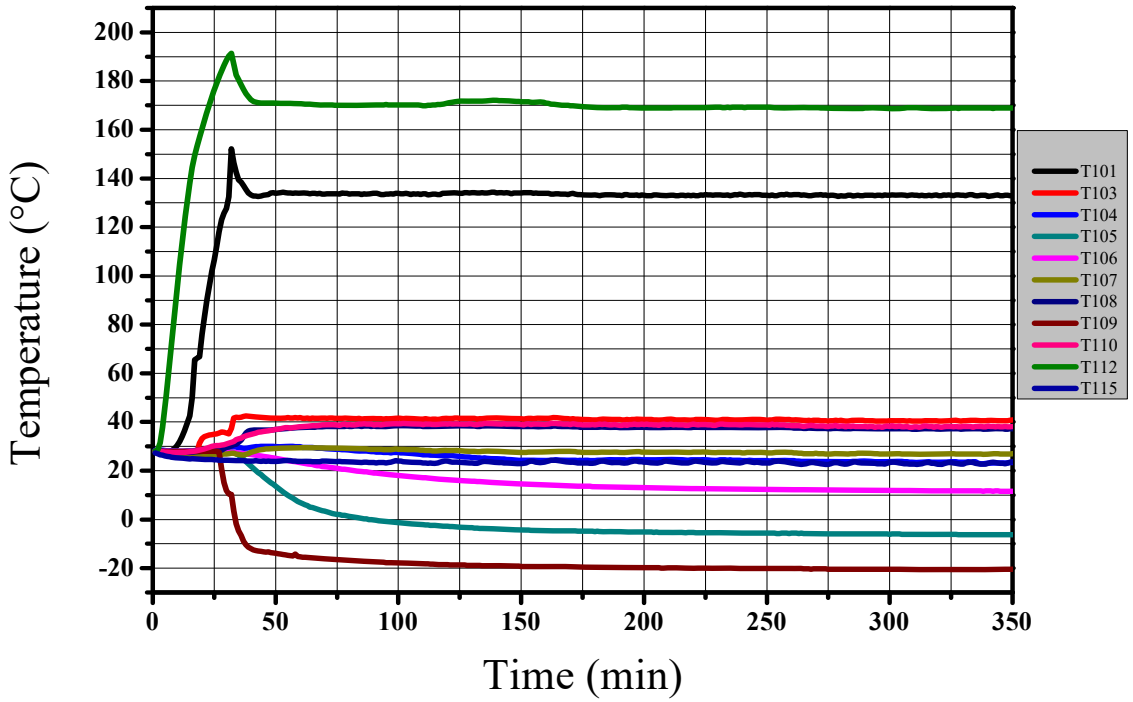

Figure 5.8. Temperature evolution in various machine components (Generator heat supply $\dot{Q}_{gen}$= 51W).

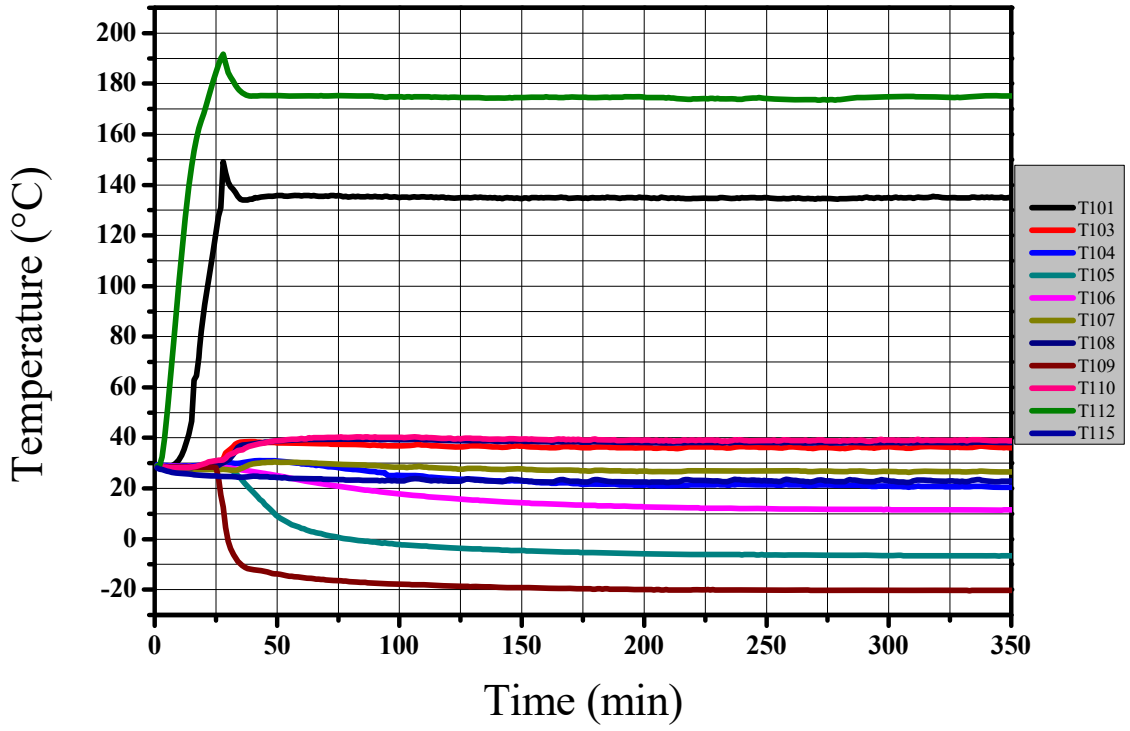

Figure 5.9. Temperature evolution in various machine components

(Generator heat supply $\dot{Q}_{gen}$= 56W).

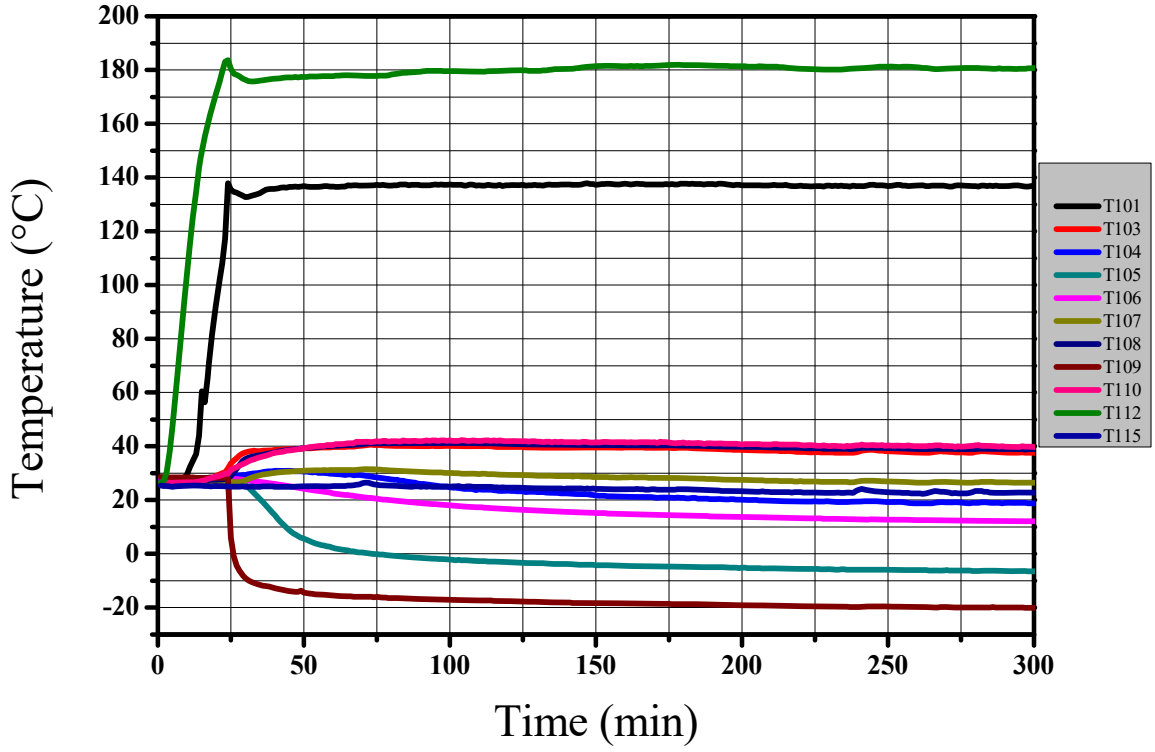

Figure 5.10. Temperature evolution in various machine components

(Generator heat supply $\dot{Q}_{gen}$= 61W).

5.4.2 Determination of the overall heat transfer coefficient $(UA)_{cab}$ of the refrigerated room

The overall heat transfer coefficient $(UA)_{cab}$ of the refrigerated room is determined applying a standardized procedure in a separate test set with the refrigerator shut down. To this purpose, the refrigerated room (cabinet) of the refrigerator was heated by an electric resistance cable (R = 135Ω) placed inside. This heater is connected to a power controller in order to vary the supplied electric power. By varying the tension of the electric current flowing in the resistance cable φ: 17, 20, 22, 26, 28, 30 and 32 V. For each test, the indoor and outdoor temperatures were measured.

When the steady-state regime is reached, the indoor temperature becomes constant, i.e. the heat generated in the electric resistance cable $\dot{Q}_{heat} = \left[{\varphi^2}/{R}\right]$ is equal to the total heat losses $\dot{Q}_{loss}$ from the refrigerated room (Eq5. 1):

$$\dot{Q}_{loss} = (UA)_{cab}(T_{int} - T_{amb}) \qquad (5.1)$$

From which it follows:

$$(UA)_{cab} = \frac{\dot{Q}_{heat}}{(T_{int} - T_{amb})} = \frac{\left[{\varphi^2}/{R}\right]}{(T_{int} - T_{amb})} \qquad (5.2)$$

T_{int} and T_{amb} refer to the measured steady state temperature in the indoor of the refrigerated room on one side, and the temperature in the outdoor of the refrigerated room, on the other side.

The experimental value of $\dot{Q}_{heat}$ are then represented *vs.* the temperature difference $(T_{int} - T_{amb})$ in Figure 5.11. The slope of the regression line representing is the average value of $(UA)_{cab} = 0.554\ \mathrm{WK^{-1}}$ with an absolute uncertainty of $\pm 0.01\ \mathrm{WK^{-1}}$. This internal heat

transfert property of the refrigerator is evaluated at steady-state regime of cooling. In this case the energy balance of the cabinet leads to:

$$\dot{Q}_{loss} = \dot{Q}_{evap} \qquad (5.3)$$

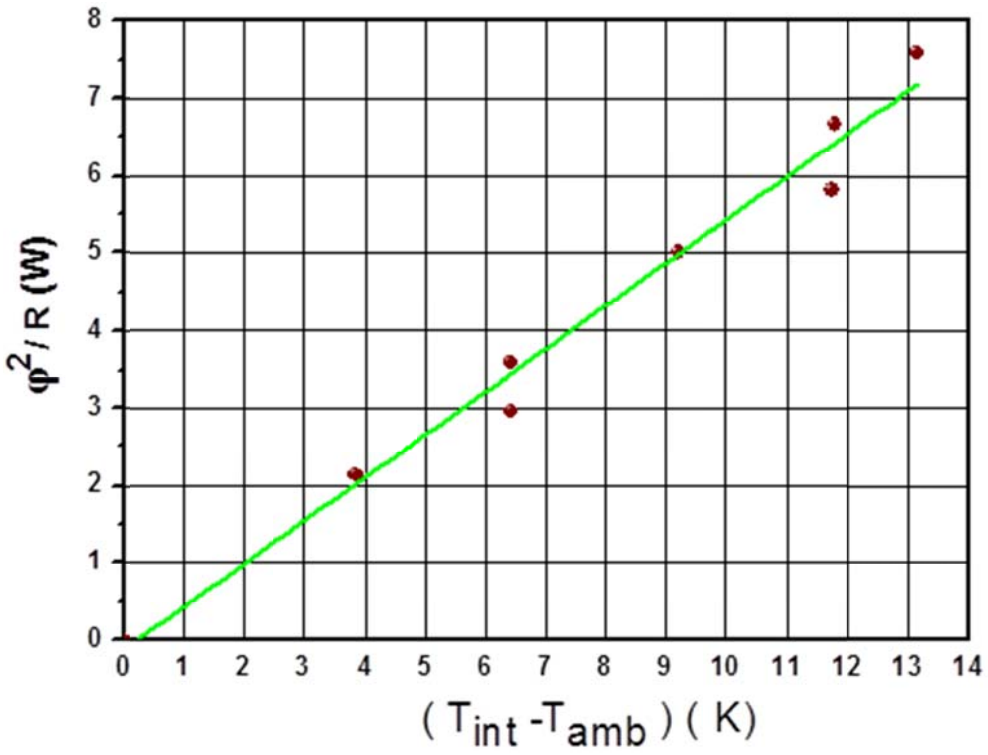

Figure 5.11. $\left[\varphi^2/_R\right]$ *vs.* $(T_{int} - T_{amb})$.

5.4.3. Estimation of the overall heat transfer coefficient $(UA)_{int}$ of the evaporator

The cooling capacity $\dot{Q}_{evap}$ is written as:

$$\dot{Q}_{evap} = (UA)_{int}\Delta T_{LMevap} \qquad (5.4)$$

ΔT_{LMevap} is the logarithmic mean temperature difference, LMTD, at the cold and hot sides of the evaporator,

$$\Delta T_{LMevap} = \frac{(T_{cab}-T_{out})-(T_{cab}-T_{in})}{\ln\left[\frac{(T_{cab}-T_{out})}{(T_{cab}-T_{in})}\right]} \qquad (5.5)$$

T_{cab}, $T_{out}$and T_{in} refer to the measured steady state temperature in the refrigerated room on one side, and the refrigerant temperature at the outlet and inlet of the evaporator, on the other side. $(UA)_{int}$ in Equation (5.4), is the heat transfer capacity of the evaporator. At steady state, the refrigerator energy balance writes $\dot{Q}_{cab} = \dot{Q}_{int}$, where $\dot{Q}_{cab}$, obtained from Equation (5.5), represents the rate of heat infiltration in the refrigerator's cabin from outside.

$$\dot{Q}_{cab} = (UA)_{cab}(T_{amb} - T_{int}) \qquad (5.6)$$

It follows then,

$$(UA)_{cab}(T_{amb} - T_{int}) = (UA)_{int}\Delta T_{LMevap} \qquad (5.7)$$

Or

$$\frac{(UA)_{cab}}{(UA)_{int}} = \frac{\Delta T_{LMevap}}{(T_{amb} - T_{int})} \qquad (5.8)$$

The last equation (5.8) indicates that the ratio $\frac{(UA)_{cab}}{(UA)_{int}}$can be deduced by plotting for various heating power supplied to the generator $(T_{amb} - T_{int})$ *vs.* ΔT_{LMevap}. It was found that $\frac{(UA)_{cab}}{(UA)_{int}} = 1.846$ with an absolute uncertainty of ±0.04.

As the value of $(UA)_{cab}$ has been already determined (0.554 WK^{-1}), the internal overall heat transfer coefficient of the evaporator, $(UA)_{int}$, can then readily be deduced $(UA)_{int} =$ 0.3 $WK^{-1}$with an absolute uncertainty of ±0.01 WK^{-1}.

5.4.4. Determination of the refrigerator's performances

The performance of the machine is evaluated using the, coefficient of performance(COP)

$$COP = \frac{\dot{Q}_{evap}}{\dot{Q}_{gen}} \qquad (5.9)$$

With $\dot{Q}_{gen}$, generator heat supply and $\dot{Q}_{evap}$, the cooling capacity.

Once the internal and external heat transfer coefficients determined, the cooling capacity and the COP were calculated by applying Equations (5.4) and (5.9), the relative uncertainty being around 4%. The results are represented in Figures 5.12 and 5.13. As Figure 5.12 illustrates, by increasing the heating power supplied to the generator, from 35W on, the cooling capacity first increases, reaches a value of 7.3W for a power supply of 46W and then remains approximately constant.

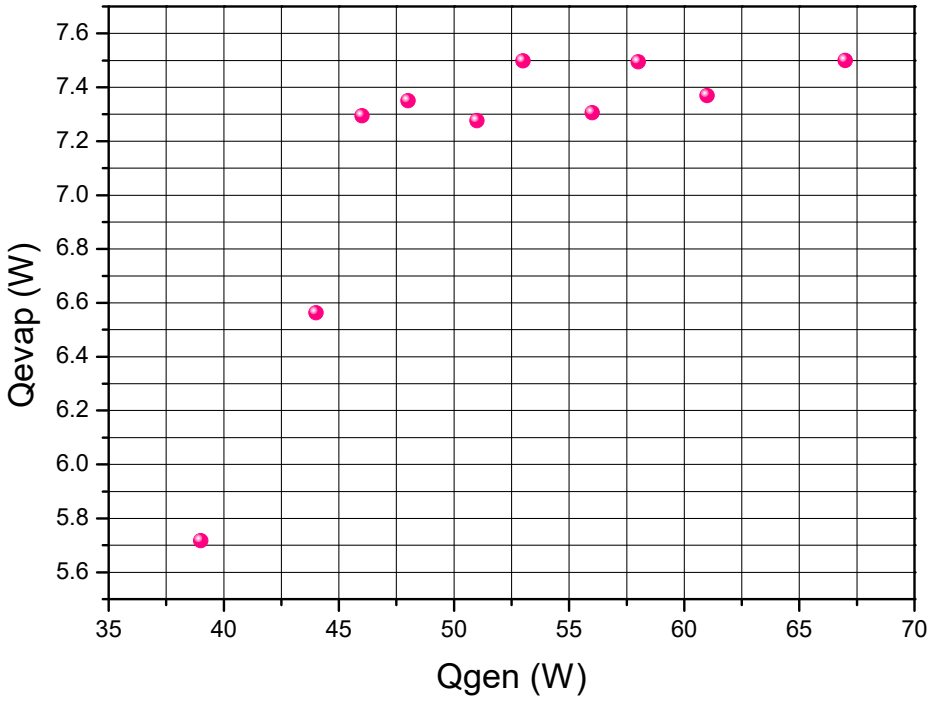

Figure 5.12. $\dot{Q}_{evap}$vs. $\dot{Q}_{gen}$.

From the trend of the COP thus depicted, it is noted that it increases first concomitantly with the refrigeration capacity for low values of the generator energy supply, reaches a maximum of 0.159, with a power supply of 46W and a generator temperature of 167°C, and then decreases gradually.

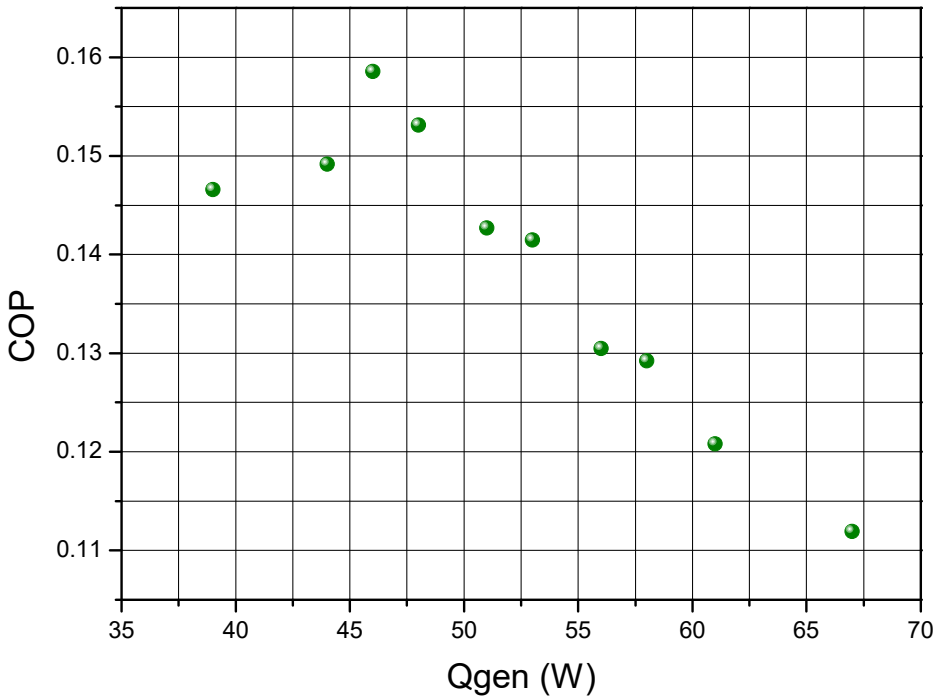

Figure 5.13. COP *vs.* $\dot{Q}_{gen}$.

In fact, by increasing the heating power supplied to the generator, the flow rates of the pumped solution and the refrigerant vapor increase simultaneously, and this leads to a progressively greater cooling capacity. On the other hand, a larger flow rate of the pumped solution allows for the absorption of a greater quantity of refrigerant vapor in the absorber. This explains the initial growth of the cooling capacity and, as a result, the concomitant increase of the coefficient of performance. Further increase of the energy supply does not lead to an improvement of the COP, rather its deterioration (Figure 5.13), because the cooling capacity comes to a stagnation point as Figure 5.12 shows. It can then be concluded that it is not necessary to apply more than 46W to ensure the functioning of the refrigerator investigated. Figure 5.14 illustrates the variation of temperature measured at 11 locations of the refrigerator from the start-up until the steady state regime for the optimal heating power supply.

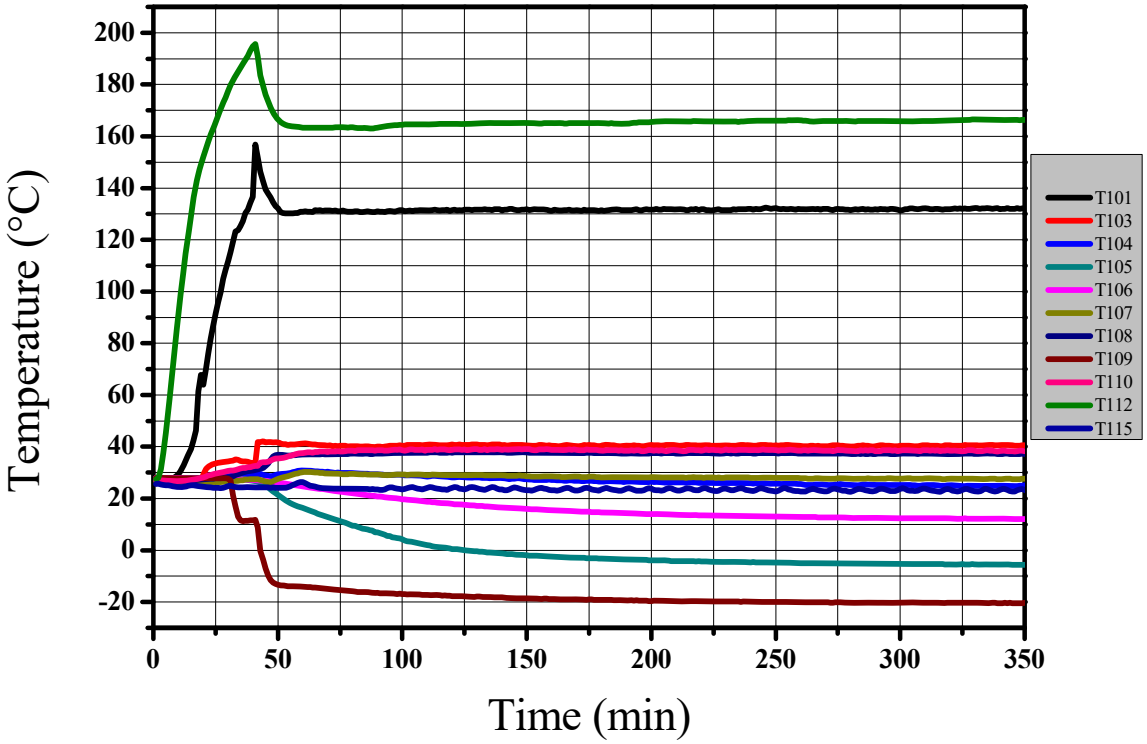

Figure 5.14. Temperature evolution in various refrigerator components (Generator heat supply $\dot{Q}_{gen}$= 46W).

5.5. Conclusion

In this chapter, a commercial diffusion-absorption refrigerator was tested under different heat inputs to the generator. The temperature at the inlet and outlet of every component was continuously recorded. The results show that a heat supply to the generator over 35W is required to ensure the functioning of the commercial (DAR) refrigerator and its stability. All the essential features of the refrigerator were determined experimentally, especially the overall heat transfer coefficients of the refrigerator's cabinet and that of the evaporator, respectively $(UA)_{cab} = 0.554\ \mathrm{WK^{-1}}$ and $(UA)_{int} = 0.3\ \mathrm{WK^{-1}}$. The best performance of the refrigerator was reached experimentally with an electric power supply of 46 W and a generator temperature of 167°C. The machine COP was found to be 0.159.

Chapter 6

Steady-state modeling of a small capacity diffusion-absorption refrigerating (DAR) machine

6.1. Introduction

Over the years, several studies have been focused on the performances of various diffusion-absorption refrigerator (DAR) cycles using graphical, numerical and experimental approaches. It is worth to note however that diffusion-absorption refrigeration systems were modeled in a variety of previous investigations using ad hoc programs but never with the process simulator Aspen-Plus Platform. To fill this gap, we propose to develop a steady state modeling of a low capacity commercial diffusion-absorption refrigerator using the software. The "Break point" approach applied in chapter 4 for the Robur chiller and used by Somers *et al.* [113] to simulate the conventional H_2O-LiBr absorption cooling cycles is used also in the present chapter to develop the refrigerator model. The theoretical model predictions are compared with the experimental data collected on the considered refrigerator at heating powers supply to the generator of 46W, 56W and 67W.

6.2. Aspen-Plus modeling of the diffusion-absorption refrigerator (DAR)

In a first step, the main assumptions and operating conditions used as inputs in the simulations were based on our experimental study carried out in a steady state regime for a heating power supply of 46 W. The state points' assumptions for the refrigerator simulation are summarized in Table 6.1.

Table 6.1. State point assumptions for the DAR simulation.

State point	Assumption
101	Determined by the generator model
103	Determined by the condenser model
104	Determined by gas heat exchanger model
105	Determined by the evaporator model
107	Determined by the absorber and solution tank model
108	Determined by the absorber model
109	Determined by gas heat exchanger model
110	Determined by the solution tank model
112	Determined by the generator model

6.2.1. Diffusion-absorption refrigerator model

Figure 6.1 shows a schematic representation of the diffusion-absorption refrigerator investigated. Material streams connecting the various components of the refrigerator are identified by their IDs given in Table 5.1, which are the same IDs given to the thermocouples placed at different locations in the refrigerator (chapter 5). The state points in the refrigerator are defined as follows. The vapor in the stream leaving the absorber in its way to the gas heat exchanger (GHX) through the solution tank is state point 107. The state point from the gas heat exchanger (GHX) exit to the evaporator is state point 109; the state point from the evaporator exit to the gas heat exchanger (GHX) is state point 105; the state point from the gas heat exchanger (GHX) exit to the absorber is state point 104. The state point from the absorber exit to the solution tank is state point 108; the state point from the solution tank exit to the solution heat exchanger (SHX) is state point 110. The state point from the generator exit to the solution heat exchanger (SHX) is state point 112; the state point from the generator

exit to the rectifier is state point 101, and the state point from the condenser exit to the gas heat exchanger (GHX) is state point 103.

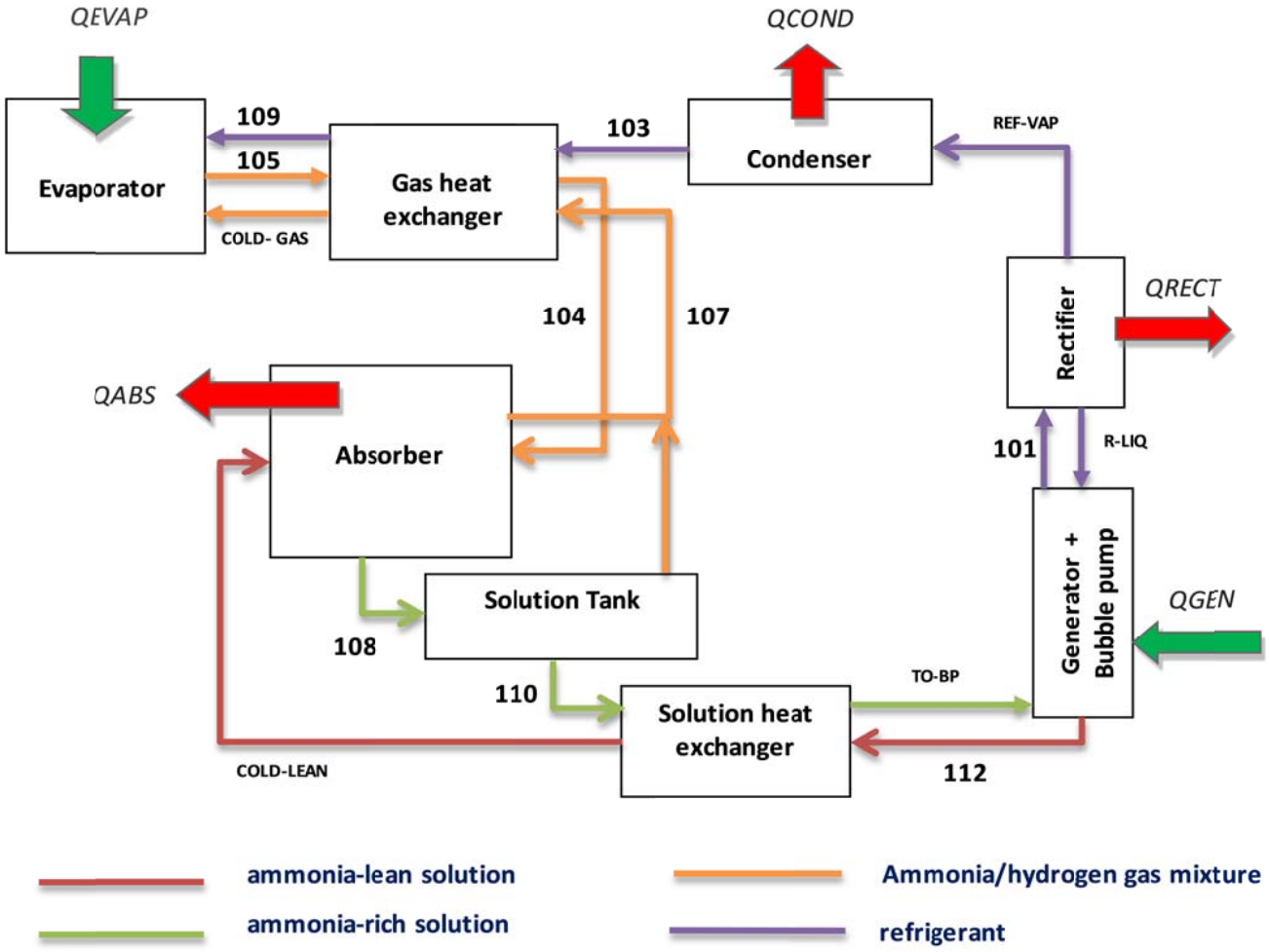

Figure 6.1. Schematic representation of the diffusion-absorption refrigerator.

6.2.2. Component models and input data

The development of a running model for a diffusion-absorption refrigerator in the Aspen-Plus environment is based on the appropriate selection of the equivalent blocks for the main components of the refrigerator. The models used for the components of the DAR machine simulated in this thesis are described in the following sub-sections.

The Aspen-Plus model developed for the diffusion-absorption refrigerator is shown in Figure 6.2. Tables 6.2 and 6.3 summarize the Aspen-Plus blocks used for the refrigerator's components and the corresponding input data, respectively.

Table 6.2. Aspen-Plus blocks used for the refrigerator's components.

Component	**Aspen-Plus Block**
Condenser (CNDNSER)	HEATER
Evaporator (EVAP)	HEATER
	MIXER
Absorber (ABSORBER)	ABSORBER
Solution heat exchanger (SOL-HX)	HEATX (Two-flow heat exchanger)
Generator (GEN)	REBOILED STRIPING BLOCK (STRIP1)
Rectifier (RECT)	RECTIFIER
TANK (TANK)	FLASH
	MIXER
Gas heat exchanger (GGHX)	LNG-HX (Three-flow heat exchanger)
Bubble pump	FLASH
	HEATER

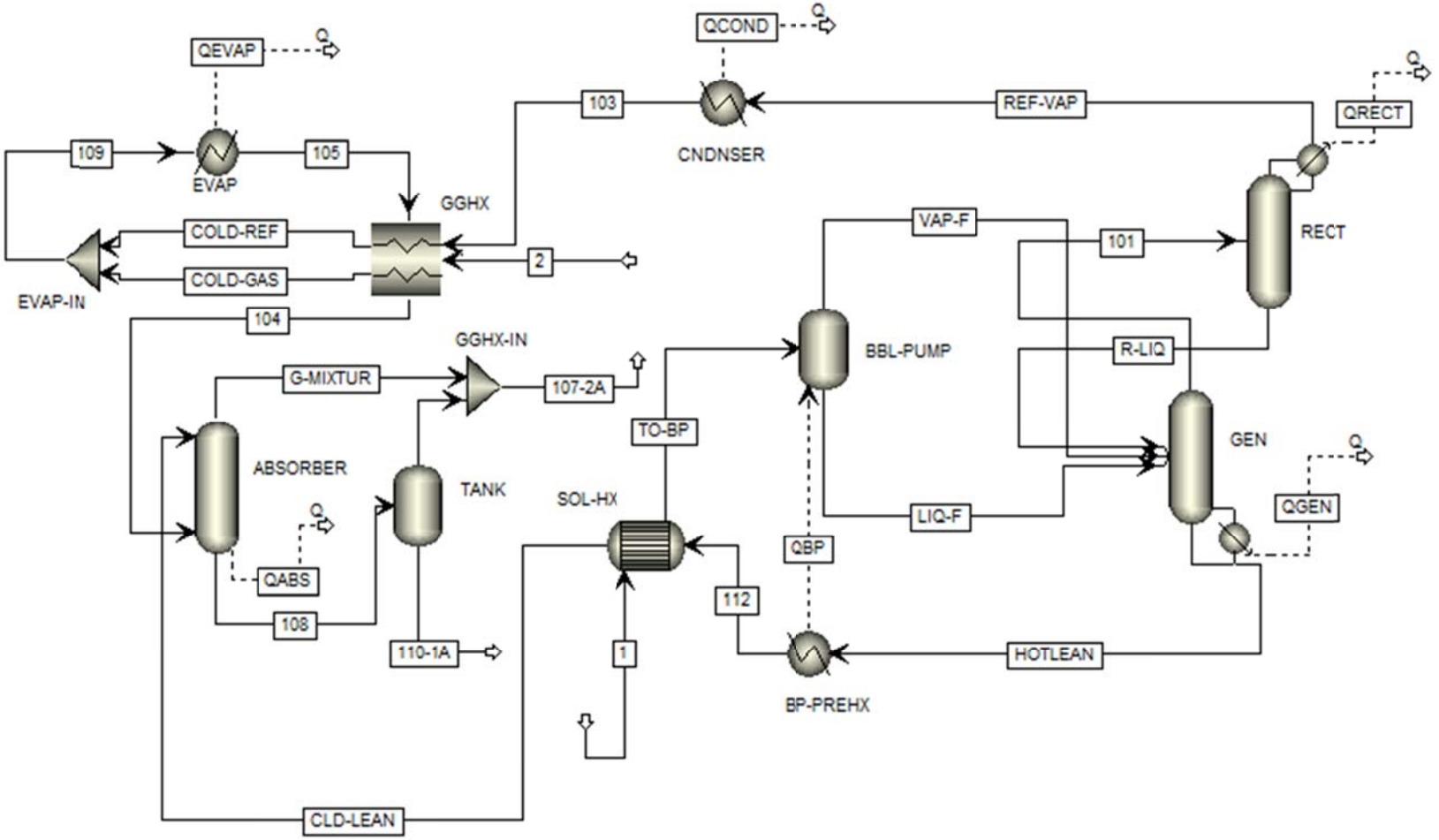

Figure 6.2. Model of the diffusion-absorption refrigerator in Aspen-Plus.

Table 6.3. Inputs used in the models of the refrigerator's components.

Block	Input
Solution heat exchanger	Cold stream outlet temperature, 110°C **Specifications of state point 1:** o Pressure = 25 bar o Temperature = 38.4°C o Total mass flow = 0.190 kg/h o NH_3 mass fraction = 0.35 o H_2O mass fraction = 0.65 o H_2 mass fraction = 0
Generator	Mass reflux ratio, 0.01 Heat duty, 46 W
Rectifier	Distillate mass rate, 0.049 kg/h
Condenser	Outlet temperature, 35°C
Gas heat exchanger	Temperature difference: inlet - outlet of stream103, -30°C Temperature difference: inlet - outlet of stream 2, -22°C **State point 2** o Pressure = 25 bar o Temperature = 27.5°C o Total mass flow = 0.019 kg/h o NH_3 mass fraction = 0.083 o H_2O mass fraction = 0.01 o H_2 mass fraction = 0.907
Evaporator	Temperature outlet, -5.6°C
Thank	Temperature, 38.4°C

- **Solution heat exchanger**

As shown in Figure 6.3, a two-flow heat exchanger HEATX model is used for the solution heat exchanger (SOL-HX) connecting the streams (state point 1 - state point TO-BP) and (state point 112 – state point CLD-LEAN). The inputs data for the solution heat exchanger (SOL-HX) model are:

- Cold stream outlet temperature, state point TO-BP = 110°C
- Specifications of the state point 1:
  - Temperature = 38.4°C
  - Total mass flow = 0.190 kg/h
  - NH_3 mass fraction = 0.35
  - H_2O mass fraction = 0.65
  - H_2 mass fraction = 0

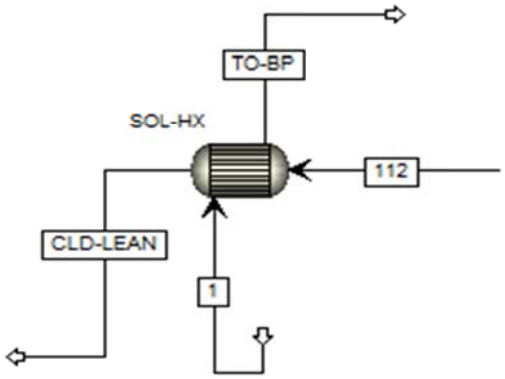

Figure 6.3. Solution heat exchanger (SOL-HX) model in Aspen-Plus.

- **Gas heat exchanger**

As regards the Gas heat exchanger (G-HX), a three-flow heat exchanger LNG-HX model is used to connect the streams (state point 105 – state point 104), (state point 103 – state point COLD-REF) and (state point 2 – state point COLD-GAS) (Figure 6.4). The inputs data for the gas heat exchanger (G-HX) model are:

- Temperature difference in the stream (103 – COLD-REF = -30°C
- Temperature difference in the stream (2 – COLD-GAS) = -22°C
- Specifications of the state point 2:
  - Temperature = 27.5°C

- Total mass flow = 0.019 kg/h
- NH_3 mass fraction = 0.083
- H_2O mass fraction = 0.01
- H_2 mass fraction = 0.907

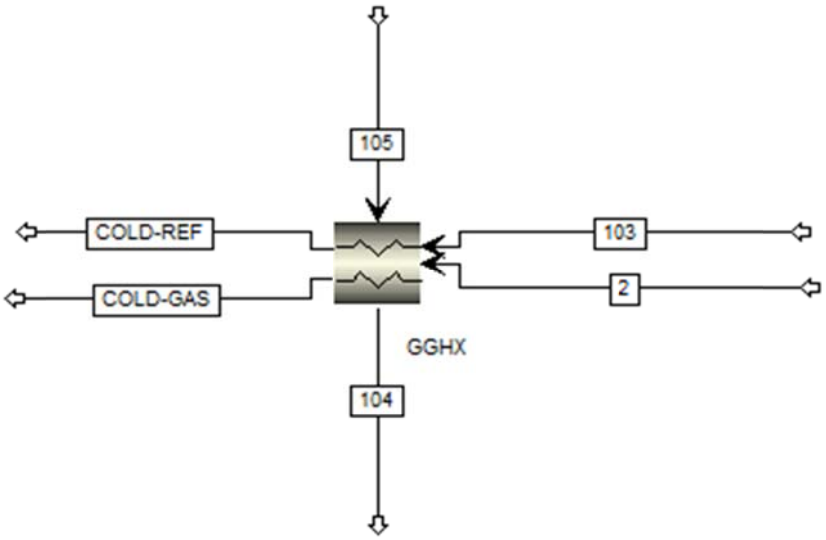

Figure 6.4. Gas heat exchanger (G-HX) model in Aspen-Plus.

- **Generator**

As shown in Figure 6.5, a REBOILED STRIPPING block is used for the generator (GEN). The streams entering the generator are: VAP-F, LIQ-F and R-LIQ. The streams HOT-LEAN and 101 leave the generator at the bottom and the top, respectively. The inputs data in the generator (GEN) model are:

- Mass reflux ratio = 0.01
- Generator heat duty, $\dot{Q}_{gen}$= 46W

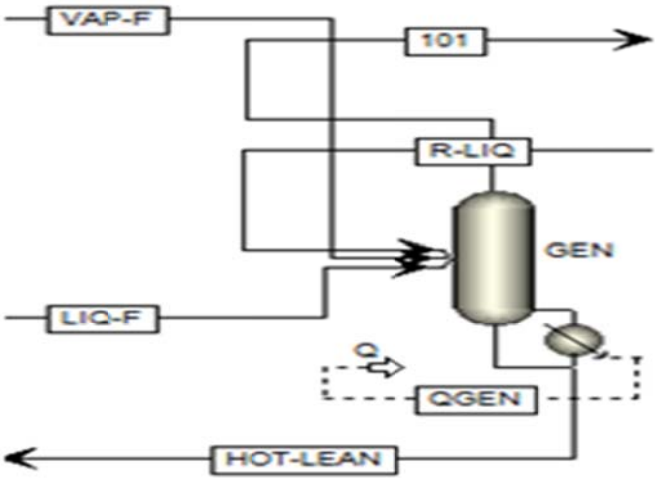

Figure 6.5. Generator (GEN) model in Aspen-Plus.

- **Bubble pump**

The bubble pump (BBL-PUMP) is modeled by combining a FLASH and a HEATER block connected with a hot stream (Figure 6.6). State point TO-BP represents the stream entering the bubble pump. State point VAP-F and state point LIQ-F represent the streams leaving the bubble pump streams outlet.

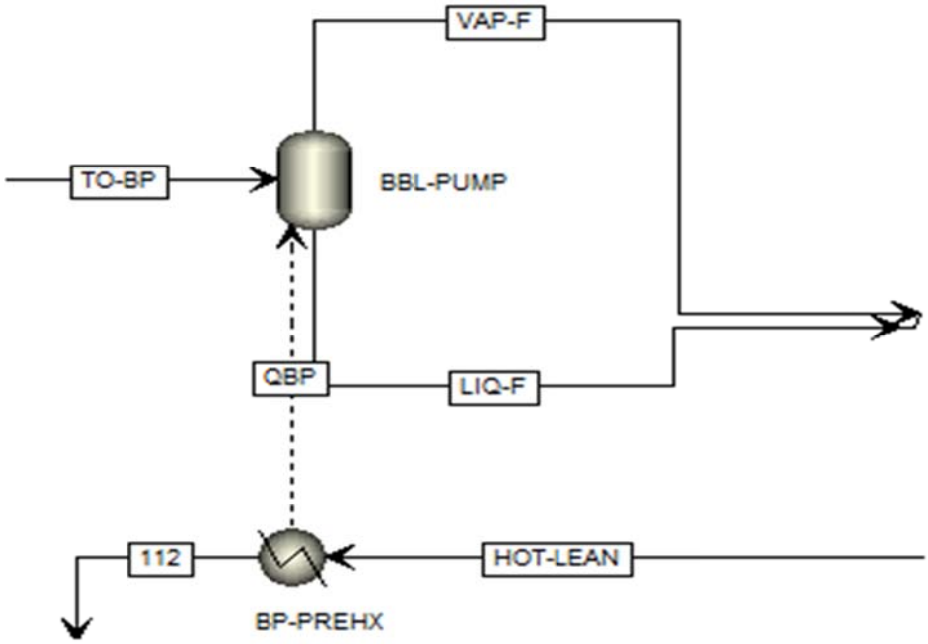

Figure 6.6. Bubble pump (BBL-PUMP) model in Aspen-Plus.

- **Rectifier**

The rectifier (RECT) is modeled using a RECTIFIER block (Figure 6.7). State point 101 represents the stream entering the rectifier. State points R-LIQ and REF-VAP represent the streams at the rectifier outlet. The inputs data in the rectifier (RECT)model are:

- Distillate mass rate = 0.049 kg/h

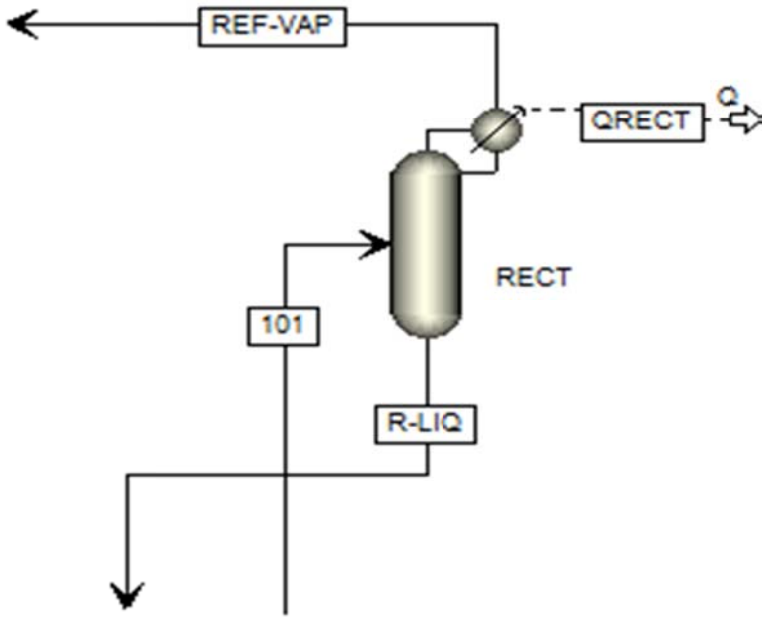

Figure 6.7. Rectifier (RECT) model in Aspen-Plus.

- **Absorber**

As shown in Figure 6.8, the absorber (ABSORBER) is modeled using an ABSORBER block. State points 101 and COL-LEAN represent the streams entering the absorber. State points G-MIXTURE and 108 represent the streams at the absorber outlet.

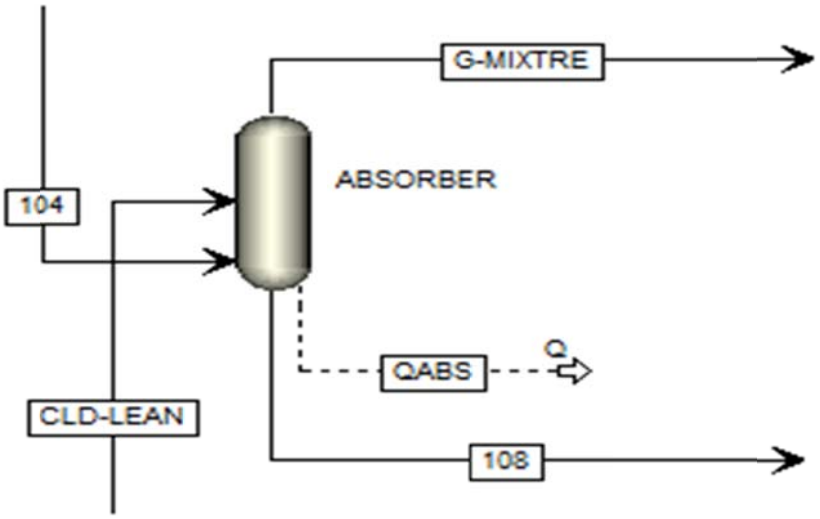

Figure 6.8. Absorber (ABSORBER)model in Aspen-Plus.

- **Solution Tank**

The solution tank (TANK) is modeled using a combination of a FLASH and a MIXER (Figure 6.9). State points 108 and G-MIXTURE represent the inlet streams in the solution tank. The streams leaving the solution tank are represented by the state points 107-2A and 110-1A. The input data in the solution tank (TANK) model is:

- ❑ Temperature outlet = 38.4°C

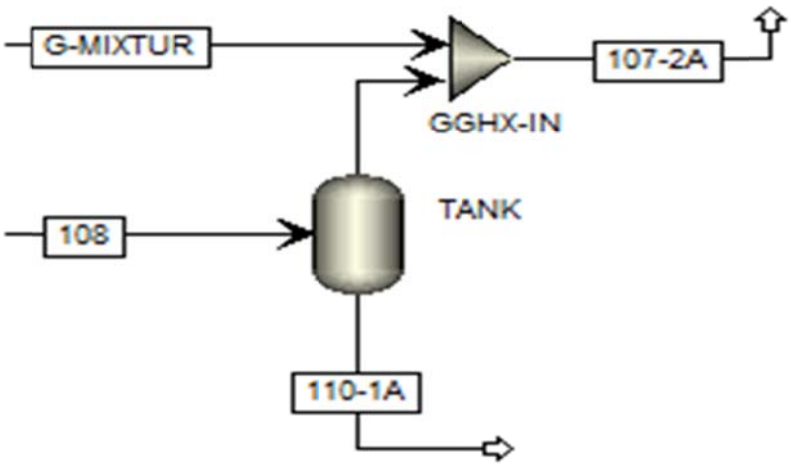

Figure 6.9. Solution tank (TANK) model in Aspen-Plus.

- **Condenser**

Regarding the condenser (CNDENSER), a HEATER block is used between the state points REF-VAP and 103 (Figure 6.10). The input data for the condenser (CNDENSER) model is:

- ❑ Outlet temperature = 35°C

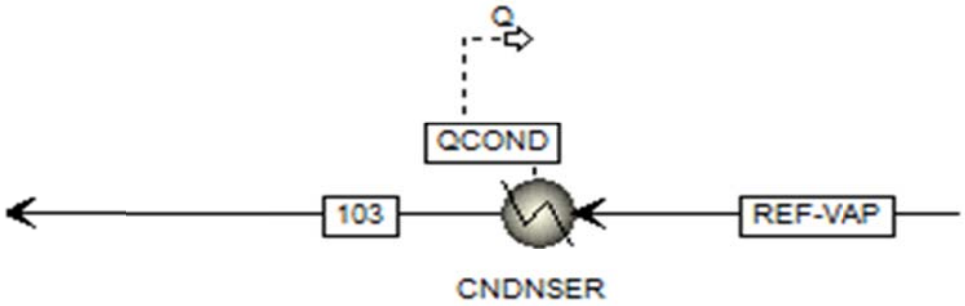

Figure 6.10. Condenser (CNDENSER) model in Aspen-Plus.

- **Evaporator**

A HEATER block is used for the evaporator (EVAP) between the state points 109 and 105 (Figure 6.11). The input data in the evaporator (EVAP) model is:

- ❑ Outlet temperature = -5.6°C

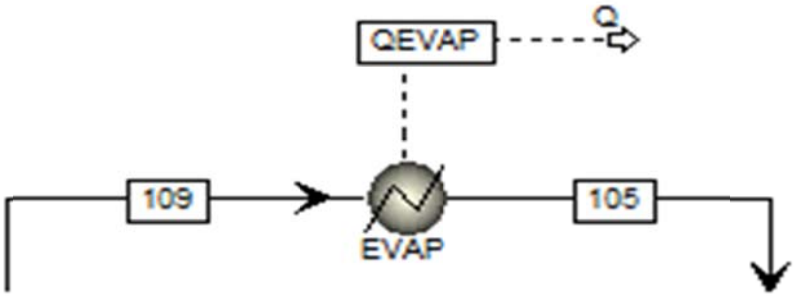

Figure 6.11. Evaporator (EVAP) model in Aspen-Plus.

6.2.3. Simulation procedure

The refrigerator model developed in this chapter uses, in a first step, a sequential modular approach in which each block is calculated separately. Two "Break points" are used in the sequential approach. The first "break" is inserted at state point 1 (ammonia-rich solution flowing to the solution heat exchanger), and the second "break" at state point 2 (ammonia/hydrogen gas mixture flowing to the gas heat exchanger). The identity of state point 1 on one side and state points 2 on the other side represent the same state points 100-1A and 107-2A, respectively. Therefore, state point 110-1A should have the same characteristics as those given as inputs at the inlet of the solution heat exchanger (ammonia-rich solution flowing to the solution heat exchanger) after the simulation is run. Also, state point 107-2A should have the same characteristics as those given as inputs at the inlet of the gas heat exchanger (ammonia/hydrogen gas mixture flowing to the gas heat exchanger) after the simulation is run. These two "Break points" constitutes the simulation convergence criterion in the sequential approach.

After convergence and synchronization, the Equation-Oriented (EO) approach is used, in a second step, to solve simultaneously in one block the governing equations of the refrigerator.

6.3. Results and discussion

As mentioned previously, in a first step to validate the Aspen-Plus model developed for the diffusion-absorption refrigerator, the measured data for a heating power of 46W are used. The corresponding simulation results are summarized in Table 6.4.

Figure 6.12 shows a graphical comparison between the measured and model calculated temperatures at 9 locations of the machine.

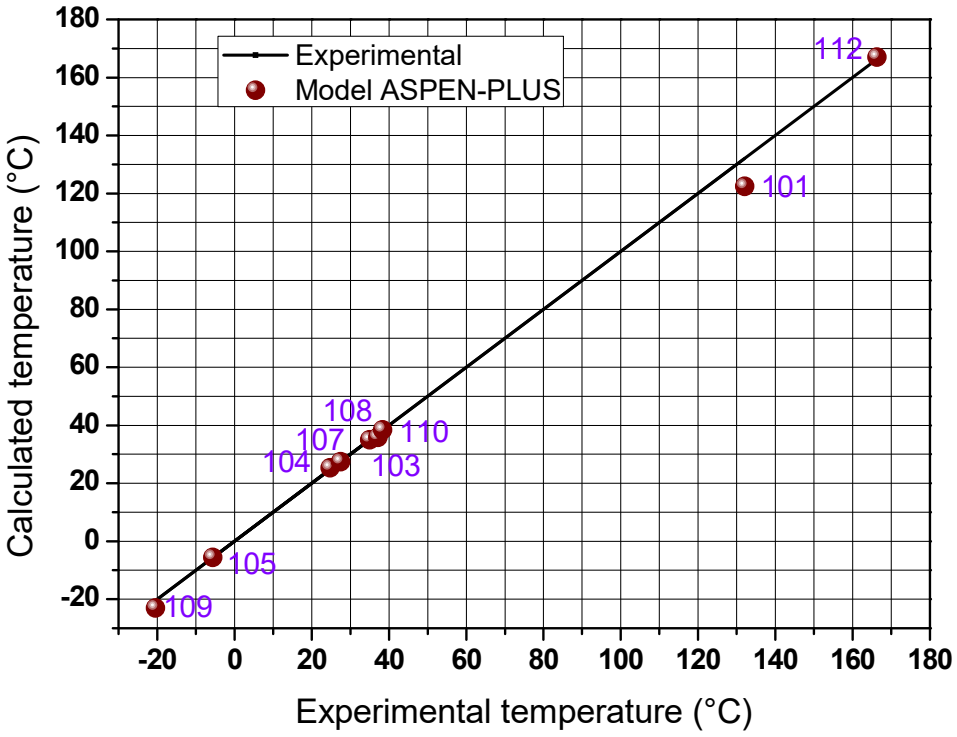

Figure 6.12. Comparison between calculated and experimental temperatures for $\dot{Q}_{gen}$=46W.

As can be noticed, this comparison shows excellent agreement between the theoretical model predictions and the experimental data.

Similar results are found when the performance parameters of the DAR machine are compared (Table 6.5): The deviations between predicted and measured COP and cooling capacity are less than 1%.

Table 6.5. Calculated and experimental performance parameters of the DAR machine.

Parameter	Experimental	Calculated
$\dot{Q}_{gen}$ (kW)	46	46
$\dot{Q}_{evap}$ (kW)	7.29	7.27
COP	0.159	0.158

Table 6.4. Simulation results of the diffusion-absorption refrigerator using the Aspen-Plus model for $\dot{Q}_{gen}$= 46W.

State point	From	To	*P* (bar)	*T* (°C)	Vapor fraction	Mass flow rate (kg/h)	NH_3 mass fraction (%)	H_2O mass fraction (%)	H_2 mass fraction (%)
1A	TANK	SOL-HX	25	38.4	0	0.190	35	65	0
107-2A	GGHX-IN	GGHX	25	27.5	1	0.019	8.3	1	90.7
101	GEN	RECT	25	122.4	1	0.091	94.5	5.5	0
REF-VAP	RECT	CNDNSER	25	62	1	0.049	99.9	0.1	0
103	CNDNSER	GGHX	25	35	0	0.049	99.9	0.1	0
COLD-REF	GGHX	EVAP-IN	25	5	0	0.049	99.9	0.1	0
COLD-GAS	GGHX	EVAP-IN	25	5.5	1	0.019	8.3	1	90.7
109	EVAP-IN	EVAP	25	-23	0.798	0.068	74.6	0.3	25.1
105	EVAP	GGHX	25	-5.6	0.873	0.068	74.6	0.3	25.1
104	GGHX	ABSORBER	25	25.3	0.997	0.068	74.6	0.3	25.1
COLD-LEAN	SOL-HX	ABSORBER	25	71.1	0	0.141	12.4	87.6	0
G-MIXTURE	ABSORBER	GGHX-IN	25	27.5	1	0.019	8.3	1	90.7
108	ABSORBER	TANK	25	35.8	0	0.190	35	65	0
110-1A	TANK	SOL-HX	25	38.4	0	0.190	35	65	0
112	BP-PREHX	SOL-HX	25	167	0	0.141	12.4	87.6	0
TO-BP	SOL-HX	BBL-PUMP	25	110	0	0.190	35	65	0
LIQ-F	BBL-PUMP	GEN	25	128.3	0	0.187	34.1	65.9	0
VAP-F	BBL-PUMP	GEN	25	128.3	1	0.003	91.2	8.8	0
HOT-LEAN	GEN	BP-PREHX	25	191.3	0	0.141	12.4	87.6	0
R-LIQ	RECT	GEN	25	64.1	0	0.042	88.1	11.9	0

In Figure 6.13 the thermodynamic cycle of the DAR machine is plotted on the Dühring diagram of the ammonia/water fluid mixture. As the whole process is taking place at a constant pressure of 25 bar, the pressure read from the diagram is significant only for liquid-vapor phase equilibrium considerations. The blue line represents the circulation of the aqueous solution of ammonia between the generator and the absorber. As indicated, the saturated ammonia-lean solution leaves the generator with an ammonia mass fraction of 12.4%, and the ammonia-rich solution the absorber with 35% mass fraction. The refrigerant vapor exits the generator at 122.4ºC and the rectifier at 62ºC. The subcooled condensate leaves the condenser at 35ºC. The evaporation process is carried out at increasing ammonia partial pressure, *i.e*. with increasing evaporation temperature so that at the evaporator exit the temperature is -5.6ºC.

In a second step, the developed Aspen-Plus model is tested for two other heating powers: 56W and 67W. Figures 6.14 and 6.15 illustrate the comparison between model predictions and measured temperatures at 9 locations of the machine for these heating rates, respectively. The figures show that the values predicted by the developed steady state Aspen-Plus model are close to the experimental data. The deviations between the predicted and measured COP and cooling capacity are also less than 1%. All these results validate the Aspen-Plus model developed for the small capacity commercial diffusion-absorption refrigerator investigated.

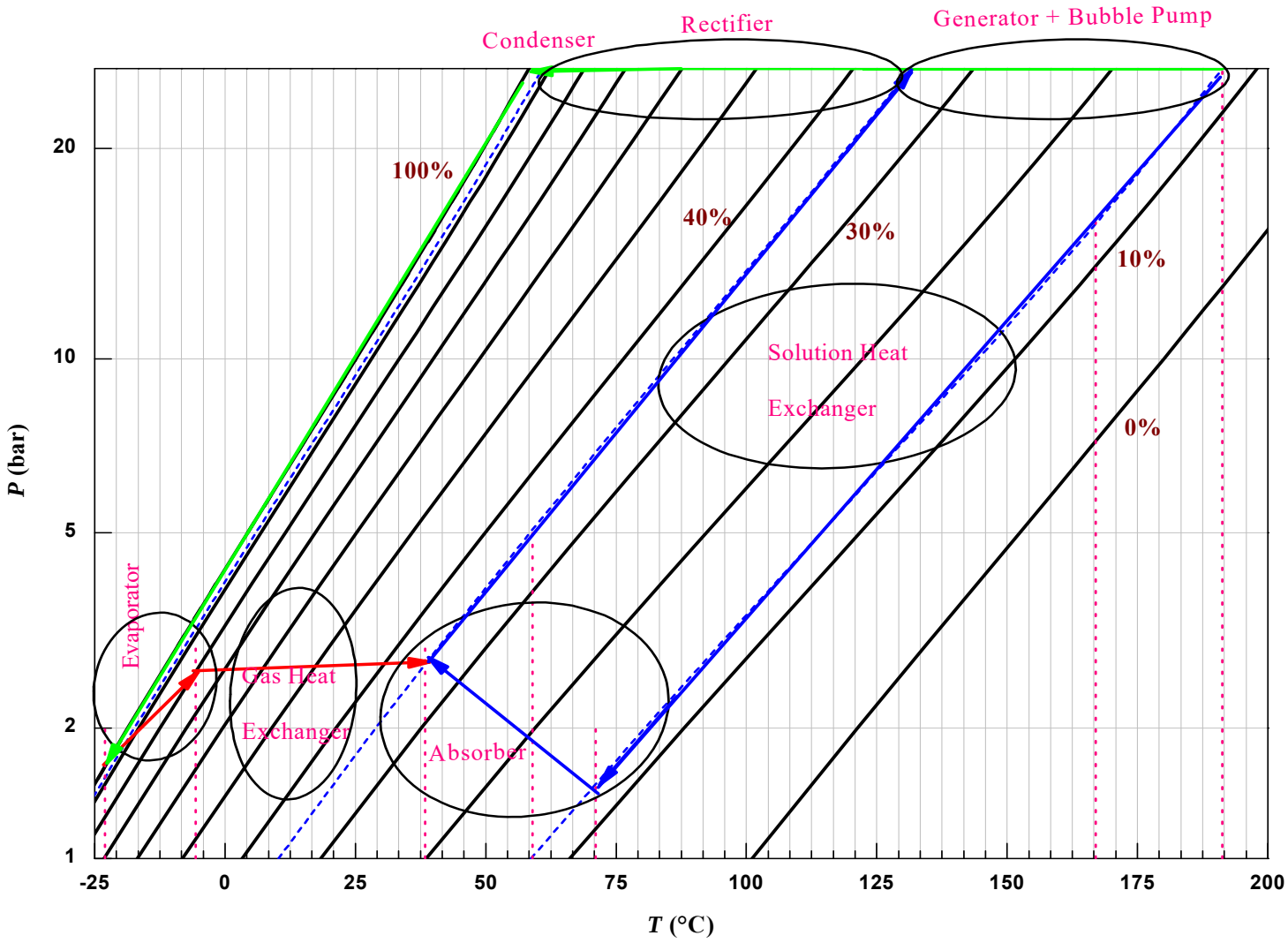

Figure 6.13. DAR cycle on Dühring diagram.

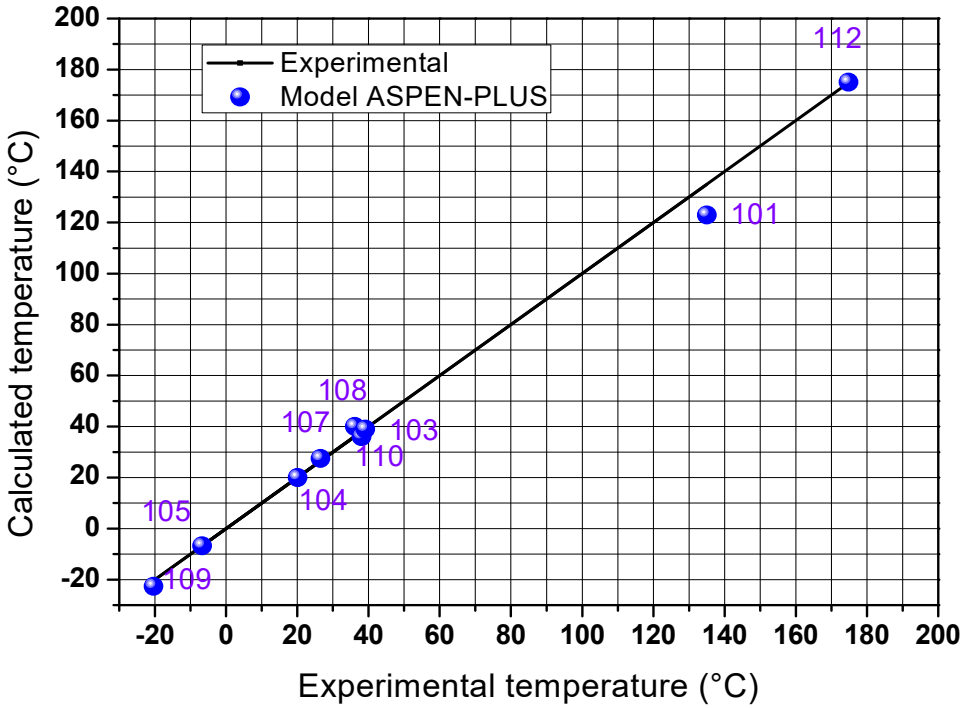

Figure 6.14. Comparison between calculated and experimental temperatures for $\dot{Q}_{gen}$=56W.

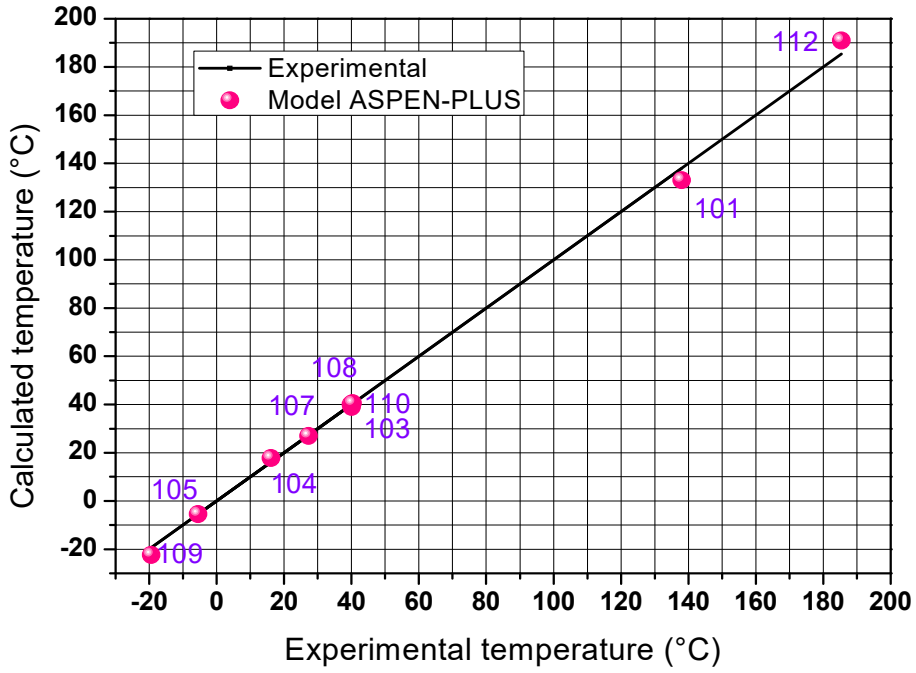

Figure 6.15. Comparison between calculated and experimental temperatures for $\dot{Q}_{gen}$=67W

6.4. Conclusion

In this chapter, an Aspen-Plus steady-state model for a small capacity diffusion-absorption refrigerator was developed. For the simulations, as well as the operating conditions, a set of assumptions based on the machine experimental tests were introduced as inputs. The calculated results for the heating rates 46W, 56W and 67W were well in agreement with the measured temperatures. The deviations between predicted and measured COP and cooling capacity were less than 1%. This indicates that the model developed represents fairly well the functioning of the commercial diffusion-absorption refrigerator working under a steady-state regime.

Chapter 7

Dynamic modeling and operational analysis of a small capacity diffusion-absorption refrigerating (DAR) machine

7.1. Introduction

The majority of published works on diffusion absorption refrigeration systems available in the literature deals with steady-state modeling associated or not to experimental tests, but few investigations have been performed on the dynamic behaviour of this kind of refrigeration system. In fact, most of the studies published on the dynamic behaviour of cooling systems [114-122] do not deal with DAR systems. However, it is of great importance to understand the dynamic operation of these systems. The present chapter is a contribution to fill this gap by investigating the operation of DAR systems in dynamic mode. A black box dynamic model was developed to predict the refrigerator performance in terms of cooling capacity and COP. The model was based on experimental measurements taken from a small capacity commercial diffusion-absorption refrigerator reported in chapter 5. The specific objectives are as follows:

i. Development of a detailed black-box dynamic model for this refrigerator using Matlab Simulink® environment.
ii. Comparisons between experimental measurements and dynamic model predictions in terms of cooling capacity and COP;

7.2. Dynamic modeling of the diffusion-absorption refrigerator

Very often process models are derived from knowledge gained of the underlying process mechanisms and describe the physicochemical processes taking place in the system. These mechanistic termed "white box" models are developed for design and optimization applications.

Contrarily, empirical models are solely the result of experiments and observation and do usually not rely on the knowledge of basic principles and mechanisms. Equation fitting is then employed to determine the model parameters, which have little or no physical meaning. These so-called "black box" models are of purely descriptive nature and with limited ranges of application however, they do constitute helpful tools for process control and automation purposes.

In this kind of modeling, the pertinent information for model identification is obtained through exciting or stimulating the system. Structure and parameter estimation methods developed in the field of process identification are then used to establish the model. These two steps are however, not really independent, as the criterion of the choice of a model from a set of candidates with unknown parameters is the best fit for the measured data.

7.2.1. Black-Box of the refrigerator

Because material properties of the cabinet's walls and thermo-physical properties of ambient air outside the refrigerator were constant during the tests, and the mean properties of air inside the refrigerator can be assumed roughly unchanged, the obtained value of $(UA)_{cab}$ in chapter 5 was used to determine the instantaneous cooling capacity $\dot{Q}_f(t)$ from the start-up of the machine until reaching the steady-state regime (Eq. 7.1),

$$\dot{Q}_f(\mathrm{t}) = (UA)_{cab}(T_{int}(t) - T_{amb}) \qquad (7.1)$$

In fact at a constant ambient temperature, the heating power supplied to the generator is the unique input that affects the operation of the refrigeration unit. Hence, the input signal to the system is $\dot{Q}_{gen}(t)$:

$$\dot{Q}_{gen}(t) = \dot{Q}_{gen}F(t) \qquad (7.2)$$

where $F(t)$ is the unit step function.

The system response to this input is the cooling effect $\dot{Q}_f(\mathrm{t})$ achieved in the refrigerated room. In terms of system theory, the considered DAR unit is then a single-input, single-output (SISO) system. To develop a dynamic black-box model for the refrigerator, nine (repeated) tests with different inputs, i.e. the heat supply to the generator of the machine $\dot{Q}_{gen}(t)$, are run and the response of the system, i.e. the time evolution of the cooling effect $\dot{Q}_f(\mathrm{t})$, noticed.

As mentioned before, the next two steps in the elaboration of a model are the model structure and the estimation of model parameters. In this chapter, these steps were performed by analyzing the experimental input and output data using the software MATLAB and its system identification package. It is found that the most adequate dynamic model for the description of the time evolution of $\dot{Q}_f(\mathrm{t})$ for every chosen energy supply $\dot{Q}_{gen}$ corresponds to the response of a first order system with a delay. Figures 7.1, 7.2, 7.3 and 7.4 show this finding, respectively, in case of four values of $\dot{Q}_{gen}$= 44W, $\dot{Q}_{gen}$= 48W, $\dot{Q}_{gen}$= 51W and $\dot{Q}_{gen}$= 53W.

This means that the transfer function $G_R(s)$ of the DAR system is of the form:

$$G_R(s) = \frac{K_P}{1+\theta_p s} e^{-\tau_d s} \qquad (7.3)$$

Where K_P is the static gain, θ_p the time constant and τ_d the time delay. When applied to the data of the refrigerator under study this simple three-parameter model describes quite accurately the time evolution of the cooling capacity for all values of the heat power supply to

the generator as shown in Figures 7.1, 7.2, 7.3 and 7.4. The fitting quality, an indicator of the quality of the regression results, ranges from 90% to 98%.

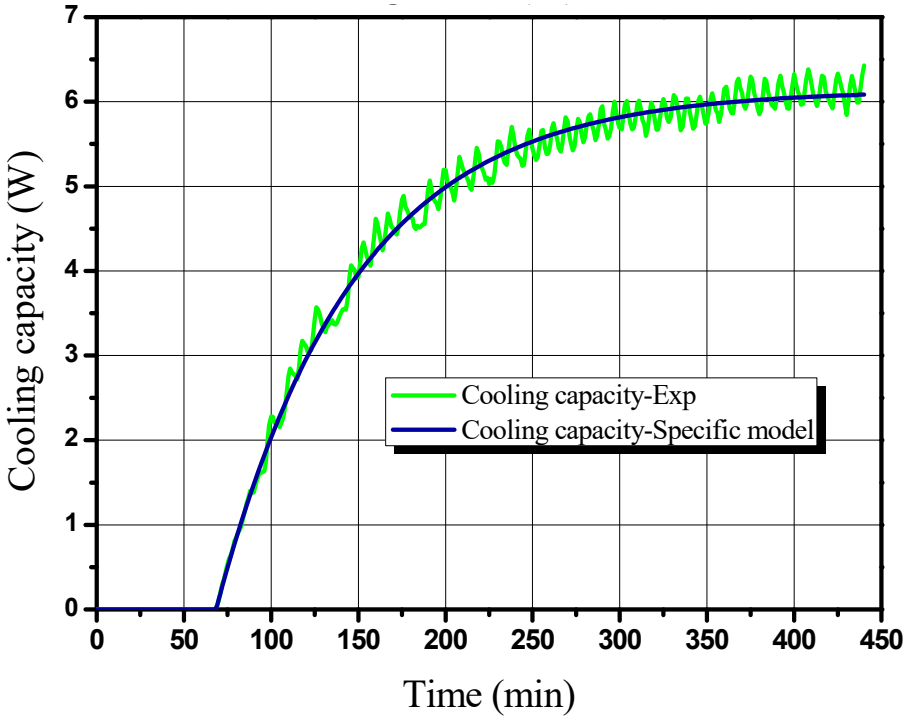

Figure 7. 1. Time evolution of the cooling capacity determined from experimental measurements and the heat-rate-specific black box model for $\dot{Q}_{gen}$= 44W.

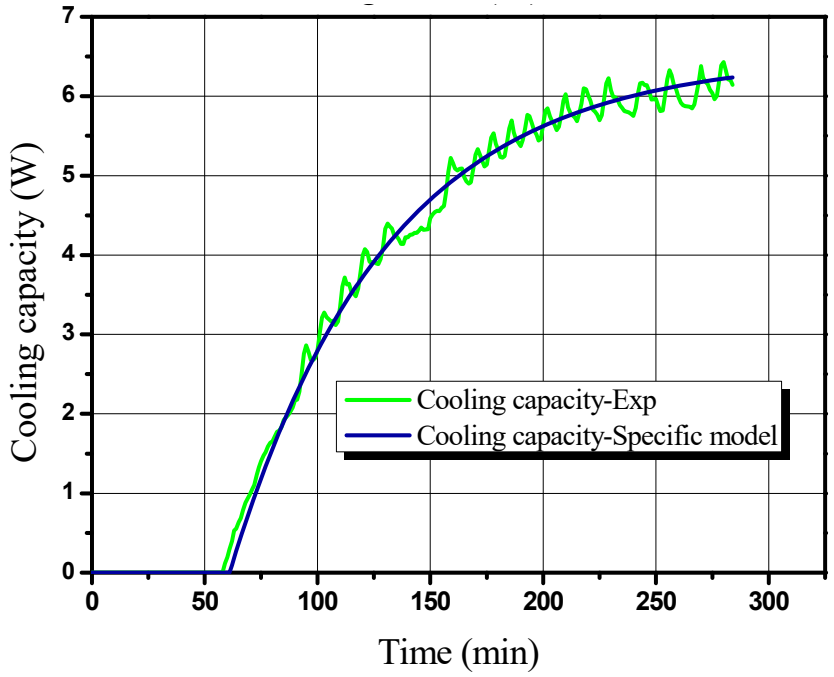

Figure 7.2. Time evolution of the cooling capacity determined from experimental measurements and the heat-rate-specific black box model for $\dot{Q}_{gen}$= 48W.

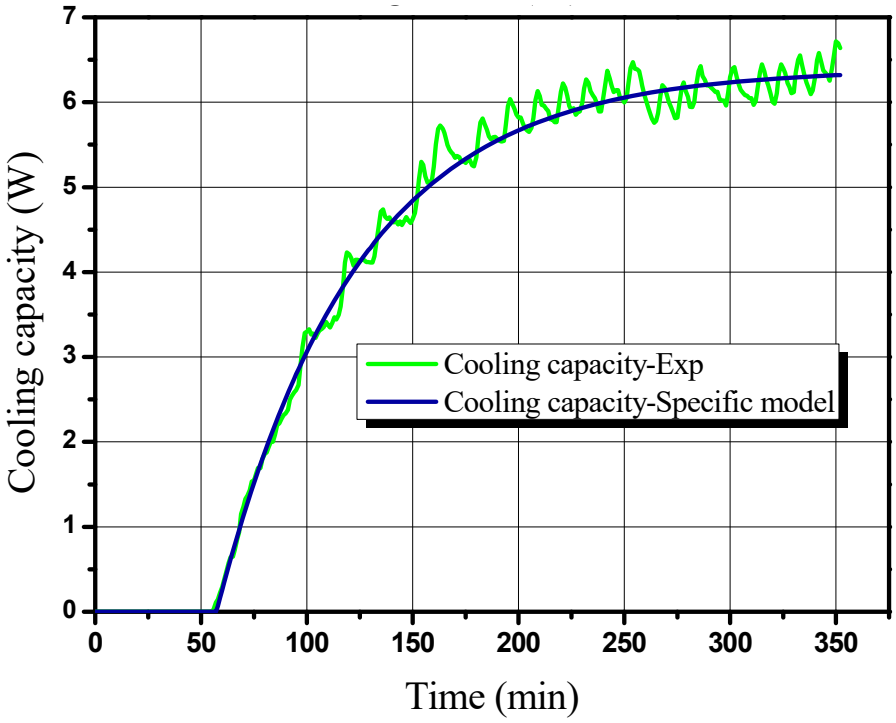

Figure 7.3. Time evolution of the cooling capacity determined from experimental measurements and the heat-rate-specific black box model for $\dot{Q}_{gen}$= 51W.

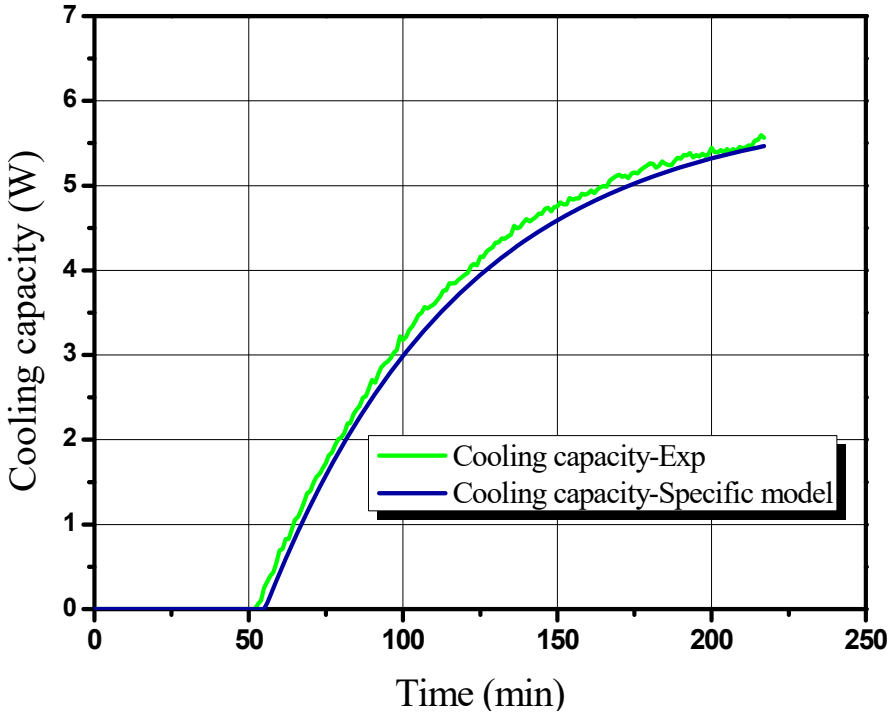

Figure 7.4. Time evolution of the cooling capacity determined from experimental measurements and the heat-rate-specific black box model for $\dot{Q}_{gen}$= 67W.

The transfer function that relates the rate of heat supply $\dot{Q}_{gen}$ as an input signal and the refrigerator cooling capacity $\dot{Q}_f(\mathrm{t})$ as an output signal is:

$$G_R(s) = \frac{Y(s)}{I(s)} = \frac{K_P}{1+\theta_p s} e^{-\tau_d s} \qquad (7.4)$$

With $I(s)$ is the Laplace transform of $\dot{Q}_{gen}(t)$,

$$I(s) = \mathcal{L}\left[\dot{Q}_{gen} F(t)\right] \qquad (7.5)$$

And $Y(s)$ the Laplace transform of the cooling capacity $\dot{Q}_f(t)$,

$$Y(s) = \mathcal{L}\left[\dot{Q}_f(t)\right] \qquad (7.6)$$

The time domain of the cooling capacity $\dot{Q}_f(\mathrm{t})$ can be deduced from equation (7.4),

$$\dot{Q}_f(\mathrm{t}) = \dot{Q}_{gen} K_P \left(1 - e^{\frac{-t-\tau_d}{\theta_p}}\right) F(t-\tau_d) \qquad (7.7)$$

Figures 7.1, 7.2, 7.3 and 7.4 show the calculated time evolution of $\dot{Q}_f(\mathrm{t})$ in comparison with the experimental profiles for the indicated values of the heating power supply to the generator. It can be appreciated that the black-box model reproduces quite accurately the unsteady-state performance of the DAR refrigerator.

Table 7.1 summarizes the model parameters and the fitting indicator quality for all investigated values of $\dot{Q}_{gen}$.

Table 7.1. Model parameters and fitting quality for all investigated values of $\dot{Q}_{gen}$.

$\dot{Q}_{gen}$ (W)	K_p	τ_d	θ_p	Fit (%)
44	0.1395	78.927	66.829	93.91
46	0.1450	71.546	66.618	91.27
48	0.1354	72.092	57.055	94.16
51	0.1253	63.109	57.24	93.08
53	0.1120	60.232	52.523	98.36
56	0.1156	69.676	55.609	93.44
58	0.1096	67.327	54.474	96.90
61	0.0965	56.378	41.623	89.86
67	0.0947	71.510	45.930	95.41

7.2.2. Generalized black-box dynamic model & validation

The analysis of the results in Table 7.1 reveals that the three model parameters K_P, θ_p and $\tau_d$depend on the heat input $\dot{Q}_{gen}$. In Figures 7.5, 7.6 and 7.7, this dependency is graphically depicted with dots representing the values of the parameters and the continuous lines their least-square fitted curves. If the corresponding regression relations $K_P(\dot{Q}_{gen})$, $\theta_p(\dot{Q}_{gen})$ and $\tau_d(\dot{Q}_{gen})$ are incorporated in the expression of $\dot{Q}_f(\mathrm{t})$ (Eq. 7.7), one obtains a generalized model of the DAR refrigerator, i.e. a function $\dot{Q}_f(t, \dot{Q}_{gen})$ which predicts the instantaneous evolution of the cooling capacity for every heating power supply to the generator within the range investigated.

$$\ln K_p = -3.37 + \frac{66.02}{\dot{Q}_{gen}} + (-12.41 * 10^{18}) e^{-\dot{Q}_{gen}}$$

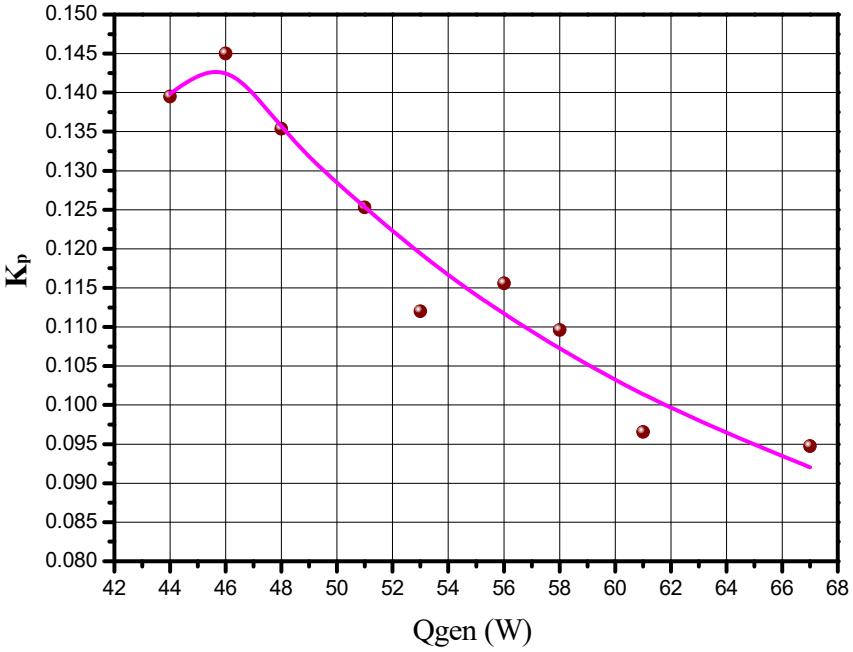

Figure 7.5. K_P vs. $\dot{Q}_{gen}$.

$$\frac{1}{\theta_p} = 0.045 + \left[(-4 * 10^{-5}) * \dot{Q}_{gen}^{1.5}\right] - \left(\frac{39.83}{\dot{Q}_{gen}^{2}}\right)$$

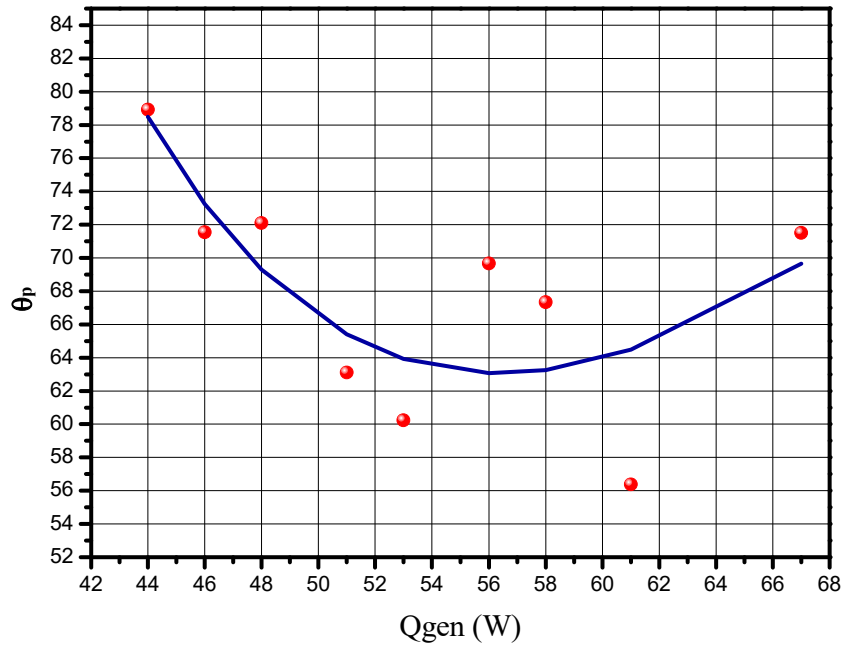

Figure 7.6. θ_P vs. $\dot{Q}_{gen}$.

$$\tau_d = 59.22 - \left(0.094 * \dot{Q}_{gen}{}^{1.5}\right) + \left[\left(8.36 * 10^{-5}\right) * \dot{Q}_{gen}{}^{3}\right] + \frac{54794.45}{\dot{Q}_{gen}{}^{2}}$$

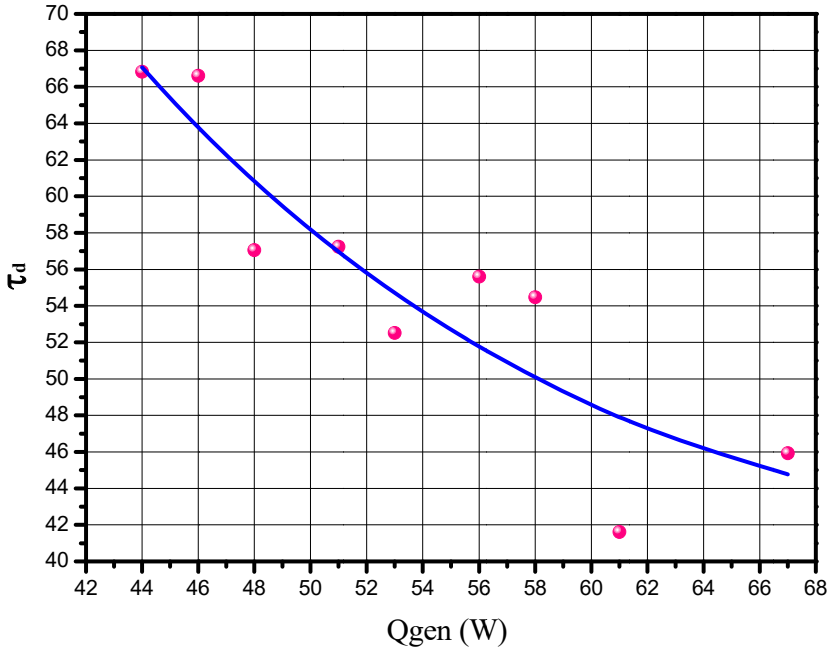

Figure 7.7. τ_d vs. $\dot{Q}_{gen}$.

The test for this generalized black-box dynamic model of the DAR refrigerator was run using the software package MATLAB SIMULINK® (Figure 7.8).

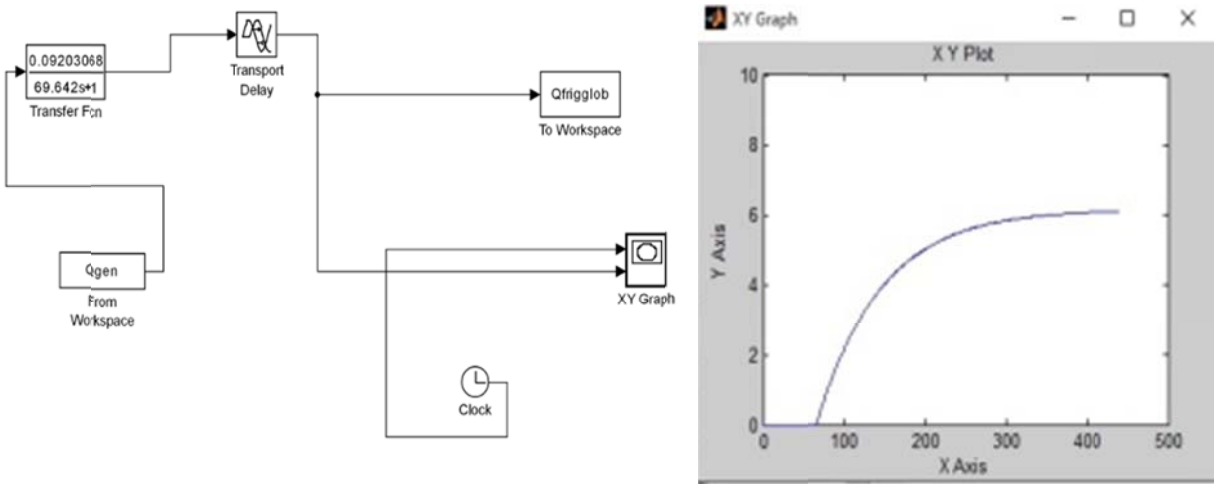

Figure 7.8. Schematic of the black-box dynamic model in the Matlab Simulink® environment.

Figures 7.9, 7.10, 7.11 and 7.12 show the time evolution of the cooling capacity calculated by both the specific and generalized models in comparison with experimental data for the four values of the heat supply, 44W, 48W, 51W and 67W. As can be seen, the generalized black-box model describes reasonably well the dynamic behavior of the DAR refrigerator and predicts fairly good the unsteady-state performance of the refrigerator. The predicted cooling capacity when the steady-state regime is achieved and the fitting quality of the generalized model for the different inputs $\dot{Q}_{gen}$ are summarized in Table 7.2.

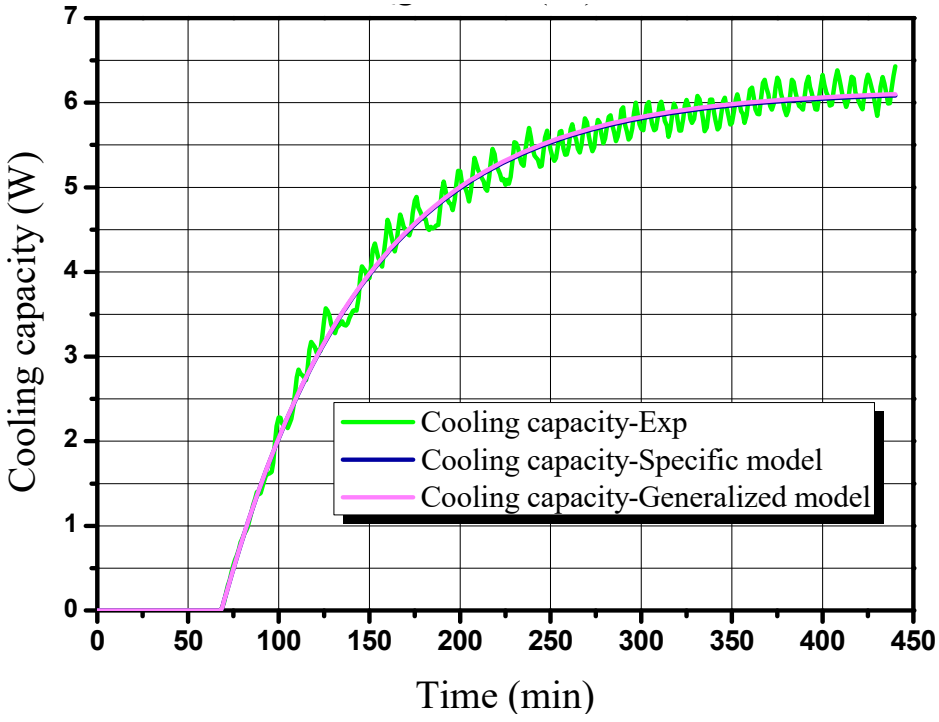

Figure 7.9. Comparison of the experimental cooling capacity and that predicted by the generalized black-box model for $\dot{Q}_{gen}$= 44W.

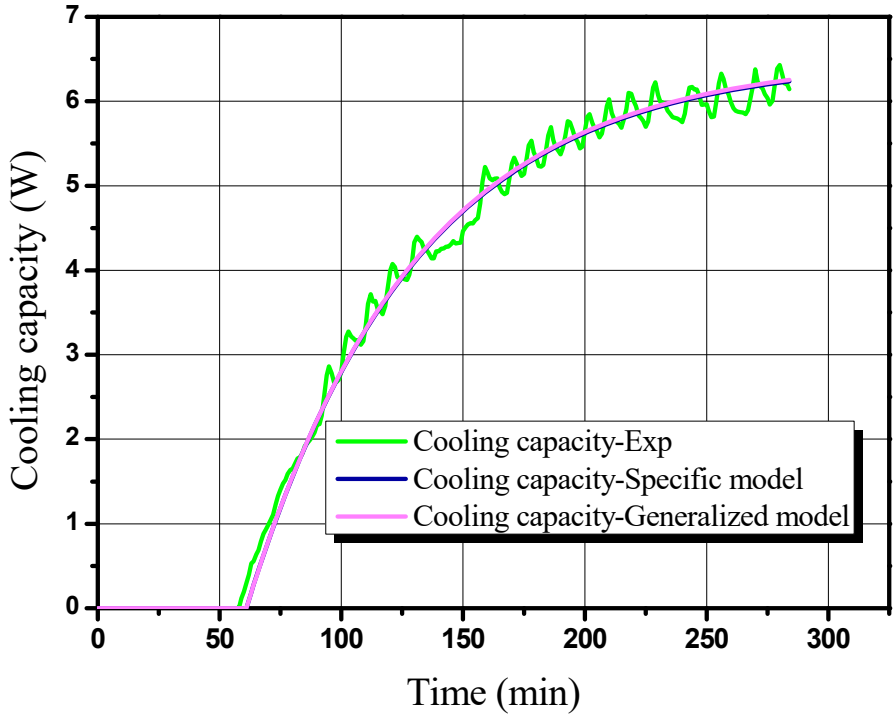

Figure 7.10. Comparison of the experimental cooling capacity and that predicted by the generalized black-box model for $\dot{Q}_{gen}$= 48W.

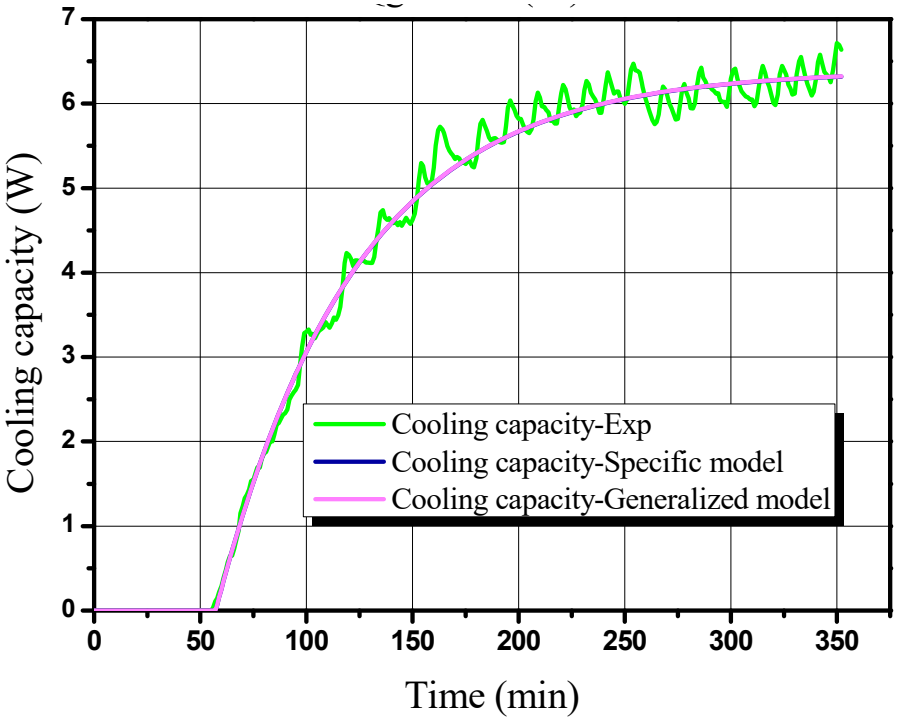

Figure 7.11. Comparison of the experimental cooling capacity and that predicted by the generalized black-box model for $\dot{Q}_{gen}$= 51W.

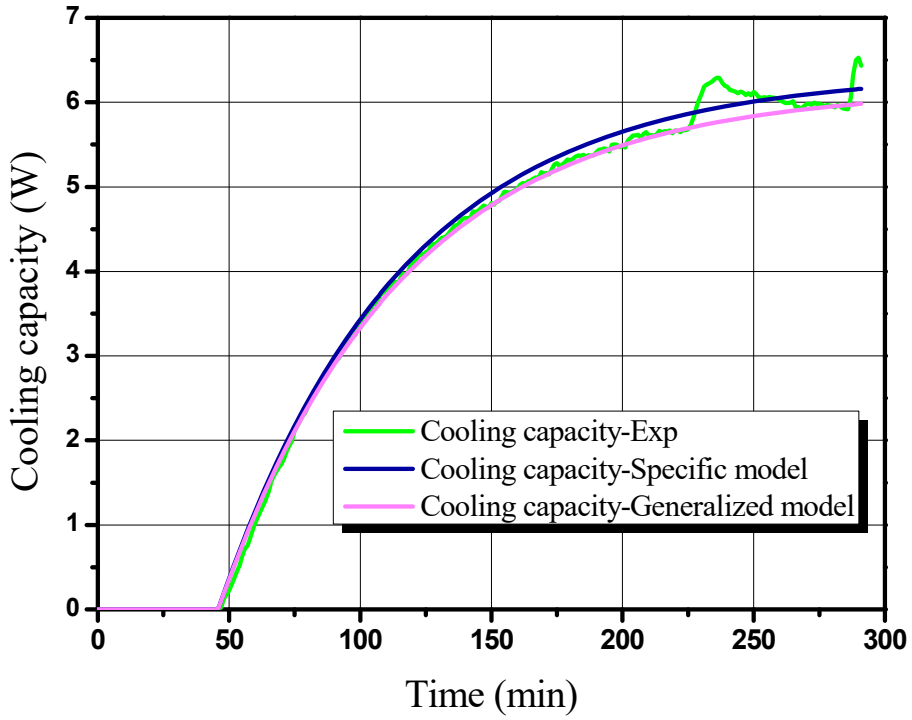

Figure 7.12. Comparison of the experimental cooling capacity and that predicted by the generalized black-box model for $\dot{Q}_{gen}$= 67W.

Table 7.2. Steady-state cooling capacity for different $\dot{Q}_{gen}$:

Experimental data and predicted values by the generalized model.

$\dot{Q}_{gen}$ (W)	Cooling Capacity (W) *Experimental*	Cooling Capacity (W) *Generalized model*	Fit (%)
44	6.43	6.10	93.88
46	6.06	6.45	85.91
48	6.14	6.25	93.21
51	6.64	6.32	92.67
53	5.56	5.82	93.78
56	6.44	6.21	90.84
58	6.10	5.97	93.15
61	6.15	6.11	84.45
67	6.44	5.98	93.58

Figure 7.13shows a further test of the black-box models. It represents a comparison for different values of $\dot{Q}_{gen}$ between the experimental cooling capacity and its calculated values by both the heat-rate-specific and generalized dynamic models. As can be seen, both models predict satisfactorily the cooling capacity of the DAR refrigerator when the steady-state regime is reached. Table 7.3 summarizes the relative deviations in predicting the cooling capacity at the different heat rates supplied to the generator. The maximum relative error is 8.2% and 7.5% for the specific and generalized models, respectively.

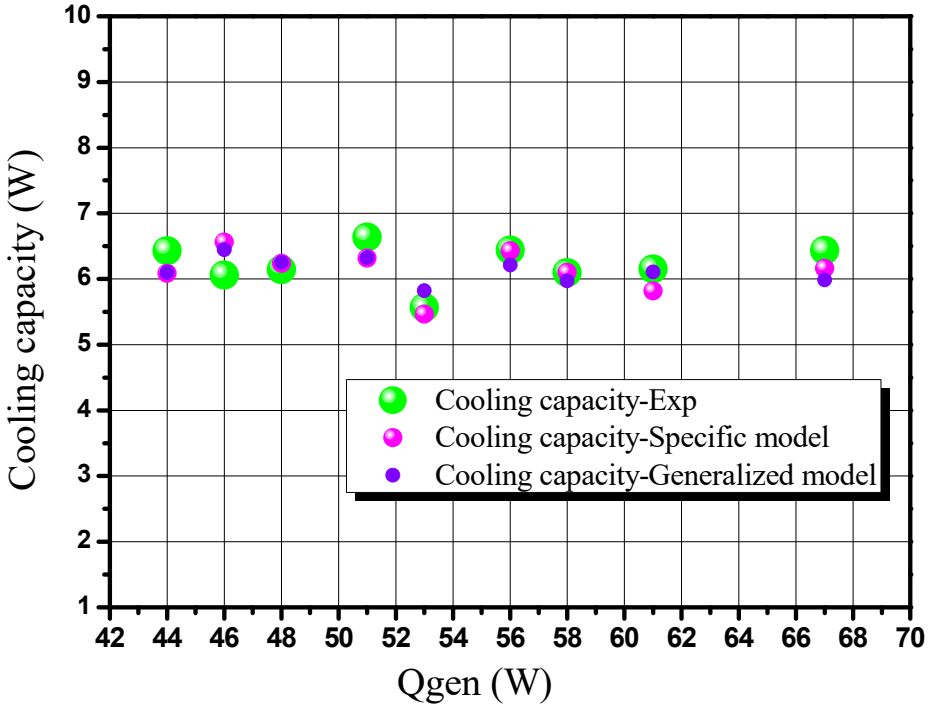

Figure 7.13. Comparison of the experimental steady-state cooling capacity and that predicted by both the heat-rate-specific and generalized models as function of the heat supply to the generator.

Table 7.3. Relative deviation in predicting the cooling capacity for both heat-rate-specific and generalized models.

$Q_{gen}\ (W)$	Cooling capacity (W) *Experimental*	Cooling capacity (W) *Specific model*	Relative deviation (%)	Cooling capacity (W) *Generalized model*	Relative deviation (%)
44	6.43	6.09	5.4	6.10	5.4
46	6.06	6.56	8.2	6.45	6.3
48	6.14	6.24	1.5	6.25	1.8
51	6.64	6.32	5.0	6.32	5.0
53	5.56	5.47	1.8	5.82	4.7
56	6.44	6.43	0.2	6.21	3.7
58	6.10	6.10	0.1	5.97	2.1
61	6.15	5.82	5.8	6.11	0.7
67	6.44	6.16	4.4	5.98	7.5

The experimental steady-state coefficient of performance(COP) of the DAR refrigerator, is depicted *vs.* $\dot{Q}_{gen}$ in Figure 7.14 and comparison with the predicted values for different values of the heat supply to the generator, it shows that the predictions of both models are in good agreement with the experimental data. Table 7.4 shows that the maximum relative deviation in the COP prediction is roughly 8%. Therefore, it can be concluded that both specific and generalized black-box models predict well the cooling capacity and the coefficient of performance of the DAR refrigerator when a steady-state regime is achieved.

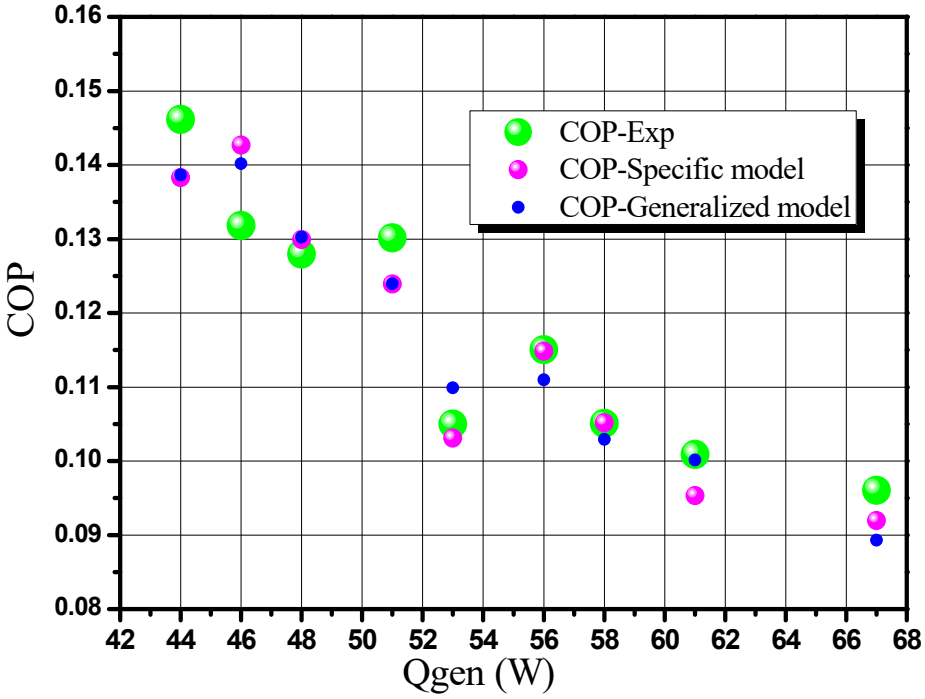

Figure 7.14. Comparison of the experimental COP and that predicted by both the heat-rate-specific and generalized models as function of the heat supply to the generator.

Table 7.4. Relative deviation in predicting the COP for both heat-rate-specific and generalized models.

Q_{gen} (W)	COP *Experimental*	COP *Specific model*	Relative deviation (%)	COP *Generalized model*	Relative deviation (%)
44	0.146	0.138	5.7	0.139	5.4
46	0.132	0.143	8.3	0.140	6.3
48	0.128	0.130	1.5	0.130	1.8
51	0.130	0.124	5.0	0.124	5.0
53	0.105	0.103	1.8	0.110	4.7
56	0.115	0.115	0.2	0.111	3.7
58	0.105	0.105	0.1	0.103	2.1
61	0.101	0.095	5.8	0.100	0.7
67	0.096	0.092	4.4	0.089	7.5

7.3. Conclusion

In this chapter, a dynamic black-box model of a small capacity commercial diffusion-absorption refrigerator (DAR) is developed. It is found that a first order transfer function with delay describes correctly the relationship between the power input to the generator and the cooling capacity as a response of the refrigerator. A maximum relative deviation of about 8.2% between the predicted values by the model and the experimental data is noted. A generalized black-box model is then built by integrating analytical expressions of the three parameters of the model as function of the heat power supplied to the generator in the original specific model. Simulations with the obtained generalized model using Matlab Simulink® environment show that the model predictions deviate by a maximum 8% from the experimental data. The steady-state COP is also well predicted by the generalized black-box model.

Chapter 8

General conclusions and Recommendations

Theoretical and experimental investigations on ammonia-based an absorption and a diffusion-absorption refrigerating machines were carried in this thesis. First, the steady-state operation of a commercial NH_3/H_2O gas-fired absorption chiller was theoretically investigated using the flow-sheeting software Aspen-Plus. Then, a small capacity diffusion-absorption refrigerator was experimentally and theoretically investigated under steady-state and dynamic regimes. The overall heat transfer coefficients and the refrigerator operation during the start-up period were established based on the experimental data. An Aspen-Plus model for the steady-state operation and a black-box model in the Matlab Simulink® environment for the dynamic operation were developed for this refrigerator. The methodology employed and most relevant results are summarized below.

In the case of the absorption chiller, the goal was to develop a reliable simulation model for the machine and to validate it basing on the published experimental data of Klein [97]. The first step in this part of the work was to select the appropriate property model for the working NH_3/H_2O fluid mixture used. Nine different models implemented in Aspen-Plus were tested in two steps. Firstly, the vapor-liquid equilibrium (VLE) calculated by each one of the Aspen-Plus property models was compared with regressed VLE data reported by Mejbri and Bellagi [91] at different pressures. It was found that none of these models predicts the NH_3/H_2O vapor-liquid equilibrium with sufficient accuracy. Secondly, the Aspen-Plus data regression tool was used to deduce the binary interaction parameters of the Aspen-Plus property models

by fitting the vapor-liquid equilibrium data reported in [91]. It was found that the Peng-Robinson-Boston-Mathias equation of state (PR-BM) with regressed interaction parameters is the most suitable property model for the NH_3/H_2O fluid mixture in the temperature and pressure ranges encountered in absorption refrigerating machines. The sum of squared deviations for the selected model was 36.55.

Once the appropriate property package for the NH_3/H_2O mixture selected, a model of a commercial 3-ton NH_3/H_2O gas-fired absorption chiller was developed using the flow-sheeting software Aspen-Plus to simulate the steady-state operation of the machine. First, the overall heat transfer coefficients of the condenser, evaporator, absorber and refrigerant heat exchanger were deduced from experimental data at 35ºC cooling air temperature. The results were then compared with the experimental data and those calculated by El May *et al*. [111]. This comparison showed a good agreement between the three sets of results. In a further step the model was modified to include the (UA) values of the heat exchangers calculated in the previous step as input parameters. The results were again compared with experimental [106] and calculated [111] data at cooling air temperatures of 26.7ºC and 38ºC. The model prediction showed a good agreement with the two sets of bibliographical data.

The second part of this work was dedicated to the investigation of a small capacity (7.5W) commercial diffusion-absorption refrigerator, tested under different heat input conditions to the generator. The temperature at the inlet and outlet of every component was continuously recorded. Monitoring the temperature profiles allowed for the determination of the minimum power supply to the generator needed to ensure the functioning of the refrigerator and its stability. The results showed that a supply of 35 W ensured the functioning of the refrigerator but not its stability, while with 39 W a steady operation of the refrigerator was reached after two and a half hours. All the essential features of the refrigerator were determined experimentally, especially the heat exchange capacities of the cabin and the evaporator,

respectively $(UA)_{cab} = 0.554\ \mathrm{WK^{-1}}$ and $(UA)_{int} = 0.3\ \mathrm{WK^{-1}}$. The best performance of the refrigerator was reached experimentally with an electric power supply of 46 W with a generator temperature of 167°C. The corresponding machine COP was found to be 0.159.

Here again an Aspen-Plus simulation model was then developed for the diffusion-absorption refrigerator for the Steady-state operating mode. To this propose, a set of assumptions based on the experimental tests were introduced as inputs. The refrigerator model developed was run, in a first step, using a sequential modular approach in which each block was calculated separately, with two "break points" constituting the convergence criterion. After convergence and synchronization, the Equation-Oriented (EO) approach was used, in a second step, to solve simultaneously in one block the governing equations of the diffusion-absorption refrigerator. The results obtained for the heating rates 46W, 56W and 67W were well in agreement with the measured temperatures. The deviations between predicted and measured COP and cooling capacity were less than 1%. This indicates that the model developed represents fairly well the functioning of the small capacity commercial diffusion-absorption refrigerator working under a steady-state regime.

Basing on the experimental data obtained for the diffusion-absorption refrigerator in non stationary mode (set-up phase), a dynamic black-box model correlating the power input to the generator and the cooling capacity of the refrigerator was developed using the Matlab identification package. A first order transfer function with delay was found to describe quite accurately the time evolution of the cooling capacity for all considered heat rates supplied to the generator. In a further step, regressed analytical expressions of the three transfer function parameters of function of the generator heat supply were incorporated in the cooling capacity function. A generalized dynamic black-box model for the refrigerator was thus obtained which was then validated using the Matlab Simulink® environment. The model predictions were found to be in good agreement with the experimental data. In particular,

the steady-state COP predictions of the model agree satisfactorily with experimental data with a maximum relative deviation of about 8%.

Regarding the future works, the investigations carried in this thesis can be completed by analyzing the integration of the DAR refrigerator in a solar cooling installation in order to optimize its operating conditions. Moreover, the dynamic modeling of the DAR refrigerator can be further improved using the neural network approach or the Aspen-Hysys platform. Also, the absorption process of ammonia in the ammonia/water solution in presence of the inert gas can be investigated in order to better understand the operation of the absorber, which is the main component in thermally driven cooling machines.

References

[1] P. Rodgers, A. Mortazavi, V. Eveloy, S. Al-Hashimi, Y. Hwang, R. Radermacher. EnhancementofLNG plant propane cyclethroughwaste heat powered absorption cooling. Applied Thermal Engineering, 2012, 48, 41-53.

[2] S. El May, Z. Sayadi, A. Bellagi. Feasibility of air-cooled solar air-conditioning in hot arid climate regions, Int. J. of Sustainable Energy, 2009, 28 (4), 183-193.

[3] K. Rajasuthan, M. PalPandi, Fabrication and Performance Evaluation of Electrolux Refrigeration System Coupled with IC Engine. Int. J. of Engineering Sciences & Research Technology, 2014, 3 (12), 478-483.

[4] B.C. Von Platen, C.G. Munters. US Patent 1, 685,764, 1928.

[5] H. Perez-Blanco. Absorption heat pump performance for different types of solution. International Journal of Refrigeration 1984, 7(2), 115-22.

[6] R.A. Marcriss, JM. Gutraj, TS. Zawacki. Absorption fluid data survey: final report on world wide data, ORLN/sub/8447989/3, Inst. Gas Tech, 1988.

[7] A.A. Berestneff. Absorption refrigeration. MechEng 1949, 72, 216-20.

[8] L.A. McNeely. Thermodynamic properties of aqueous solutions of lithium bromide. ASHRAE Trans 1979, 85(2), 413-34.

[9] M.R. Patterson, H. Perez-Blanco. Numerical fits of properties of lithium-bromide water solutions. ASHRAE Trans 1988, 94(2), 2059-77.

[10] R.J. Lee, R.M. DiGuilio, S.M. Jeter, A.S. Teja. Properties of lithium bromide-water solutions at high temperatures and concentrations-part II: density and viscosity. ASHRAE Trans 1990, 96, 709-14.

[11] S.M. Jeter, J.P. Moran, A.S. Teja. Properties of lithium bromide-water solutions at high temperatures and concentrations-part III: specific heat. ASHRAE Trans 1992, 98, 137-49.

[12] J.L.Y. Lenard, S.M. Jeter, A.S. Teja. Properties of lithium bromide-water solutions at high temperatures and concentrations-part IV: vapor pressure. ASHRAE Trans 1992, 98, 167-72.

[13] R.J. Modahl, P.J. Lynch. Arsenic trioxide corrosion inhibitor for absorption refrigeration system, US Patent No. 3609086, 1971.

[14] S. Iyoki, T. Uemura. Studies on corrosion inhibitor in water-lithium bromide absorption refrigerating machine. Reito 1978, 53(614), 1101-5.

[15] T.C. Wen, S.M. Lin. Corrosion inhibitors the absorption system. J Chin Inst ChemEng 1992, 22, 311-6.

[16] S.K. Verma, M.S. Mekhjian, G.R. Sandor, N. Nakada. Corrosion inhibitor in lithium bromide absorption fluid for advanced and current absorption cycle machines. ASHRAE Trans 1999, 105(1), 813-5.

[17] C.E. Albertson, RH. Krueger. Heat transfer additives for absorbent solution, US Patent No. 3580759, 1971.

[18] W.C. Chang, RA. Marcriss, W.F. Rush. Secondary alcohol additives for lithium bromide-water absorption refrigeration system, US Patent No. 3609087, 1971.

[19] YM. Elkassabgi, H. Perez-Blanco. Experimental study of the effects of alcohol additives in lithium bromide/water pool absorber. ASHRAE Trans 1991, 97, 403-5.

[20] H. Daiguji, E. Hihara, T. Saito. Mechanism of absorption enhancement by surfactant. International Journal Heat Mass transfer, 1997, 40(8), 1743-52.

[21] E. Hihara, T. Saito. Effect of surfactant on falling film absorption. International Journal of Refrigeration, 1993, 16(5), 339-46.

[22] K. Herold, R. Radermacher, S.A. Klein. Absorption Chillers and Heat Pumps. 1996. CRC Press.

[23] R. Renz, F. Steimle. Comparison of thermodynamic properties of working fluids for absorption systems. I.I.F-I.I.R. Commission E1, E2, Jerusalem, 1982, 61-67.

[24] P. Srikhirin, S. Aphornratana, S. Chungpaibulpatana. A review of absorption refrigerationtechnologies. Renewable and Sustainable Energy Reviews,2001, 5, 343-372.

[25] J.Labus, J.C. Bruno, A. Coronas. Review on absorption technology with emphasis on small capacity absorption machines. Thermal Science, 2013, 17 (3), 739-762.

[26] C. Amaris. Intensification of NH_3 bubble absorption process using advanced surfaces and carbon nanotubes for $NH_3/LiNO_3$absorption chillers. PhD thesis, Universitat Rovira i Virgili, Tarragona, Spain, 2013.

[27] S. Raghuvanshi, G. Maheshwari. Analysis of Ammonia-Water (NH_3-H_2O) Vapor Absorption Refrigeration System based on First Law of Thermodynamics. International Journal of Scientific & Engineering Research, 2011, 2, ISSN 2229-5518.

[28] D. Kong, J. Liu, L. Zhang, H. He, Z. Fang. Thermodynamic and Experimental Analysis of an Ammonia-Water Absorption Chiller. Energy and Power Engineering, 2010, 2, 298-305.

[29] N. Ben Ezzine, M. Barhoumi, Kh. Mejbri, A. Bellagi. Second law study of ammonia-water double effectabsorption chiller. International Refrigeration and Air Conditioning Conference, 2004, Paper 673.

[30] Y.T. Ge, S.A Tassou, I. Chaer. Modelling and performance evaluation of a low-temperature ammonia-waterabsorption refrigeration system. International Journal of Low-Carbon Technologies, 2009, 4, 68-77.

[31] C.J. Jawahar, B. Raja, R. Saravanan. Thermodynamic studies on NH_3-H_2O absorption coolingsystem using pinch point approach. International Journal of Refrigeration, 2010, 33, 1377-1385.

[32] A. Sozen, M. Ozalp. Performance improvement of absorption refrigeration system using triple-pressure-level. Applied Thermal Engineering, 2003, 23 (13), 1577-93.

[33] S.Q. Abu-Ein, S.M. Fayyad, W. Momani, M. Al-Bousoul. Performance analysis of solar powered absorption refrigeration system. Heat Mass Trans, 2009, 46, 137-45.

[34] I. Horuz, T.M.S. Callander. Experimental investigation of a vapor absorption refrigeration system. Int. J. of Refrigeration, 2004, 27 (1), 10-16.

[35] N.A. Darwish, S.H. Al-Hashimi, A.S. Al-Mansoori. Performance analysis and evaluation of a commercial absorption-refrigeration water-ammonia (ARWA) system. Int. J. of Refrigeration, 2008, 31 (7), 1214-1223.

[36] D.K. Priedeman, M.A. Garrabrant, J.A. Mathias, R.E. Stout, R.N. Christensen. Performance of a residential sized GAX absorption chiller. Transactions of the ASME, 2001, 123 (3), 236-241.

[37] K.C. Ng, K. Tu, H.T. Chua, J.M. Gordon, T. Kashiwagi, A. Akisawas, B.B. Saha. Thermodynamic analysis of absorption chillers: Internal dissipation and process average temperature. AppliedThermal Engineering, 1998, 18 (8), 671-682.

[38] D. Zheng, W. Deng, H. Jin, J. Ji. α-h diagram and principle of exergy coupling of GAX cycle. Applied Thermal Engineering, 2007,27 (11- 12), 1771-1778.

[39] R. Mansouri, I. Boukholda, M. Bourouis, A. Bellagi. Modelling and testing the performance of a commercial ammonia/water absorption chiller using Aspen-Plus platform. Energy, 2015, 93, 2374-2383.

[40] GC. Blytas, F. Daniels. Concentrated solutions of NaSCN in liquid ammonia. Solubility, density, vapor pressure, viscosity, thermal conductance, heat of solution and heat capacity. J Am ChemSoc, 1962, 84, 1075-83.

[41] JF. Wang, GC. Gao, GM. Chen. An improved absorption refrigeration cycle driven by unsteady thermal sources below 100 8C. Int J Energy Res, 2000, 24, 633-40.

[42] W. Wu, XL. Zhang, XT. Li, WX. Shi, BL. Wang. Comparisons of different working pairs and cycles on the performance of absorption heat pump for heating and domestic hot water in cold regions. Applied Thermal Engineering, 2012, 48, 349-58.

[43] ROE. Davis, LB. Olmstead, FO. Landstrum. Vapor pressure of lithium nitrate: ammonia system. J Am ChemSoc, 1921, 43, 1575-80.

[44] JCV. Chinnappa. Experimental study of the intermittent vapour absorption refrigeration cycle employing the refrigerant-absorbent systems of ammonia water and ammonia lithium nitrate. Solar Energy, 1961, 5(1), 1-18.

[45] R. Best, MAR. Eisa, FA. Holland. Thermodynamic design data for absorption heat pump systems operating on ammonia-water-Part I. Cooling. Heat Recover Syst CHP, 1987, 7(2), 167-75.

[46] R. Best, MAR. Eisa, FA. Holland. Thermodynamic design data for absorption heat pump systems operating on ammonia-water-Part II. Heat Recover Syst CHP, 1987, 7(2), 177-85.

[47] R. Best, MAR. Eisa, FA. Holland. Thermodynamic design data for absorption heat pump systems operating on ammonia-water-Part III. Simultaneous cooling and heating. Heat Recover Syst CHP, 1987, 7(2), 187-94.

[48] R. Best, MAR. Eisa, FA. Holland. Thermodynamic design data for absorption heat transformers-III. Operating on ammonia-water. Heat Recover Syst CHP, 1987, 7(3), 259-72.

[49] R. Best, L. Porras, FA. Holland. Thermodynamic design data for absorption heat pump systems operating on ammonia-lithium nitrate-Part one. Cooling. Heat Recover Syst CHP, 1991, 11(1), 49-61.

[50] R. Best, L. Porras, FA. Holland. Thermodynamic design data for absorption heat pump systems operating on ammonia-lithium nitrate-Part two. Cooling. Heat Recover Syst CHP, 1991, 11(2–3), 103-11.

[51] R. Best, L. Porras, FA. Holland. Thermodynamic design data for absorption heat pump systems operating on ammonia-lithium nitrate-Part three. Cooling. Heat Recover Syst CHP, 1991, 11(4), 199-212.

[52] R. Best, W. Rivera, I. Pilatowsky, FA. Holland. Thermodynamic design data for absorption heat transformers-Part four. Operating on ammonia-lithium nitrate. Heat Recover Syst CHP, 1990, 10(5–6), 539-48.

[53] R. Best, W. Rivera, J. Hernández, A. Oskam. Thermodynamic design data for absorption heat pump systems operating on ammonia-sodium thiocyanate-I. Cooling. Heat Recovery Syst CHP, 1993, 13(1), 1-9.

[54] R. Best, W. Rivera, J. Hernández, A. Oskam. Thermodynamic design data for absorption heat pump systems operating on ammonia-sodium thiocyanate-II. Heating. Heat Recover Syst CHP, 1993, 13(1), 11-21.

[55] R. Best, W. Rivera, J. Hernández, A. Oskam. Thermodynamic design data for absorption heat pump systems operating on ammonia-sodium thiocyanate-III. Simultaneous cooling and heating. Heat Recover Syst CHP, 1993, 13(1), 23-31.

[56] R. Best, W. Rivera, J. Hernández, FA. Holland. Thermodynamic design data for absorption heat transformers-Part 5. Operating on ammonia-sodium thiocyanate. Heat Recover Syst CHP, 1992, 12(4), 347-56.

[57] K.A. Antonopoulos, E.D. Rogdakis. Performance of solar-driven ammonia-lithium nitrate and ammonia-sodium thiocyanate absorption systems operating as coolers or heat pumps in Athens. Applied Thermal Engineering, 1996, 16(2), 127-47.

[58] DW. Sun. Comparison of the performances of NH_3-H_2O, NH_3-$LiNO_3$ and NH_3-NaSCN absorption refrigeration systems. Energy Conversion and Management, 1998, 39(5-6), 357-68.

[59] CO. Rivera, W. Rivera. Modeling of an intermittent solar absorption refrigeration system operating with ammonia-lithium nitrate mixture. Solar Energy Mater Sol C, 2003, 76(3), 417-27.

[60] LH. Zhu, JJ. Gu. Second law-based thermodynamic analysis of ammonia/sodium thiocyanate absorption system. Renewable Energy, 2010, 35, 1940-6.

[61] W. Rivera, R. Best. Boiling heat transfer coefficients inside a vertical smooth tube for water/ammonia and ammonia/lithium nitrate mixtures. International Journal Heat Mass Transfer, 1999, 42, 905-21.

[62] M. Venegas, M. Izquierdo, M. De Vega, A. Lecuona. Thermodynamic study of multistage absorption cycles using low-temperature heat. International Journal ofEnergy Research, 2002, 26, 775-791.

[63] G. Moreno-Quintanar, W. Rivera, R. Best. Comparison of the experimental evaluation of a solar intermittent refrigeration system for ice production operating with the mixtures$NH_3/LiNO_3$ and $NH_3/LiNO_3/H_2O$. Renewable Energy, 2012, 38 (1), 62-68.

[64] R. Ventas, A. Lecuona, A. Zacarías, M. Venegas. Ammonia-lithium nitrate absorption chiller with an integrated low-pressure compression booster cycle for low drivingtemperatures. Applied Thermal Engineering, 2010a, 30, 1351-1359.

[65] M. Bourouis, A. Coronas, M. Vallès, M. Zamora. Air/water or water/water absorption water cooler using ammonia and lithium nitrate. OEPM Madrid P200930758. 29/09/2009, PCT/ES2010/070608.

[66] M. Zamora, M. Bourouis, A. Coronas, M. Vallès. Pre-industrial development and experimental characterization of new air-cooled and water-cooled ammonia/lithium nitrate absorption chillers. International Journal of Refrigeration, 2014, 45, 189-197.

[67] M. Zamora, M. Bourouis, A. Coronas, M. Vallès. Part-load characteristics of a new ammonia/lithium nitrate absorption chiller. International Journal of Refrigeration, 2015, 56, 43-51.

[68] F. Táboas, M. Bourouis, M. Vallès. Boiling heat transfer and pressure drop of $NH_3/LiNO_3$ and $NH_3/(LiNO_3+H_2O)$ in a plate heat exchanger. International Journal of Thermal Sciences, 2016, 105, 182-194.

[69] C. Amaris, M. Bourouis, M. Vallès. Effect of advanced surfaces on the ammonia absorption process with $NH_3/LiNO_3$ in a tubular bubble absorber. International Journal Heat Mass Transfer, 2014, 72, 544-552.

[70] C. Amaris, M. Bourouis, M. Vallès. Passive intensification of the ammonia absorption process with $NH_3/LiNO_3$ using carbon nanotubes and advanced surfaces in a tubular bubble absorber. Energy, 2014, 68, 519-528.

[71] C. Oronel, C. Amaris, M. Bourouis, M. Vallès. Heat and mass transfer in a bubble plate absorber with $NH_3/LiNO_3$ and $NH_3/(LiNO_3+H_2O)$ mixtures. International Journal of Thermal Sciences, 2013, 63, 105-114.

[72] Electrolux, http ://group.electrolux.com.

[73] D.A. Kouremenos, A. Stegou-Sagia. Use of helium instead of hydrogen in inert gas absorption refrigeration. International Journal of Refrigeration, 1988, 11, 6-341.

[74] A. Zohar, M. Jelinek, A. Levy, I. Borde. Numerical investigation of a diffusion absorption refrigeration cycle. International Journal of Refrigeration, 2005, 28 (4), 515-525.

[75] A. Zohar, M. Jelinek, A. Levy, I. Borde. The influence of diffusion absorption refrigeration cycle configuration on the performance. Applied Thermal Engineering, 2007, 27 (13), 2213-2219.

[76] A. Zohar, M. Jelinek, A. Levy, I. Borde. Performance of diffusion absorption refrigeration cycle with organic working fluids. International Journal of Refrigeration, 2009, 32 (6), 1241-1246.

[77] N. Ben Ezzine, R. Garma, A. Bellagi. A numerical investigation of a diffusion-absorption refrigeration cycle based on R124-DMAC mixture for solar cooling. Energy, 2010, 35 (5), 1874-1883.

[78] G. Starace, L. De Pascalis. An advanced analytical model of the Diffusion Absorption Refrigerator cycle. International Journal of Refrigeration, 2012, 35 (7), 605-612.

[79] Z. Sayadi, N. Ben Thameur, M. Bourouis, A. Bellagi. Performance optimization of solar driven small air-cooled absorption–diffusion chiller working with light hydrocarbons. Energy Conversion and Management, 2013, 74, 299-307.

[80] Z. Long, Y. Luo, H. Li, X. Bu, W. Ma. Performance analysis of a diffusion absorption refrigeration cycle working with TFE–TEGDME mixture. Energy Building, 2013, 58, 86-92.

[81] J.L. Rodríguez-Muñoz, J.M. Belman-Flores. Review of diffusion-absorption refrigeration technologies. Renewable and Sustainable Energy Reviews, 2014, 30, 145-153.

[82] A.S. Rattner, S. Garimella. Low-source-temperature diffusion absorption refrigeration. Part I: Modeling and cycle analysis. International Journal of Refrigeration, 2016, 65, 287-311.

[83] A.S. Rattner, S. Garimella. Low-source-temperature diffusion absorption refrigeration. Part II: Experiments and model assessment. International Journal of Refrigeration, 2016, 65, 312-329.

[84] J. Chen, K.J. Kim, K.E. Herold. Performance enhancement of a diffusion absorption refrigerator. International Journal of Refrigeration, 1996, 19 (3), 208-218.

[85] G.Vicatos. Experimental investigation on a three-fluid absorption refrigeration machine. Journal of Process Mechanical Engineering, 2000, 214, 157-172.

[86] A. Koyfman, M. Jelinek, A. Levy, I. Borde. An experimental investigation of bubble pump performance for diffusion absorption refrigeration system with organic working fluids. Applied Thermal Engineering, 2003, 23 (15), 1881-1894.

[87] U. Jakob, U. Eicker,D. Schneider, A.H. Taki, M.J. Cook. Simulation and experimental investigation into diffusion absorption cooling machines for air-conditioning applications. Applied Thermal Engineering, 2008, 28 (10), 1138-1150.

[88] A. Yıldız, M.A. Ersöz. Energy and exergy analyses of the diffusion absorption refrigeration system. Energy, 2013, 60, 407-415.

[89] S. Mazouz, R. Mansouri, A. Bellagi. Experimental and thermodynamic investigation of an ammonia/water diffusion absorption machine. International Journal of Refrigeration, 2014, 45, 83-91.

[90] Aspen-Plus. Version 7.3.0.13 (25.0.4987), 2009. Aspen Technology, Inc., Ten Canal Park, Cambridge, MA, USA. www.aspentech.com.

[91] Kh. Mejbri, A. Bellagi. Modeling of thermodynamic properties of the water-ammonia by three different approaches.Int. J. of Refrigeration, 2006, 29 (2), 211-218.

[92] B.E. Poling, J.M. Prausnitz, J.P. O'Connell. The properties of gases and liquids. 5th Edition, McGraw-Hill, 2001.

[93] Z. Duan, N. Moller, J.H. Weare. Equation of state for the NH_3-H_2O System. Journal of Solution Chemistry, 1996, 25 (1), 43-50.

[94] S.C.G . Schulz. Equations of state for the system ammonia-water for use with computers. Proceedings of 13th International Congress of Refrigeration, Paper nº 2.06, pp. 431-436, Washington DC, 1971.

[95] B. Ziegler, Trepp Ch. Equation of state for ammonia-water mixtures.International Journal of Refrigeration, 1984, 7 (2), pp. 101-106.

[96] H. Renon, J.L. Guillevic, D. Richon, J. Boston, H. Britt. A cubic equation of state representation of ammonia-water -liquid equilibrium data.International Journal of Refrigeration, 1986, 9 (2), 70-73.

[97] J.P. Ruiter. Simplified thermodynamic description of mixtures and solutions.International Journal of Refrigeration, 1990, 13 (4), 223-236.

[98] J. Pátek, J. Klomfar. Simple functions for fast calculations of selected thermodynamic properties of the ammonia-water system.International Journal of Refrigeration, 1995, 18 (4), 228-234.

[99] M. Barhoumi, A. Snoussi, N. Ben Ezzine, K. Mejbri, A. Bellagi. Modeling of the thermodynamic properties of the ammonia/water mixture.International Journal of Refrigeration, 2004, 27 (3), 271-283.

[100] J. Vidal. Equation of state – reworking the old forms. Fluid Phase Equilibria, 1983, 13 (C), 15-33.

[101] R. Tillner-Roth, D.G. Friend. A Helmholtz free energy formulation of the thermodynamic properties of the mixture {water+ammonia}. Journal of Physical and Chemical Reference Data, 1998, 27 (1), 63-77.

[102] V. Abovsky. Thermodynamics of ammonia+water mixture. Fluid Phase Equilibria, 1996, 116 (2), 170-176.

[103] L.J. Van Poolen, J.C. Rainwater. Critical-region model for bubble curves of ammonia-water with extrapolation to low pressures. Fluid Phase Equilibria, 1998, 150 (151), 451-458.

[104] M. Moshfeghian, A. Shariat, R.N. Maddox. Prediction of refrigerant thermodynamic properties by equations of state: vapor liquid equilibrium behavior of binary mixtures. Fluid Phase Equilibria, 1992, 80 (C), 33-44.

[105] L.A. Weber. Estimating the virial coefficients of the ammonia+water mixture. Fluid Phase Equilibria, 1999, 162 (1-2), 31-49.

[106] S.A. Klein. A model of the steady-state performance of an absorption heat pump. US Department of Commerce, National Bureau of Standards, National Engineering Laboratory, Center for Building Technology, NBSIR 82-2606, Washington DC, 1982.

[107] R.M.Lazzarin, A. Gasparella, G.A. Longo. Ammonia-water absorption machines for refrigeration: Theoretical and real performances. International Journal of Refrigeration, 1996, 19 (4), 239-246.

[108] H.T. Chua, H.K. Toh, K.C. Ng. Thermodynamic modeling of an ammonia-water absorption chiller. International Journal of Refrigeration, 2002, 25 (7), 896-906.

[109] J.A. Rossa, E. Bazzo. Themodynamic modeling of an ammonia-water absorption system associated with a microturbine.International Journal of Themodynamics, 2009, 12 (1), 38-43.

[110] S. El May, I. Boukholda, A. Bellagi. Modular simulation and thermodynamic analysis of absorption heat pumps. Engineering with Computers, 2010, 26 (2), pp. 185-192.

[111] S. El May, I. Boukholda, A. Bellagi. Energetic and exergetic analysis of a commercial ammonia-water absorption chiller. International Journal of Exergy, 2011, 8 (1), 33-50.

[112] Règlement délégué (UE) n°1060/2010 de la commission du 28 septembre 2010, Journal officiel de l'union européenne, L314/17.

[113] C. Somers, A. Mortazavi, Y. Hwang, R. Radermacher, P. Rodgers, S. Al-Hashimi, Modeling water/lithium bromide absorption chillers in Aspen Plus. Applied Energy, 2011, 88 (11), 4197-4205.

[114] D. Butz, K. Stephan. Dynamic Behavior of an Absorption Heat Pump. International Journal of Refrigeration, 1989, 12 (4), 204- 212.

[115] S. Jeong, B. H. Kang, S. W. Karng. Dynamic Simulation of an Absorption Heat Pump for Recovering Low Grade Waste Heat. Applied Thermal Engineering,1998, 18 (1-2), 1-12.

[116] D. G. Fu, G. Poncia, Z. Lu. Implementation of an Object-Oriented Dynamic Modeling Library for Absorption Refrigeration Systems. Applied Thermal Engineering, 2006, 26 (2-3), 217-225.

[117] B. Kim, J. Park. Dynamic Simulation of a Single-Effect Ammonia–Water Absorption Chiller. International Journal of Refrigeration. 2007, 30 (3), 535-545.

[118] P. Kohlenbach, F. Ziegler. A Dynamic Simulation Model for Transient Absorption Chiller Performance. Part I: The Model. International Journal of Refrigeration, 2008a, 31 (2), 217-225.

[119] P. Kohlenbach, F. Ziegler. A Dynamic Simulation Model for Transient Absorption Chiller Performance. Part II: Numerical Results and Experimental Verification. International Journal of Refrigeration, 2008b, 31 (2), 226-233.

[120] H. Matsushima, T. Fujii, T. Komatsu, A. Nishiguchi. Dynamic Simulation Program with Object-Oriented Formulation for Absorption Chillers (Modelling, Verification, and Application to Triple-Effect Absorption Chiller). International Journal of Refrigeration, 2010, 33 (2), 259-268.

[121] W. Cai, M. Sen, S. Paolucci. Dynamic Simulation of an Ammonia-Water Absorption Refrigeration System. Industrial & Engineering Chemistry Research,2011, 51, 2070-2076.

[122] M. Zinet, R. Rulliere, P. Haberschill. A Numerical Model for the Dynamic Simulation of a Recirculation Single-Effect Absorption Chiller. Energy Conversion and Management, 2012, 62, 51-63.

[123] R. Mansouri, M. Bourouis, A. Bellagi. Experimental investigations and modelling of a small capacity diffusion-absorption refrigerator in dynamic mode. Applied Thermal Engineering, 2017, 113, 653-662.

[124] R. Mansouri, M. Bourouis, A. Bellagi. Steady state investigations of a commercial diffusion-absorption refrigerator: Experimental study and numerical simulations. Applied Thermal Engineering, 2018, 129, 725-734.